UNIVERSITA' DEGLI STUDI DI MILANO
Facoltà di Medicina e Chirurgia
Dipartimento di Morfologia Umana e Scienze Biomediche "Città Studi"
Dottorato di Ricerca in Scienze Morfologiche
XXIII ciclo
Settore Disciplinare BIO16-17

Immunomodulation and intestinal barrier protection activities of a novel synthetic glucose analogue in inflammatory animal model of colitis and asthma.

Coordinatore: Chiar.ma Prof.ssa Magda Enrica Gioia
Tutor: Prof. Cristiano Rumio

Tesi di Dottorato di Ricerca di
Giuseppina Dusio
Matr. R07773

Anno Accademico 2009-2010

INDEX

4. RESULTS

4.1. Synthetic glucose analogues: synthesis and screening

4.1.1. *Stability studies*

4.1.2. *BLF501 affects LPS-induced IL-8 release in intestinal epithelial cells*

4.1.3. *Protection afforded by BLF501 in LPS-induced shock in mice*

4.2. SGLT-1 a new therapeutic target for epithelial barrier function

4.2.1. *SGLT-1 activation by BLF-501 5 µg/l effects on permeability of Caco-2 monolayer against inflammatory stimuli (INF-γ and TNF-α) and "chemical-DSS" damage*

4.2.2. *BLF501-mediated barrier functionality protection is associated to a morphological conservation of two TJ proteins*

4.2.3. *BLF501 protection against inflammatory bowel disease in vivo*

4.3. SGLT-1 a new therapeutic target in lung inflammatory disease

4.3.1. *Engagement of SGLT-1 inhibits the response of human pneumocytes to LPS*

4.3.2. *BLF501 inhibits LPS-induced interleukin IL-8 production in human pneumocytes A549 cells at 100,000-fold lower concentrations than D-glucose*

4.3.3. *Protective anti-inflammatory effects induced by BLF501 engagement of SGLT-1 in lung after aerosol administration of LPS*

4.3.4. *Anti-inflammatory effects of BLF501 in an OVA-induced model of allergic asthma*

4.3.5. *Orally administered BLF501 inhibits OVA-induced lung inflammation*

4.3.6. *Hsp27 mediates the anti-inflammatory effects of BLF501 through induction of IL-10 production by dendritic cells*

Abstract.

The mucosal surfaces of the gastrointestinal and respiratory tracts are the main interfaces between the environment and the host. All two are protected by continuous epithelia that prevents the entry of microbes and integrity loss of these epithelia commonly predispose to infection. On the other hand the epithelial surfaces provide essential absorptive functions for the intake of food and air. SGLT-1 is a co-transporter able to absorb D-glucose, against a concentration gradient, together with Na^+. The expression of SGLT-1 on the apical membrane of enterocytes, the cells that line the gut and overlook to the intestinal lumen, is fundamental in order to obtain the maximum D-glucose absorption from the digested alimentary bolo that transits through the gut. Accumulating data support the notion that SGLT1 orchestrates a number of fundamental cellular processes besides its canonical absorptive function. Presented results show a novel role of SGLT-1: this protein if appropriately activated modulates the immune response and protect barrier function.

Our recent findings indicate that the activation of SGLT-1, present at apical membrane of enterocytes inhibits bacteria-induced inflammatory processes and lifesaving treatments, assuming a role as an immunological player. The main drawback of this activation is the high level of glucose that must be administrated (2.5 g/kg) *in vivo* so to achieve protection. In this contest we have developed a new glucoderivatives, named BLF501, able to "activate" SGLT-1 in order to achieve the protection against damages induced by LPSs while avoiding the disadvantages caused by high glucose concentration.. Thus our new synthetic molecule BLF501, acting as a potent activator of SGLT-1 at very low dosages, might represent a new pharmacological drug for the treatment of IBD, given the cytoprotective and anti-inflammatory effects linked to SGLT-1 activation. Infact BLF501 stabilizes TJ-protein localization preventing INF-γ/TNF-α. or DSS-mediated degradation.

BLF501 is very effective at preventing functional (FD-3 flux) and morphological (TJ protein) permeability defects induced by inflammatory or chemically stimuli. *In vivo* experiments utilizing a chemically-induced mouse model of intestinal inflammation, we found that mice with acute or chronic colitis BLF-501-treated not presents typical mucosal injury, shows a weight recovery and not develops severe clinical symptoms, including bleeding and dehydratation. The TJ protein has been reported to be deregulated in IBD. We have analyzed occludin and ZO-1 localization in colon tissue of different treatments and we have evaluated that intestinal permeability recovery observed with Ussing Chamber analysis is mediated by TJ protein protection. Results suggest that the BLF-501-mediated action involves stabilization of epithelial junction complex also *in vivo*. Moreover, we observed that activation of pro-inflammatory cytokines, such as TNF-α, and IL-12 in acute and chronic colitis was suppressed by oral administration of BLF-501. We have observed a marked increase of IL-10 levels in mice treated with BLF-501 and acute and chronic cycles of DSS in comparison with DSS alone or with untreated mice. The continuous IL-10 production from immune system components, guaranteeing an endogenous source of this anti-inflammatory cytokine, is able, to down-

The sodium-dependent glucose transporter-1 (SGLT-1) molecule is expressed by intestinal epithelial cells and by pneumocytes. We show here that BLF501, induces protective anti-inflammatory effects in lung of mice exposed to aerosolized lipopolysaccharide (LPS) or to ovalbumin (OVA), as assessed by analysis of serum, brochoalveolar lavage and lung morphology of the mice in both experimental models. Findings in the OVA-induced asthma murine model that aerosol and oral, administration of BLF501 led to a marked decrease of bronchoalveolar cellular infiltrate and of IL-4, IL-5, NO and IgE levels, and increased levels of the anti-inflammatory cytokine IL-10, suggest

the promise of SGLT-1 activation by BLF501 as a new approach to improving asthma pathology.

We can conclude thatBLF-501 as ligand of SGLT-1 may be suggested as a new pharmacological approach for the treatment of different inflammatory diseases as IBD and asthma.

1.INTRODUCTION

1.1 Sodium-dependent glucose transporter-1.

1.1.1 SGLT-1 and its classical role.

Luminal content influences intestinal epithelium function and the components of diet certainly play a role in the modulation of enterocytes response. The large surface of the gut is a wide area that protects and constitutes a easy way to the whole organism for pathogen bacteria. On the other hand a so large line on external environment is necessary to an appropriate absorption of the nutrients. Often the absorption is a against gradient transport because the concentration of nutrient molecules is lower in the lumen than that found inside the cells. For this reason a wide range of transporters are evolved in order to guarantee the absorption of water and electrolytes, minerals and vitamins, sugars, fatty acids, amino-acids and small peptides. The same molecules probably exert different effects on the role of IECs in mucosal immunity. D-glucose, in particular, is considered prevalently as energetic substrate for cells but a possible role as immuno-modulator is poorly analyzed**.**

Glucose is among the more abundant monosaccharides in the diet, and its absorption in the intestine is mediated by the high-affinity, sodium-dependent glucose transporter (SGLT)-1, located in the apical membrane of enterocytes [1]. SGLT1 is found in brush border membrane of mature enterocytes in the small intestine, with very small amounts detectable in the kidneys and the heart. Recently, SGLT1 has also been detected in the luminal membrane of intracerebral capillary endothelial cells, where it may participate in the transport of glucose across the blood brain barrier [3]. During the process of intestinal

sugar transport, on the luminal side of the brush border membrane, two Na^+ ions bind to SGLT1 and produce a conformational change that permits sugar binding. Another conformational change allows the substrates to enter the enterocyte. The sugar, followed by the Na^+, dissociates from SGLT1 because the affinity of the cytosolic sites is low, and also because the intracellular concentration of Na^+ is low (10 *vs* 140 mEq/L). The Na^+K^+-ATPase in the basolateral membrane is responsible for maintaining the Na^+ and K^+ electrochemical gradients across the cell membrane. A number of factors influence the transport function of SGLT1. For example, the regulation of SGLT1 by dietary sugars was examined by Miyamoto *et* [3]. Using Northern blotting, they showed that SGLT1 mRNA was increased by feeding rats 55% sugar diets containing glucose, galactose, fructose, mannose, xylose, or 3-O-methylglucose. Because 3-O-methylglucose is transported by SGLT1, but is not metabolized, and because SGLT1 does not transport fructose, mannose or xylose, the up-regulation of SGLT1 does not appear to depend on either metabolism or transport of the sugar in question. Veyhl *et al* [4] demonstrated the presence of an intracellular regulatory protein (RS1) that may modify the activity of SGLT1. Heat shock proteins (hsp) may also play a role in regulating SGLT1 function. A study done in renal epithelial cells showed that treatment with hsp70 increased glucose transport, but not the abundance of SGLT1 protein[5]. The increase in sugar transport was inhibited by an antibody directed against transforming growth factor β (TGF- β), leading the investigators to explore the effect of TGF-β on SGLT1: there was an increase in SGLT1 activity, as well as an increase in hsp70 protein when TGF-β was added to the culture media. The researchers speculated that hsp70 might stabilize SGLT1 expression in the membrane. This concept was supported by confocal microscopy studies, which demonstrated that TGF-β appears to move both SGLT1 and Hsp70 near the apical membrane site. The

transcription factors hepatocyte nuclear factor- 1 (HNF-1) and Sp1 may also regulate SGLT1 [5].

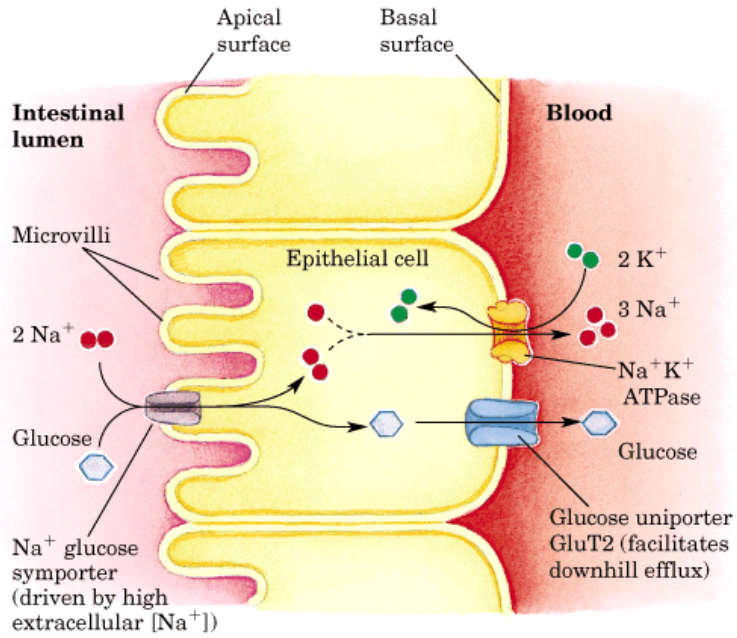

Fig 1 Classical model of intestinal sugar transport**.** SGLT1 is the sodium dependent glucose/galactose transporter on the brush border membrane. The Na+K+-ATPase on the basolateral membrane maintains the gradient necessary for the functioning of SGLT1. GLUT5 is a facilitative transporter on the brush border membrane which transports fructose into the cell. GLUT2 transports glucose, galactose and fructose out of the cell.

1.1.2 SGLT-1 as a new immunological player

Since 2005 SGLT-1 assumes a novel protective role. SGLT-1 activation loads to a local and systemic anti-inflammatory and cytoprotective response, in different inflammatory conditions. Firstly the effect of glucose has been analyzed in enterocytes exposed to agonists of TLR4 and TLR9. The encouraging in vitro results prompted us to analyze the effects of glucose on a systemic inflammatory response syndrome (endotoxic shock) in mice. Oral ingestion of glucose was found to protect 100% of mice from lethal endotoxic shock induced by intraperitoneal LPS administration; protection was only observed when glucose was administered orally, not by i.p. route, suggesting the important role of

intestinal epithelial cells[6]. Subsequently the study investigated the possibility that orally administered D-glucose exerts a systemic anti-inflammatory activity on hepatic liver failure. In this study[7] that D-glucose prevents LPS-induced liver injury, as well as liver injury and death induced by acetaminophen overdosing. In both of these models, physiological liver morphology is maintained and organ protection was confirmed also by unchanged levels of circulating markers of hepatotoxicity, such as ALT or LDH. In addition, D-glucose was found to protect liver from alpha-amanitin intoxication. In this case, however, a second signal had to be present in addition to glucose in order to achieve protective efficacy.

In addition, we observed that the in vivo protections depends from a systemic increase of anti-inflammatory cytokine IL- 10 as shown in schematic representation (fig.2). The cornerstone of the observed immunomodulatory effects resides in activation of SGLT-1; in fact, the glucose analogue 3-OMG, which induces the transporter activity but is not metabolized, exerted the same effects as glucose both in vitro and in vivo. Thus, we propose that activated SGLT-1, apart from its classical metabolic function, may be a promising target for inhibition of bacteria-induced inflammatory processes and life-saving treatments, assuming a novel role as an immunological player.

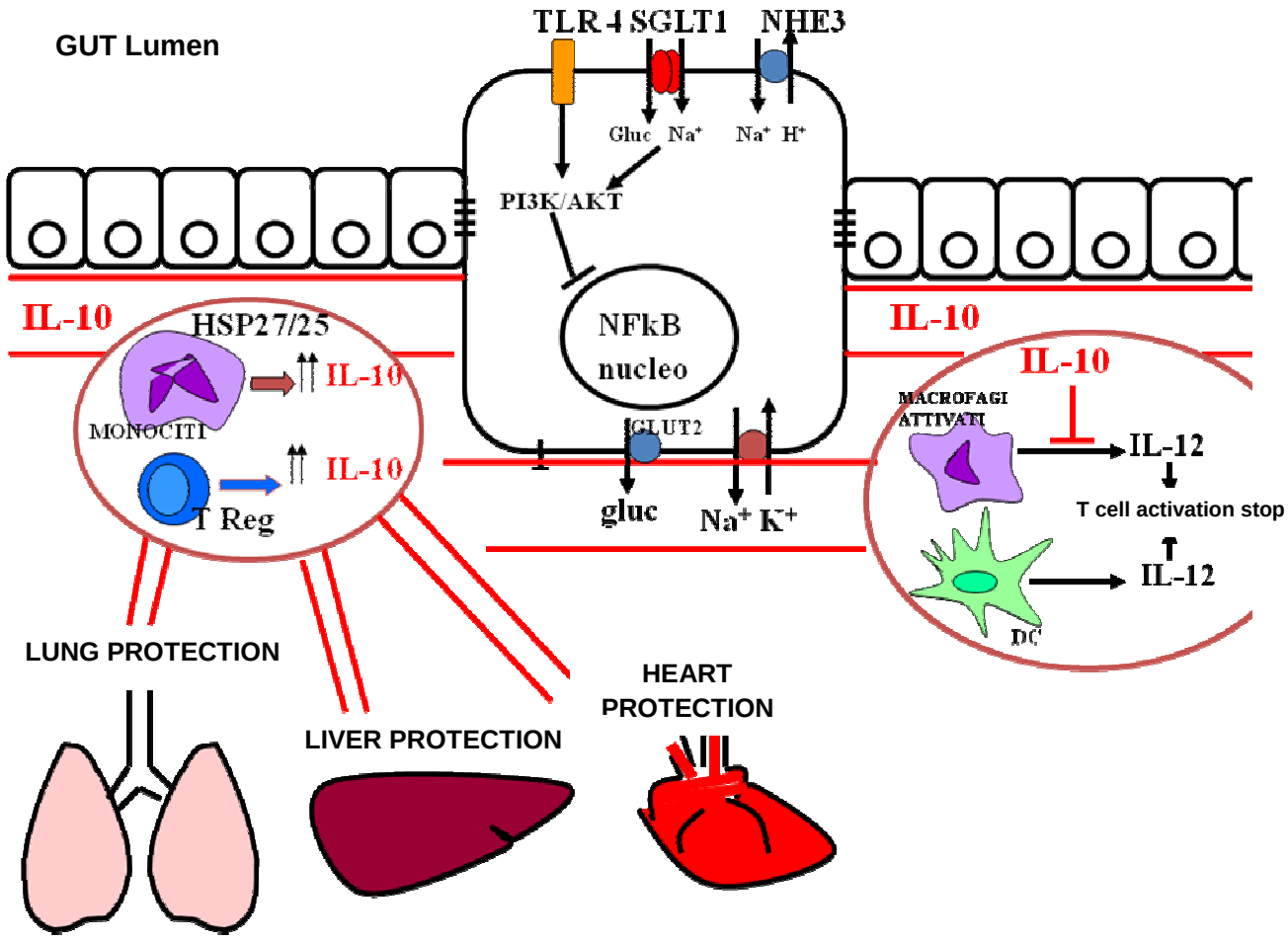

Fig. 2 Schematic representation of local and systemic protection by SGLT-1 activation against inflammatory damage.

1.2 Epithelial barrier and its role in chronic inflammatory disease.

Multicellular organisms, from sea sponges to mammals, require tissue compartmentalization to interface with the external environment while supporting specialized functions internally. In advanced animals, triploblasts include formation of three cell layers during embryogenesis. The endoderm forms the gastrointestinal tract; the nervous system and external skin develop from the ectoderm; and the mesoderm gives rise to musculoskeletal, genitourinary, and circulatory systems. Each of these layers includes cells specialized to establish distinct compartments, including gastrointestinal and respiratory epithelia derived from endoderm, epidermal squamous epithelium and accessory glands derived from ectoderm, and renal epithelium and vascular endothelium derived from mesoderm. Thus, cells that define the interface between the organism and the external world are a characteristic of all multicellular eukaryotes.

Complex multicellular organisms interface with their external enviromments at multiple sites, including mucosae of the airway, oral cavity, digestive and genitourinary tracts, and the skin. Although the skin is the most visible site of interface, the combined area of the mucosal surface is much greater than that of the skin. Epithelial cells that define the interface between the organism and external world forms barriers that are essential to life. This is particularly true in the intestine, where the epithelial barrier supports nutrient and water transport while preventing microbial contamination of the interstitial tissue.

1.2.1 Gut epithelial. Cellular components of intestinal mucosa with active immune function

Mucosae are also the primary sites at which the *mucosa-associated lymphoid tissue* (MALT) is exposed to and interacts with the external environment. The magnitude of these interactions is greatest in the gastrointestinal tract, which is the largest mucosal surface and is also in continuous contact with dietary antigens and diverse microorganisms. Thus, mucosal surfaces, particularly in the intestines, are crucial sites of innate and adaptative immune regulation. A central mediator of interactions between MALT and the external enviroment is the epithelium that cover the mucosa. Epithelial cells establish a active barrier between sometimes hostile external enviromments and the internal milieu.

Gut epithelial surfaces are composed of four cells lineages that arise from a pluripotent stem cell progenitor: absorptive globet cells, Paneth cells, enteroendocrine cells and enterocytes. Each of which contributes in a unique way to mucosal defence and the maintenance of barrier integrity. Goblet cells, found in both the small and large intestines, secrete large quantities of mucin, which is composed of highly glycosylated proteins that form a protective layer of gel-like mucus over the surface epithelium. Mucus acts trapping the vast majority of antigens that, in the intestinal tract, are cleared by peristalsis. By keeping microbes moving, these physical factors limit the time available for adherence to the epithelia and thus restrict invasion. The importance of mucus gel hydration is shown by cystic fibrosis, in which the production of hyperviscous mucus contributes to pulmonary, pancreatic and intestinal disease[8] Defective mucus production has also been reported in various immune-mediated disease, and spontaneous colitis develop in mice that lack specific mucin genes[9].

In the small intestine, granulocytic Paneth cells are the key effectors of antimicrobial defence. These specialized epithelial cells are situated at the base of small intestinal

crypts and harbor secretory granules containing several microbicidal proteins including defensins, lysozyme, and phospholipase A2. Paneth cells sense bacterial proximity and react by discharging their microbicidal granule contents into the gut lumen[10]. Only the microbes that can survive these harsh innate chemical defences have the ability to infect and cause disease.

The epithelial and sub-epithelial region of mucosal surfaces contains abundant immunocytes of many varieties. Indeed, in a healthy human adult, the mucosal immune system contributes almost 80% of all immunocytes[11]. The number of immunoglobulin Ig-secreting cells in this population exceeds by several fold the number of Ig-secreting cells in all other lymphoid organs (spleen, bone marrow, and lymph nodes) combined[12]. Importantly, these cells also have the ability to directly sense danger through expression of surface receptors specific for conserved microbial products. Under the influence of signals from the epithelium, stimulation through these receptors induces these cells to secrete cytokines and other modulatory factors. These factors work in concert with the epithelial signals to alert and dictate adaptive effector functions[13]. In this way, cooperation of leukocytes and epithelial cells extends the definition of the innate immune system to include all cells of the body[14].

Enteroendocrine cells (EEC) form the largest endocrine system in the body. They secrete multiple regulatory molecules which control physiological and homeostatic functions, particulary postprandial secretion and motility. Their key purpose act as a sensors of luminal contents, either in a classical endocrine fashion, or by a paracrine effect on proximate cells, notably vagal afferent fibres. They also play a pivotal role in the control of food intake, and emerging data add roles in mucosal immunity and repair[15].

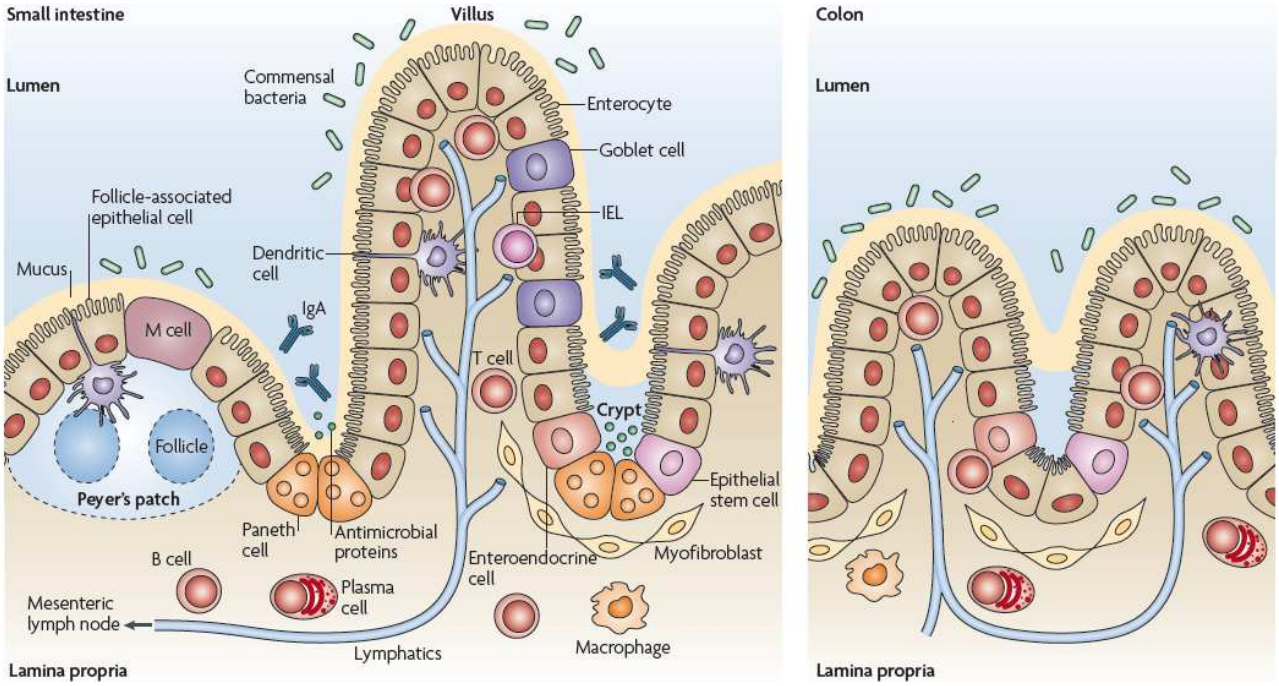

Figure 3 Anatomy of the intestinal immune system. A single layer of intestinal epithelial cells (IECs) provides a physical barrier that separates the trillions of commensal bacteria in the intestinal lumen from the underlying lamina propria. The IECs lining the lumen are bathed in nutrients, commensal bacteria, IgA and goblet cell-produced mucus. Epithelial stem cells proliferate and give rise to daughter cells with the potential to proliferate. These IECs then differentiate into villous or colonic enterocytes, which absorb nutrients (small intestine) and water (colon). In addition to differentiated enterocytes and goblet cells, progenitor IECs differentiate into both enteroendocrine cells, which secrete enteric hormones, and Paneth cells at the base of the small intestinal crypts. Beneath the IECs, the lamina propria is made up of stromal cells (myofibroblasts), B cells (especially IgA-producing plasma cells), T cells, macrophages and dendritic cells. Certain subsets of T cells and dendritic cells localize between the IECs. The small intestine has regions of specialized epithelium termed follicle-associated epithelium and microfold (M) cells that overlie the Peyer's patches and sample the intestinal lumen. IEL, intraepithelial lymphocyte.

Enterocytes, enteroendocrine cells, Paneth cells and globet cells expres Toll-like receptors (TLR) that has been shown to be involved in recognition of commensal- and pathogen associated molecular patterns (PAMPs). Moreover, TLR signalling has been shown to be involved in epithelial cell proliferation, IgA production, maintenance of tight junction and

antimicrobial peptide expression, which are functions that are crucial for maintaining a healthy epithelial barrier.

IECs are structurally and functionally polarized, with an apical surface facing the intestinal lumen and a basolateral surface facing the underlying basement membrane and the lamina propria. The polarized structure of IECs is established through exclusive targeting of certain membrane proteins to either the apical or basolateral surface and is maintained under normal conditions by tight junction complexes. This, together with a layer of mucus on the apical surface, establishes a barrier that is generally thought to be impermeable to commensal bacteria and other intestinal microorganisms in the gut lumen. However, it is likely that a low number of intestinal bacteria, and perhaps other microorganisms such as viruses and fungi, traverse the epithelium under steady-state conditions, as gut flora-derived microorganisms can be cultured from the spleens of mice, especially from mice that lack TLR signalling ability. Disruption of the epithelial barrier, such as that which occurs during intestinal ulceration or infection with a pathogen, can allow PAMPs to access the basolateral surface.

Given the juxtaposition between IECs and the gut flora, how does the intestinal epithelium respond to luminal PAMPs that are largely derived from nonpathogenic commensal microorganisms? Consistent with the known function of TLRs, indiscriminate recognition of PAMPs by TLRs on the epithelium would be expected to trigger an inflammatory response. Such a response to PAMPs from commensal, non-pathogenic bacteria would disadvantage the host. Instead, the intestinal epithelium seems to tolerate the presence of luminal PAMPs and does not mount an acute inflammatory immune response. Moreover, the epithelium require these signals for its normal function and for sensing a breach in its barrier.

Toll-like receptors (TLRs) are a key group of pattern recognition receptors in mammals. To date, 13 mouse and 10 human TLRs have been identified. The members of the TLR family are expressed variably throughout the epithelial barrier of the gut. It is still not entirely clear which TLRs are expressed in the gut in vivo and which cell types support their expression. TLR4, for example, is expressed on several intestinal epithelial cell lines[16] and is present in intestinal crypt epithelial cells in vivo[17]. These molecular patterns include bacterial cell wall components such as LPS and peptidoglycan or protein components of specialized bacterial structures such as flagella. Upon ligand binding, each of the TLRs initiates a signalling cascade that trigger the activation and nuclear translocation of the transcription factor NF-kB, which directs expression of proinflammatory genes such as IL-8 and IL-6.

1.2.2 Gut epithelial is a dinamic barrier.

The primary responsibility for mucosal barrier function resides with the epithelial cell plasma membrane, which is impermeable to most hydrophilic solutes in the absence of specific transporters. Accordingly, direct epithelial cell damage, such as that induced by mucosal irritants or cytotoxic agents, including some drugs used for cancer chemotherapy, results in a marked loss of barrier function. However, in the presence of an intact epithelial cell layer, the paracellular pathway between cells must be sealed. This function is mediated by the apical junctional complex, which is composed of the tight junction and subjacent adherens junction (fig. 4). Both tight and adherens junctions are supported by a dense perijunctional ring of actin and myosin that can regulate barrier function. As implied by the name, the adherens junctions, along with desmosomes, provide the strong adhesive bonds that maintain cellular proximity and are also a site of intercellular communication. Loss of adherens junctions results in disruption of cell–cell and cell–

matrix contacts, ineffective epithelial cell polarization and differentiation, and premature apoptosis [18]. Adherens junctions are composed of cadherins, a family of transmembrane proteins that form strong, homotypic interactions with molecules on adjacent cells. Adherens junctions are required for assembly of the tight junction, which seals the paracellular space.

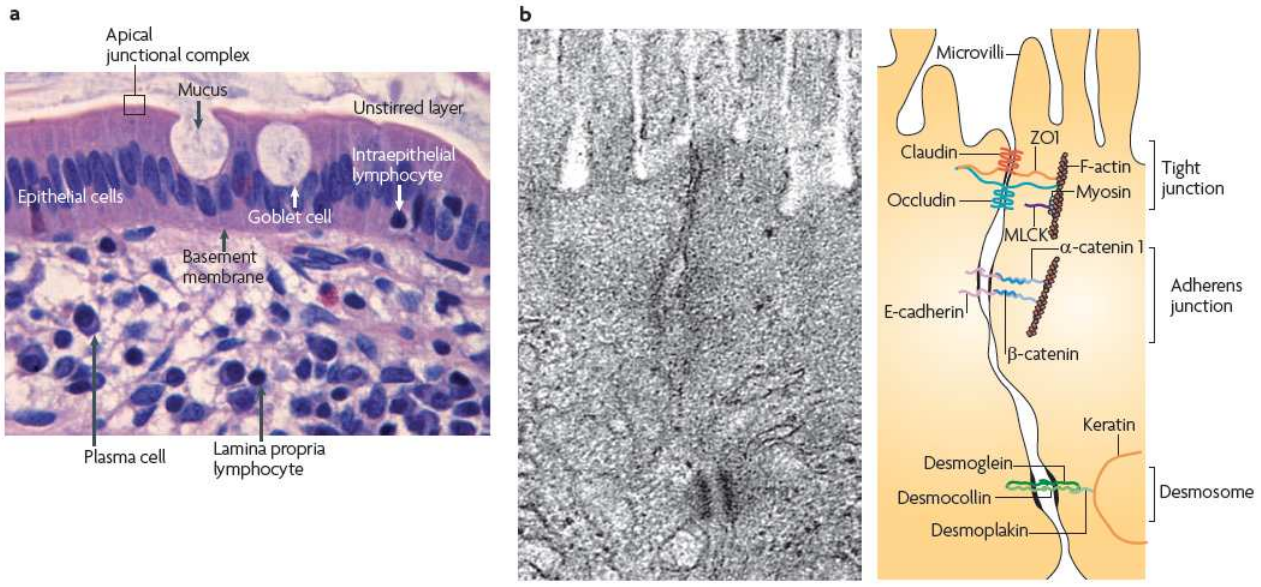

Figure 4 Anatomy of the mucosal barrier**. a** | The human intestinal mucosa is composed of a simple layer of columnar epithelial cells, as well as the underlying lamina propria and muscular mucosa. Goblet cells, which synthesize and release mucin, as well as other differentiated epithelial cell types, are present. The unstirred layer, which cannot be seen histologically, is located immediately above the epithelial cells. The tight junction, a component of the apical junctional complex, seals the paracellular space between epithelial cells. Intraepithelial lymphocytes are located above the basement membrane, but are subjacent to the tight junction. The lamina propria is located beneath the basement membrane and contains immune cells, including macrophages, dendritic cells, plasma cells, lamina propria lymphocytes and, in some cases, neutrophils. **b** | An electron micrograph and corresponding line drawing of the junctional complex of an intestinal epithelial cell. Just below the base of the microvilli, the plasma membranes of adjacent cells seem to fuse at the tight junction, where claudins, zonula occludens 1 (ZO1), occludin and F‑actin interact. E‑cadherin, α‑catenin 1, β‑catenin, catenin δ1 (also known as p120 catenin; not shown) and F‑actin interact to form the adherens junction. Myosin light chain kinase (MLCK) is associated

with the perijunctional actomyosin ring. Desmosomes, which are located beneath the apical junctional complex, are formed by interactions between desmoglein, desmocollin, desmoplakin and keratin filaments.

Tight junctions are multi-protein complexes composed of transmembrane proteins, peripheral membrane (scaffolding) proteins and regulatory molecules that include kinases At present, the most well-understood tight junction proteins are the claudins, a large family that includes at least 24 members [19-21]. These proteins have four transmembrane helices with a very short intracellular amino-terminal sequence and a somewhat longer carboxy-terminal tail. The first extracellular loop is approximately 50 residues long, although there is some variation among claudin family members. More importantly, sequence variation within the first extracellular loop determines tight junction charge selectivity[22], consistent with the view that the array of claudin proteins expressed in a given cell type defines the paracellular pore[23] through which ions and perhaps nonionic solutes travel. The second extracellular loop of claudins is smaller than the first, ranges from 16 to 33 amino acids in length, and is poorly characterized Importantly, almost all claudin proteins terminate with a three-aminoacid motif that binds to PDZ domains[24]. The cytoplasmic plaque, or peripheral membrane, proteins of the tight junction include ZO-1 as well as the related proteins ZO-2 and ZO-3[25,26]. ZO-1 and ZO-2 are each able to direct claudins to developing tight junctions; simultaneous elimination of ZO-1 and ZO-2 expression prevents claudin recruitment, tight junction formation, and development of barrier function[27].

Occludin, the first transmembrane protein discovered at the tight junction[28], continues to be enigmatic. An abundance of data making use of cultured cell lines and *Xenopus* embryos suggests that this protein is very important to barrier development and regulation[29-35]. However, occludin knockout embryonic stem cells can differentiate into polarized epithelial cells with functional tight junctions, and although occludin knockout

mice have severe disease with a complex phenotype [36,37], they do not appear to have defects in intestinal transport or barrier function. Thus, although the knockout mice may have partially compensated for the absence of occludin, the specific in vivo role of this protein remains controversial. Notably, human mutations in the occludin-related tight junction protein tricellulin have been linked to autosomal recessive hearing loss [38,39].

Physiological mechanisms of tight junction regulation. The best-characterized example of tight junction regulation in response to physiological stimuli remains the reversible increase in intestinal paracellular permeability induced by apical Na+-nutrient cotransport[40,41]. . The signal transduction pathway that enhances paracellular permeability following initiation of Na+–glucose co-transport has been characterized and includes activation of mitogen-activated protein kinase cascades, trafficking of Na+–H+-exchange protein 3 (NHE3) to the apical membrane and myosin light chain kinase (MLCK) (fig.5). activation [40]. Increased NHE3 activity at the apical membrane enhances Na+ absorption, which (along with the Na+ absorbed as a result of Na+–glucose co-transport) increases the transcellular Na+ gradient and promotes paracellular water absorption.

This increase in paracellular permeability is thought to allow passive paracellular flux of nutrients, along with water, pathways have been saturated. Ultrastructural analyses of tight junctions showed that activation of Na+-nutrient cotransport induced condensation of perijunctional microfilaments[42]. This was interpreted as an indicator of actomyosin contraction, but at the time the tools needed to study these biochemical events in intact tissue did not exist. To circumvent this problem, an in vitro model that recapitulated Na+-glucose cotransport–induced tight junction regulation was developed through use of cultured intestinal epithelial cell monolayers[40]. Based on the ultrastructural data, phosphorylation of myosin II regulatory light chain (MLC), a trigger for actomyosin

contraction, was examined and shown to increase following activation of Na+-glucose cotransport[42]. Moreover, pharmacological MLC kinase (MLCK) inhibition prevented both MLC phosphorylation and barrier regulation induced by Na+-glucose cotransport in cultured monolayers and also blocked barrier regulation in intact intestinal mucosa[42]. These data suggest that MLCK is a critical physiological regulator of tight junction permeability. Within months, similar data showing an association of MLCK-dependent MLC phosphorylation with increased tight junction permeability induced by enteropathogenic *Escherichia coli* infection were published[43,44], suggesting that MLCK-dependent MLC phosphorylation may be both a physiological and a pathophysiological regulator of barrier function.

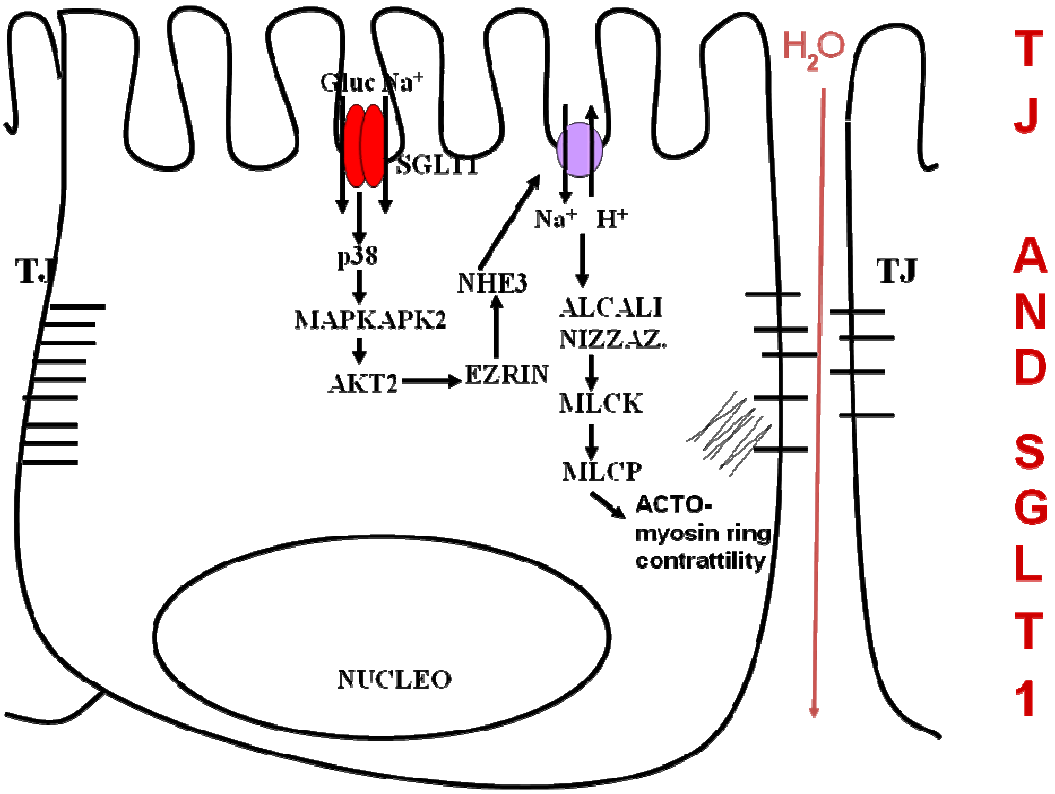

Fig. 5 Schematic representation of intracellular pathway after SGLT-1 activation that leads to physiological acto-myosin ring contractility and water flux across paracellular via.

Barrier regulation by immune stimulation The ability of cytokines, such as TNF-α and IFN-γ, to regulate the function of the tight junction barrier was first described 20 years ago. Since then, increased tight junction protein transcription, vesicular removal of proteins from the tight junction, tight junction protein degradation, kinase activation and cytoskeletal modulation have all been proposed to mediate cytokine-induced loss of tight junction barrier function. Although extensive apoptosis of epithelial cells may also cause barrier loss, the relevance of single-cell apoptosis to barrier dysfunction remains controversial owing to differing results in diverse experimental systems.

TNF-α and IFN-γ modify tight junction barrier function in intestinal[45,46], renal[47], pulmonary[48] and salivary gland[49] epithelia as well as between endothelial cells[50]. The effects of TNF on barrier integrity have been best studied in the gut, where this cytokine has a central role in many diseases associated with intestinal epithelial barrier dysfunction, including inflammatory bowel disease[51], intestinal ischaemia [46,52] and graft-versus host disease[53]. For example, although the effect of therapy with TNF-specific antibodies may be largely due to the overall reduction in inflammation. MLCK has been shown to have a central role in TNF-α induced epithelial and endothelial barrier dysregulation, both *in vitro* and *in vivo* [54-58]. Similarly, MLCK expression and activity are increased in intestinal epithelial cells of patients with inflammatory bowel disease [59]. The degree to which MLCK expression and activity are increased correlates with local disease activity, suggesting that these processes may be regulated by local cytokine signalling in these patients [59].

MLCK is also a fundamental intermediate in barrier dysfunction induced by the TNF family member LIGHT[60], interleukin-1β (IL-1β)[61], enteropathogenic *Escherichia coli* infection[43,44], *Helicobacter pylori* infection[62], giardiasis[63], lipopolysaccharide[64,65] and the ethanol metabolite acetaldehyde[66]. Thus, MLCK activation can be viewed as a common final

pathway of acute tight junction regulation in response to a broad range of immune and infectious stimuli.

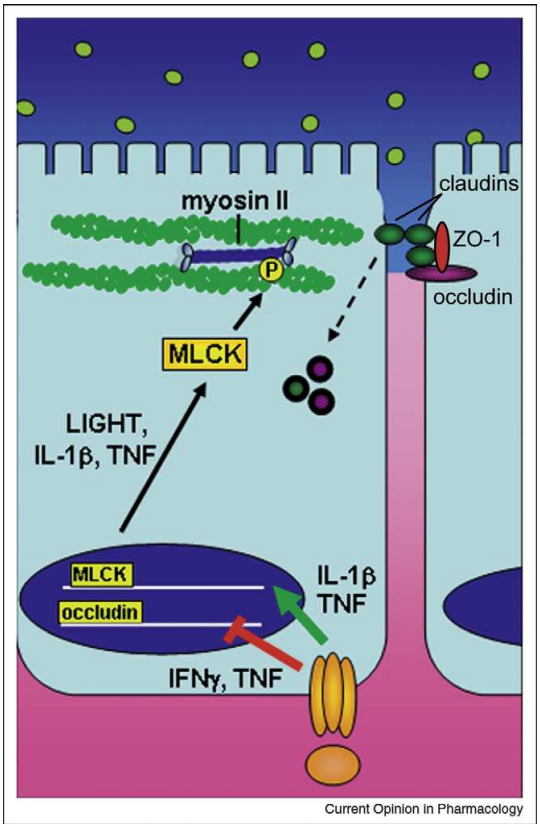

Fig. 6 Cytokine regulation of epithelial barrier function. Pro-inflammatory cytokines such as TNF, IL-1b, and LIGHT promote barrier dysfunction by inhibiting transcription of junction proteins and inducing cytoskeleton mediated redistribution of tight junction proteins. These cytokines promote transcription of MLCK, which when activated phosphorylates myosin II, resulting in reorganization of tight junction proteins, including endocytic removal from the apical junctional complex.

1.2.3 Barrier defects in inflammatory bowel disease.

Idiopathic IBDs such as Crohn disease and ulcerative colitis occur in clinically immunocompetent individuals whose characteristic symptoms and signs arise from a robust, cytokine-driven (yet noninfectious) inflammation of the gut[67]. Crohn disease is associated with excess IL-12/IL-23 and IFN-γ/IL-17 production that affects the small bowel and colon with discontinuous ulceration and full thickness bowel wall inflammation often including granulomas[67,68]. Patients report gastrointestinal symptoms of abdominal pain, diarrhea, and rectal bleeding as well as systemic symptoms of weight loss, fever, and fatigue. Crohn disease patients can also develop obstructing structures of the bowel and inflammatory connections (fistulae) between segments of bowel or between the bowel and skin and other organs. In comparison, ulcerative colitis is associated with excess IL-13 production, primarily affecting the colon, with a continuous inflammation of the mucosa nearly always involving the rectum and extending proximally[69].

It has been proposed that three main features should be present for IBD to occur: (1) a genetically susceptible mucosal immune system; (2) an antigen, or pro-inflammatory compound, which reaches the gut and can trigger the susceptible immune system; and (3) an alteration in gut barrier function which allows antigens to have contact with the mucosal immune system [67,68,70].

Since the studies about Crohn's disease have shown immunological factors underlying onset of this disease, the conventional treatments for IBD as corticosteroids, mesalamine, and immunosuppressants, provide mostly to block downstream inflammatory events. Medical therapy relies on classic antiinflammatory and immunosuppressant drugs: corticosteroids, mesalamine compounds, azathioprine, and derivatives of the latter[72,73]. These agents vary in their ability to induce and maintain control of symptoms as well as in their tolerability and toxicities. Newer biological drugs such as anti–TNF-α antibodies

targeting the general inflammatory cytokine, TNF-α, have added greatly to our ability to control IBD, but even this therapy is limited by lack or loss of efficacy and associated toxicities[51].

In recent years, several lines of evidence suggested that an increased intestinal permeability play a central role in the pathogenesis of IBD. In different animal models of Crohn's disease, an increased small intestinal permeability has been shown, even before disease expression, and the reversal of this barrier defect can attenuate the disease, implying that the increased permeability is not simply an epiphenomenon but rather is an important aetiological event. IL-10-deficient and SAMP1/yit mice, which develop spontaneous colitis and enteritis, respectively, show increased intestinal permeability before disease onset[74,75]. The suggestion that permeability is merely a sensitive indicator of mucosal immune activation would also explain the observation that, during clinical remission, increased intestinal permeability is a predictor of relapse in patients with Crohn's disease[76]. However, barrier dysfunction must also be regarded as a potential contributor to disease progression.

Because a subset of healthy first-degree relatives of patients with Crohn's disease will ultimately develop the disease, and because a similar fraction of these healthy relatives have increased intestinal permeability, it has been suggested that tight junction barrier dysfunction is one factor that contributes to the development of inflammatory bowel disease[77]. This hypothesis is consistent with a case report documenting increased intestinal permeability eight years prior to disease onset in a healthy relative of a patient with Crohn's disease[78]. In the human condition it is also evident that increased small intestinal permeability is commonly observed in populations at high risk of developing Crohn's disease.

This would suggest that there is a subtle alteration of function, independent of inflammation, which can be visible as an increase in paracellular permeability. This raises the possibility that restoration of barrier function may be therapeutic in CD. Consistent with this hypothesis, emerging data indicate that inhibition of cytoskeletally mediated barrier dysfunction may be able to prevent disease progression. Recently, Zolotarevsky and Turner have shown that impaired TJ functionality can be restored in vitro by inhibition of MLCK using a short peptide (PIK) that emulates a specific sequence of the regulatory domain of this protein[79]. Thus, peptide-based therapeutics for the treatment of IBD could be readily absorbed following oral administration and PIK specifically has the ability to reduce the permeability properties of the TJ barrier. Barrier restoration may, therefore, represent a non-immunosuppressive approach to achieving or maintain disease remission.

1.2.4 Lung epithelial barrier

Lung epithelium, like intestinal epithelium, provides a physical barrier between host and environment, thereby affording passive protection against infectious or otherwise noxious agents. In addition, the lung epithelium may initiate active responses, such as mechanical clearance, production of antimicrobial molecules, and participation in the generation of adaptive immune responses. Each breath carries in the inhaled air thousands of micro-organisms and microparticles into the respiratory tract. This exposure appears well tolerated by the host, which rarely reacts to this continuous stimulation. Thus, in normal conditions, the respiratory tract appears to be well equipped to efficiently eliminate exogenous material without generating a major inflammatory or immune response. The defence of the respiratory tract against pathogens relies on two distinct mechanisms, located in the airways (upper and lower) and the alveolar space, respectively. In the airways, mechanical defence appears to predominate and includes the deposition on the nasal and oropharyngeal surfaces and elimination through cough, sneezing, and mucociliary clearance. In contrast, the alveolar epithelium lacks mucociliary properties and therefore relies mostly on the alveolar macrophages to remove particles and micro organisms reaching the alveolar space[80]. In addition, the respiratory tract can also call on several protective mechanisms whenever required. For example, the contribution of polymorphonuclear neutrophils (PMNs) to the defence of the lung against bacterial infection is well recognized, and recent research has elucidated important mechanisms of recruitment and activation of PMNs at sites of infection. Another area of research where major progress has been made concerns the epithelial cells. Thus, the bronchial epithelial cell which has long been recognized as a key element of the mucociliary system is now also considered as a pivotal cell in the control of inflammatory and immune responses against pathogens and biotoxics. The respiratory epithelium is able to initiate and

perpetuate an inflammatory reaction in response to a variety of stimuli. In particular, bronchial epithelial cells produce IL-5, IL-8 and growth factors such as granulocyte macrophage-colony stimulating factor (GM-CSF), all implicated in attraction and/or activation of inflammatory cells [81]. Interestingly, IL-8, the most potent neutrophil chemoattractant, is released by bronchial epithelial cells in response to bacterial products [82]. In addition, the epithelium can probably participate in the immune response at an early stage after antigen deposition. This participation can occur since epithelial cells are recognized as antigen presenting cells, both in the respiratory and digestive mucosa. Also, while it is well accepted that inflammatory mediators such as oxidants and proteases can damage the airways, conversely, it is likely that remodelling of the bronchial structures (as observed in chronic disorders such as asthma, chronic bronchitis or cystic fibrosis) could modify the response of the host against inhaled pathogens and toxins. Although lymphocytes are scarce in the normal airway and alveolar lumen, they are detected in the submucosa of the bronchi and when they are abundant, such as in some pathologies, they are sometimes organized in lymphoid tissue called bronchu sassociated lymphoid tissue (BALT). A part of their role is related to the mucosal humoral immune response and more specifically to the production of immunoglobulin (Ig)-A. The defence mechanisms of the bronchial tree and lung parenchyma against infection, often associated with an inflammatory or immune response, have been the topic of extensive reviews and of several workshops [83]. However, the most recent information on the role of the mucosal humoral immune system (namely the secretory IgA system) has rarely been addressed in the literature devoted to the lung.

Receptors for microbial ligands in lung

The pulmonary epithelium contributes to lung defense in several ways. First, it serves as a structural barrier and in clearance of inhaled particles and microbes by the ‘muco-ciliary

escalator'. As in other organs, lung epithelial cells form intercellular junctions (tight and adherens junctions) that divide the epithelial cells into apical and basal surfaces and restrict the passive movement of particles and molecules across the epithelium. In addition, epithelial cells actively participate in the inflammatory response and are capable of mounting an immune response and potentially even killing microbial pathogens by internalization of organisms and secretion of cytotoxic and anti-microbial peptides[84,85]. Epithelial cells can be stimulated by bacterial components, such as LPS, and by cytokines such as TNF-α and IL-1β espresse by cells of the immune system as well as by some parenchymal cells that recognize conserved epitopes in microbial pathogens. Analogously to intestinal epithelial cells, in lung the cells that have a direct contact with the external environment express receptors able to recognize bacterial and harmful agents and to stimulate the immune response.

Antimicrobial peptides in respiratory system

All of the β-defensins are present in the respiratory system. These AMPs are expressed at various levels in the epithelia of trachea and lung as well as in the serous cells of the submucosal glands. Cathelicidins are also present in the conducting airway epithelium, pulmonary epithelium, and submucosal glands [86]. Functionally, the importance of these AMPs in the respiratory system has been suggested by several investigations. Mice deficient in β-defensin 1, for example, show decreased ability to clear *Haemophilus influenzae* instilled into their lungs [87].

2. MATERIALS AND METHODS.

BLF501 role in intestinal inflammation: *in vitro* and *in vivo* experiments.

2.1 *In vitro:*

2.1.1 Cell lines and treatments.

HT-29 and CaCo-2 human colorectal carcinoma epithelial cells were obtained from the American Type Culture Collection (Manassas, VA). HT-29 cells were maintained in Dulbecco's modified Eagle's medium (DMEM) (Sigma-Aldrich, St. Louis**,** MO) with L-glutamine, supplemented with 10% fetal bovine serum (FBS) (Gibco, Invitrogen Corp., Auckland, NZ), 200 U/ml penicillin and 200 μg/ml streptomycin (Sigma-Aldrich) (complete medium). CaCo-2 cells were maintained in DMEM with L-glutamine, supplemented with 10% FBS, 200 U/ml penicillin and 200 μg/ml streptomycin, 1 mmol/L sodium pyruvate, 1% non-essential amino acids. Cells were grown at 37℃ in a 5% CO_2 humidified atmosphere. To analyze effects of BLF501 on IL-8 release after LPS stimulation HT29 cells were cultured for 18 h in complete medium, or in medium with synthetic molecules (50mg/l – 0.05 μg/l concentration), before stimulation with LPS (1 μg/ml) for 6 h. Supernatants were collected at the end of treatment and stored at -80℃.

Caco-2 cells were grown as monolayers on collagen-coated polycarbonate membrane Transwell supports (Corning-Costar, Acton, MA) and used 17 to 20 days after confluence. Transwell supports with 0.33 cm^2 area were used for paracellular flux assays. Caco-2 monolayer were cultured for 24 hours in complete medium, or in medium additioned with BLF501 5 μg/l. Other Caco2 monolayers were incubated with IFN-γ (10 ng/ml) for 16 hours

and after with TNF-α (2.5 ng/ml) for 8 hours. Cythokines were added to the basal chamber without manipulating the apical media.. In other samples, Caco-2 monolayers were cultured with BLF501 5 µg/l, with concomitant INF-γ plus TNF-α administration, for 24 h total.

Moreover,. Caco-2 monolayer were cultured for 24 hours in complete medium, or in medium additioned with BLF501 5 µg/l. Other Caco2 monolayers were incubated with only DSS 5%-added medium for 24 hours or with BLF501 5 µg/l and DSS 5%.

Same treatments were performed in Caco-2 grown in coverslips on 24 well in order to detect TJ protein with immunofluorescence methods.

2.1.2 Paracellular Flux Assay.

Flux of isothiocynate-labeled dextran (molecular weight, 3kD, Molecular Probes, Eugene, OR) was evaluated across Caco-2 monolayer. Epithelial monolayers were washed free of media and equilibrated with Hanks bilance salt solution (HBSS from Sigma) at 37℃ prior to addition of fluorescent tracer. Apical medium was removed and 250 µl of FD-3 1 mg/ml (diluted in HBSS) was added to the apical chamber. At 30 minutes and 90 minutes after the end of different treatments monolayer recevoirs were agitated by pipetting and 50 µl samples were removed from basal chambre. Fluorescent intensity (excitation, 485 nm; emission, 530 nm) was measured on a fluorescent plate reader (Citofluor^{TM} 2300, Millipore Inc. Bedford, MA). Tracer concentrations were determinated from standard curves generated by serial diluition of known concentrations of FD-3 in HBSS. All data were normalized for background fluorescence by substraction of fluorescence intensity of semples collected from monolayer incubated in buffer only, without addition of fluorescent tracer.

2.1.3. Immunofluorescence microscopy analysis

Caco-2 cells were grown as monolayer on coverslips in 24-well plates. For occludin detection monolayers were permeabilized in ice for 2 minutes with 0.2% Triton X-100 in Tris-HCl and fixed with 3.7% paraformaldehyde 30 minutes at room temperature. After incubation for 1 hour in ice with rabbit anti-occludin (from Zymed, Invitrogen) antibody, Caco2 monolayers were washed and incubated with 546 Alexa conjugated secondary antibody goat anti-rabbit (from Molecular Probes) for 45 min at room temperature.

For staining of ZO-1, Caco-2 monolayers were permeabilized and fixed in methanol for 10 min at -20℃ and after were incubated with rabbit a nti-ZO-1 antibody (from Zymed, Invitrogen) for 1 hour at room temperature, followed by incubation with 546 Alexa conjugated secondary antibody for 45 min.

In staining of both TJ protein nuclei were stained with 4', 6'-diamidino-2-phenylindole (DAPI) and mounted with Mowiol 4-88 (from Calbiochem). Monolayers immunofluorescence was observed with a Nikon Eclipse 80i Video Confoccal microscope equipped with a digital Nikon DS-L1 camera.

2.1.4 Knockdown of SGLT-1 using small interfering RNA

SGLT-1 was silenced by small interfering RNA (siRNA) transfection. Briefly, HT-29 cells (3 x 105/well) seeded in 6-well plates at 60–80% of confluence were washed in Optimem (Invitrogen Life Technologies) medium and then transfected with a pool of siRNA oligonucleotides targeting human SGLT-1 or a scrambled RNA duplex (Santa Cruz), at a final concentration of 100 nM. Six µg/µl Lipofectamine 2000 (Invitrogen) were used as transfection reagent. After 24 h, the transfection mixture was aspirated, replaced with

culture medium and the cells has been treated for 24 h with BLF501 (50 mg/l) and TLR agonists (LPS) as reported above.

2.2 In vivo

2.2.1 Mice

C57BL/6 female mice were purchased from Charles River, Italy (Head Office Wilmington, MA). Mice were housed under specific pathogen-free conditions, maintained at constant temperature and humidity, with food and water given ad libitum, and used at 8-12 weeks of age. Experimental protocols were approved by the Ethics Committee for Animal Experimentation of Istituto Nazionale Tumori, Milano, and carried out according to guidelines of the United Kingdom Co-ordinating Committee on Cancer Research for animal welfare in experimental neoplasia(1998).

2.2.2 Experimental model of sepsis.

For the experimental model of sepsis, mice (n=10) were injected i.p. with 250 µg/kg of LPS and 1 g/kg of GalNH2 (D-galactosamine), with or without oral pretreatment with BLF501 25 or 13,43 or 7,57 or 4,3 or 2,5 or 0,025 µg/kg 1 h before LPS/GalNH2 administration. One control group was treated with sterile water,and another with only BLF501 (25 µ g/kg). Animal deaths were recorded in the first 24 h and in the week following LPS treatment.

2.2.3 Induction of acute and chronic colitis

Mice weighting 20-22 g received 2% dextran sodium salt (molecular mass 40 kilodaltons, MP Biomedicals, Irvine, CA) ad libitum in filter-purified drinking water for 7 days. For treatments studies mice undergoing DSS from day 4 at day 7 received oral administration of BLF501 250 µg/kg or 25 µg/kg or 2,5 µg/kg or glucose 2,5 g/kg once day. BLF501 and

glucose were administrated with a steril stomach tube In other mice groups received only BLF501 250 μg/kg or 25 μg/kg or 2,5 μg/kg or glucose 2,5 g/kg. One group received only DSS 2% in drinking water (as rapresented inn table 1 and 2).

Day 1	Day 2	Day 3	Day 4	Day 5	Day 6	Day 7	Day 8
DSS 2%	DSS 2%	DSS 2%	DSS 2% +BLF501 or glucose	DSS 2% +BLF501 or glucose	DSS 2% +BLF501 or glucose	DSS 2% +BLF501 or glucose	Sacrifice

Table 1.Schematic presentation of different treatments in the time. Mice received DSS 2% in drinking water. BLF501 250 μg/kg or 25 μg/kg or 2,5 μg/kg or glucose 2,5 g/kg were administrated (diluited in physiological solution) once per day at day 4, 5, 6, 7 and at 8th mice were sacrificated.

Groups	**Treatment**
1	Untreated
2	DSS 2% only
3	DSS 2% + Glucose 2,5 g/kg
4	DSS 2% + BLF501 250 μg/kg
5	DSS 2% + BLF501 25 μg/kg
6	DSS 2% + BLF501 2,5 μg/kg
7	Glucose 2,5 g/kg only
8	BLF501 250 μg/kg
9	BLF501 25 μg/kg
10	DSS 2% + physiological solution

Table 2 Schematic representation mice groups. 5 mice/groups.

To induce chronic colitis four groups of 10 mice/groups mice received three cycles of DSS 2%. Each cycle consists of 2% DSS dissolved in filter-purified drinking water for 7 days,

followed by a 14 days interval with normal water administration. After ten days from the last DSS cycle we started different treatments.

The first group of animals (control group) received normal drinking water only, during the whole time of the experiment. The second group of 12 mice received only three cycles of treatment with DSS, as previously described, and no any further treatment. Four mice of this group were sacrificated one week after DSS cycle completion; four mice of this group were sacrificated two weeks after DSS cycle completion; and 4 mice were sacrificated after three weeks.

After DSS cycles completion, third mice group received oral administration of 25 µg/kg BLF501 four times/week for one week; forth received 25 µg/kg BLF501 four times/week for two consecutive weeks; and fifth received 25 µg/kg BLF501 four times/week for three consecutive weeks.

Groups	**Treatments**
1	Untreated
2	DSS 2% +physiological solution
3	DSS 2%+ BLF501 25 µg/kg for 1 week
4	DSS 2% + BLF501 25 µg/kg for two week
5	DSS 2% + BLF501 25 µg/kg for three weeks

Table 2 Schematic representation mice groups. 12 mice in group 1. In goups 2, 3, 4 and 5 10 mice/group.

TREAT.	DSS	H_2O	DSS	H_2O	DSS	H_2O	BLF501 25 µg/kg	Death Group3 and 2	BLF501 25 µg/kg	Death Group4 and 2	BLF501 25 µg/kg	Death Group5 and 2
N days	7	14	7	14	7	10	7	X	7	X	7	X

Table 3 Schematic presentation of different treatments time. N days is for number days of water DSS 2% added or water only administration. After ten days of the last DSS cycle BLF501 was orally administrated 4 times/week for 1 or 2 or 3 consecutive week. X is for sacrifice day.

Evaluation of intestinal inflammation in acute and chronic colitis

Acute colitis was scored daily using standard parametres that includes evaluation of body weight and stool consistence. Body weight of mice was registered daily at 5.00 p.m.. Stool consistence was valuated daily, but comparative analysis between differents groups was conducted at the end of experiments.

Score	**Stool consistence**	**Blood**
0	Normal	No visible
1	Soft but still formed	No visible
2	Very soft	Blood traces in stool visible
3	Diarrhea	Rectal bleeding

Table 4 Scoring system for the comparative analysis of stool consistence.

At the end of treatments the colon of mice was cut close to the ileo-cecal valve and rectum, and the length was measured with and .for acute colitis experiment photos were captured.

Ussing Chamber analysis..

In order to measure the colon permeability in 5 mice/group, organ segments were mounted between the two chambers of a Ussing System (0.125 cm^2 opening). Two calomel voltage-sensitive electrodes and two Ag-AgCl current passing electrodes (EVC-4000 World Precision Instrument Inc., Sarasota, FL) were connected to the Ussing chamber via agar bridges. Both the mucosal and serosal sides of the chamber were connected to sterilized circulating reservoirs containing 10 ml of oxygenated Krebs buffer (115 mM NaCl, 8 mM KCl, 1.25 mM $CaCl_2$, 1.2 mM $MgCl_2$, 2 mM KH_2PO_4, and 225 mM $NaHCO_3$; pH 7.35). The buffers were maintained at 37℃ by a heated water jacket and will circulate by a gas lift column of 95% oxygen/5% CO2. Glucose (5.5 mM) was added to the serosal and mucosal sides. Colonic membrane mounted in the Ussing chamber, the system was allowed to stabilize for 20 minutes, in order to test the system functionality and the integrity of the colonic mucosal membrane. Trans-epithelial electrical potential difference in millivolt across the mucosal membrane was measured directly, while the trans-membrane resistance was calculated indirectly as ohms x cm^2, using Ohm's law.

Organotypic culture of colon.

Colon from 3 mice/group was excised, opened, and cut transversely into 3 parts. Each segments was washed in cold phosphate-buffered saline (PBS) containing penicillin, streptomycin, and amphotericin B (Cambrex; BioWhittaker, Walkersville, MD) and incubated in serum-free RPMI 1640 medium containing 0.1% penicillin, streptomycin, and amphotericin B at 37℃ in 5% CO_2. After 2 hours, supernatants were collected, centrifuged, and stored at -80℃ to cytokines.

Histological evaluation of colitis severity.

Murine colon specimens of 5 mice/group will be fixed in 10% neutral buffered formalin, embedded in paraffin, sectioned at 4 μm and collected on silanized slides. Histopathological analysis using hematoxylin-eosin-stained sections of distal colon samples of mice were performed. Samples were observed with a Nikon Eclipse 80i microscope equipped with a digital Nikon DS-L1 camera. To quantify/evaluate acute and chronic colitis-associated histological alteration in the colon we used a scoring system, provided in table 5.

Score	**Histologic changes**
0	No evidence of inflammation
1	Low level of inflammation with scattered infiltranting mononuclear cells
2	Moderate inflammation with multiple foci
3	High level of inflammation with increate vascular density and marked wall thickening
4	Maximal severity of inflammation with transmural leukocyte infiltration and loss of globet cells.

Table 5 Scoring system for inflammation associated histological changes in the colon

2.2.4 Enzyme-linked immunosorbent assay.

In HT29 treatments concentrations of IL-8 were evaluated using ELISA kits obtained respectively from Endogen (Woburn, MA), and Pierce Biotechnology (Rockford, IL) and carried out according to the manufacturers' instructions.

Evaluation TNF-α, IL-10 and IL-12 in supernatants of organ cultures and in murine plasma samples were obtained using ELISA kits respectively from R & D Systems (Minneapolis, MN), Endogen (Woburn, MA), and Pierce Biotechnology (Rockford, IL) and carried out according to the manufacturers' instructions. . Plasma samples were collected from each mouse before sacrifice , for cytokines evaluation.

2.2.5 Immunofluorescence analysis in tissue

Murine colon specimens were fixed in 10% neutral buffered formalin, embedded in paraffin, sectioned at 4 µm and collected on silanizated slides; samples were deparaffinized, rehydrated, and incubated for 10 minutes at 37 ℃ in a humidified chamber with protease type XIV 2 mg/ml (from Sigma) in Tris HCl; samples were then incubated with glycine 0,1 M for 20 minutes at room temperature, washed with TrisHCl + Triton X-100 0.01%, incubated with $NaBH_4$ 0.5mg/ml for 20 minutes at room temperature, washed with TrisHCl + Triton X-100 0.01%, incubated with Image-IT FX signal enhancer (Invitrogen) for 30 minutes, blocked with 2% goat serum for 20 minutes at room temperature and incubated with rabbit anti-occludin or anti-ZO-1 antibody 4 µg/ml (both from Invitrogen). Incubation with secondary antibody 546 Alexa conjugated goat anti-rabbit and staining of the nuclei with DAPI were performer. Samples were observed with a Nikon Eclipse 80i microscope equipped with a digital Nikon DS-L1 camera.

3.5 Statistical analysis.

Student's *t*-test (paired two-tailed) and GraphPad Prism software (GraphPad Prism Software Inc., San Diego, CA) were used for comparisons between groups. Differences were considered significant at $p<0.005$.

3. MATERIALS AND METHODS.

BLF501 role in lung inflammation

3.1 Cell lines and treatments.

A549 human lung carcinoma epithelial cells (derived from type II pneumocytes), HT-29 and CaCo-2 human colorectal carcinoma epithelial cells, and 16-HBE human bronchial epithelial cells were obtained from the American Type Culture Collection (Manassas, VA). A549, HT-29 and 16-HBE cells were maintained in Dulbecco's modified Eagle's medium (DMEM) (Sigma-Aldrich, St. Louis**,** MO) with L-glutamine, supplemented with 10% fetal bovine serum (FBS) (Gibco, Invitrogen Corp., Auckland, NZ), 200 U/ml penicillin and 200 μg/ml streptomycin (Sigma-Aldrich) (complete medium). CaCo-2 cells were maintained in DMEM with L-glutamine, supplemented with 10% FBS, 200 U/ml penicillin and 200 μg/ml streptomycin, 1 mmol/L sodium pyruvate, 1% non-essential amino acids. Cells were grown at 37℃ in a 5% CO_2 humidified atmosphere. HUH 7 human liver hepatoma cells (kindly provided by F. Marincola, National Institutes of Health, Bethesda, MD) were maintained in DMEM with L-glutamine, supplemented with 10% FBS, 10 mM Hepes, 200 U/ml penicillin and 200 μg/ml streptomycin.

A549, 16-HBE and HT-29 cells were cultured for 18 h in complete medium or in complete medium supplemented with high D-glucose concentration (5 g/L) (Merck, Darmstadt, Germany) or in medium containing BLF501 (50 μg/L) before stimulation with LPS from *Pseudomonas aeruginosa* (100 μg/ml) (Sigma-Aldrich) for 6 h. Supernatants were collected at the end of treatment and stored at -80℃. In some experiments with HT-29

cells, TNF-α (Peprotech Inc., Rocky Hill, NJ) was added at 50 ng/ml for 6 h at the end of the 18-h culture period.

3.1.1 Coculture of HT-29 and human MoDCs.

Human PBMCs were isolated by Ficoll-Paque density gradient centrifugation of buffy coats obtained from healthy volunteers (Fondazione IRCCS, Istituto Nazionale dei Tumori, Milan, Italy). CD14+ monocytes were positively selected using anti-CD14+ microbeads. Monocytes were induced to differentiate to immature MoDCs in 5- to 6-day culture in RPMI 1640 complete medium supplemented with 50 ng/ml GM-CSF and 50 ng/ml IL-4. Purity of monocytes and MoDCs, routinely checked by flow cytometric analysis using anti-CD14-FITC (M5E2) and anti-CD1a-FITC (HI149) (both from BD Bioscience Pharmingen, San Diego, CA), was more than 90%. MoDCs cells ($1x10^5$) were cultured in a multi-well support for 1 day, and confluent HT-29 cells grown in the upper part of a Transwell growth support (Millipore, Billerica, MA) were added to the same wells; cells were incubated for 18 h with BLF501 and stimulated for 6 h with TNF-α as described above. Cells treated with BLF501 alone or TNF-α alone or left untreated served as controls. Supernatants were collected and analyzed as reported below.

3.1.2 Small interfering RNA (siRNA).

Expression of SGLT-1 was silenced by transfection with siRNA. Briefly, cells ($2x10^5$/well) seeded in 6-well plates, harvested at 60-80% confluence, washed in Optimem medium (Invitrogen Corp.), and transfected with a pool of siRNA oligonucleotides targeting human SGLT-1 mRNA or a scrambled RNA duplex (Santa Cruz Biotechnology Inc., Santa Cruz, CA) at a final concentration of 100 nM using Lipofectin 200 (6 μg/αμl; Invitrogen Corp.) as transfection reagent. After 24 h, the transfection mixture was aspirated, replaced with

culture medium, and cells were incubated for 24 h as above with BLF501 or glucose in the presence of LPS or TNF-α.

3.2 Mice and *in vivo* treatments

3.2.1 Exposure of mice to aerosolized LPS.

Male 8 weeks-old C57BL/6 mice (purchased from Charles River, Calco, Italy) were maintained under specific pathogen-free conditions. Experimental protocols were approved by the Ethics Committee for Animal Experimentation of the Istituto Nazionale Tumori, Milan, Italy according to UKCCCR guidelines. Mice (n=5/group) were exposed to aerosolized LPS from *Pseudomonas aeruginosa* in a whole-animal exposure system, in which animals were placed in wire-mesh cages within a 55-l Plexiglas cylinder connected via 10-cm ducting to a 16-l aerosol chamber. Airflow through the system was maintained at 20 l/min by negative pressure. Aerosols were generated from twin jet nebulizers (Salter Labs, Arvin, CA), each containing 3 ml of LPS suspension (3 mg/ml) and driven by forced air at 15-18 psi. After 30 min, the chamber was purged with ambient air and mice were returned to their microisolator cages. Some mice were concomitantly exposed to aerosolized BLF501 (266 ng/ml, for a total of 3 ml). These treatments were carried out daily for 5 consecutive days. In another experiment, mice were treated orally with BLF501 before exposure to aerosolized LPS.

3.2.2 Asthma model.

Male 8 weeks-old C57BL/6 mice (n=5/group) were immunized i.p. weekly for 2 weeks with 100 μg ovalbumin (OVA grade V; Sigma-Aldrich) and 500 μg aluminum hydroxide (Alum, Sigma-Aldrich). Two weeks after the first immunization, mice were challenged for 25 min with an aerosol of 5% (wt/vol) OVA in PBS each day for 5 consecutive days. A second

group of mice was analogously treated with OVA but additionally treated with aerosolized BLF501 (266 ng/ml, total of 3 ml, diluted in saline solution) during the 5 days of aerosolized OVA challenge. A third group of mice was analogously treated with OVA and received OVA plus oral BLF501 (25 µg/kg, diluted in saline solution) both on the days of i.p. OVA challenge and during the 5 days of aerosolized OVA challenge. A group of mice was also injected i.p. with a neutralizing anti-TNF-α antibody (R & D System, Minneapolis, MN) at 15 □g/mouse during the 4th and 5th day of OVA plus BLF501 administration. Two hours after the last inhalation, blood samples were collected retroorbitally and mice were sacrificed and BALF performed.

3.2.3 Bronchoalveolar lavage (BALF).

BALF was performed by 3 instilliations of 1 ml saline into the lungs through a tracheal cannula, followed by gentle aspiration of the fluid and filtration of the recovered fluid through double-layer gauze to remove mucus. The resulting BALF was centrifuged (1000 rpm, 4ºC, 10 min), supernatants were collected and stored at –80ºC, while cells were formalin-fixed with the addition of sucrose (VWR International, Poole, England). BALFs were assessed for total cell counts, and aliquots were pelleted on glass slides by cytocentrifugation (Shandon Inc., Pittsburgh, PA). Differential counts were performed on Giemsa (Fluka, St. Gallen, Switzerland)-stained cytospins.

3.2.4 Hematoxylin-eosin staining.

Lung samples collected from mice and fixed in 10% paraformaldehyde and embedded in paraffin were sectioned (4 µm thickness}, deparaffinized, rehydrated, stained with hematoxylin and eosin, and mounted in Entellan® (Merck). Slides were observed under a

Nikon Eclipse 80i microscope equipped with a digital Nikon DS-L1 camera (Nikon Instruments, Firenze, Italy).

3.2.5 Immunohistochemistry.

Expression of ICAM-1 and caveolin-1 in lung samples was assessed immunohistochemically. Briefly, 4-μm sections of paraffin-embedded samples were deparaffinized and endogenous peroxidases were quenched for 20 min with 0.3% (v/v) hydrogen peroxide in PBS. Sections were incubated for 1 hour at room temperature with goat anti-mouse ICAM-1 (1:10 in PBS, R&D Systems) or rabbit anti-mouse caveolin-1 (1:200 in PBS, Santa Cruz Biotechnology, Inc.) polyclonal antibodies, washed with PBS, and incubated with secondary antibodies at room temperature Specific labeling was detected with a DAB Substrate Kit for peroxidase (Vector Laboratories).

3.2.6 Immunofluorescence assay.

Antigen retrieval was carried out in mouse lung sections, followed by sequential incubation with 0.1 M glycine buffer and sodium tetrahydroborate solution, each for 20 min at room temperature. Immunofluorescence detection of SGLT-1 expression on pneumocytes was carried out using polyclonal anti-SGLT-1 antibody (Millipore), diluted 1:1000 in PBS, for 1 h at room temperature, followed by addition of goat anti-rabbit antibody Alexa 488 (Invitrogen Corp.), diluted 1:200 in PBS and 3% BSA, for 30 min at room temperature. Nuclei were counterstained with 4,6-diamidino-2-phenylindole and slides were mounted with Mowiol mounting medium.

3.2.7 Isolation of murine dendritic cells.

Lung tissue was placed in PBS, DTT (145 μg/ml) and EDTA (0.37 mg/ml), dissected, digested with collagenase type 2 (Sigma Aldrich) (final concentration of 10 mg/ml in

RPMI), and DNAse (bovine pancreatic DNAse, Sigma-Aldrich) (final concentration of 25 mg/ml) for 60 min at 37℃ with gentle shaking. Aft er gentle disruption using a 2-ml syringe to produce a single-cell suspension, samples were centrifuged at 1500 rpm for 5 min at 4° C, washed with PBS containing 0.5% FBS, and cells were counted. Samples were incubated with anti-Fc receptor antibody (Miltenyi Biotec S.r.l., Calderara di Reno, Italy), followed by incubation at the appropriate ratio with MACS CD11c microbeads (Miltenyi Biotec S.r.l.) for 15 min at 4℃. After further was hes with PBS containing 0.5% FBS, cells were separated by passing the antibody-coated cell suspension over a VS+ column on a SuperMACS magnetic cell separator (all from Miltenyi Biotec S.r.l.), flushed with PBS-0.5% FBS to collect CD11e-positive cells, washed with RPMI medium, counted and plated *in vitro* at constant cell density for 18 h, when supernatants were harvested for analysis of cytokine levels.

3.3 Enzyme-linked immunosorbent assays (ELISA).

Levels of KC, NO, IgE, IL-4, IL-5, IL-8, IL-10, and TNF-α in serum samples or culture supernatants were quantitated using ELISA kits (Quantikine, R&D Systems, Minneapolis, MN; Promega Corp., Madison, WI; MD Biosciences, Zürich, Switzerland; Endogen, Woburn, MA; BD Biosciences, San Diego, CA), according to the manufacturers' instructions. Enzymatic reactions were detected in an automatic microplate photometer (Multiskan Ascent, Thermo Electron Corporation, Vantaa, Finland).

3.3.1 hsp/hsp25 ELISA.

To quantitate expression of hsp27 and its murine homologue hsp25, 96-well plates (NUNC Thermo Fisher Scientific Inc., Rochester, NY) were coated with 10 µl/well of HT29 cell supernatant or mouse serum, left overnight at 4℃, washed 3 times with PBS, 0.5% Tween

20, and incubated for 60 min at room temperature with primary rabbit anti-hsp27 antibody (Abcam, Cambridge, UK) (cross-reacts with mouse hsp25) diluted 1:2,000 in assay diluent (PBS, 0.5% Tween 20, 5% FBS, 100 μl/well); after 3 further washes, plates were incubated for 60 min at room temperature with secondary biotinylated anti-rabbit antibody (Vector Laboratories, Burlingame, CA) diluted 1:1000 in assay diluent (100 μl/well), washed 3 times, and incubated with streptavidin-conjugated horseradish peroxidase (SA-HRP, 1:250 in assay diluent, 100 □l/well) for 30 min. After seven further washes, 100 μl of tetramethylbenzidine (TMB) substrate (0.1 mg/ml 0.05 M phosphate-citrate buffer, pH 5.0) was added to each well and incubated at room temperature for 50 min, when the reaction was stopped by addition of 20 μl of 2 M H_2SO_4. Plates were examined at 450 nm (absorbance filter) using the automatic microplate photometer.

3.4 Western blot analysis.

Cell protein extracts were quantified using the BCA Protein Assay Kit (Pierce, Rockford, IL). Total proteins (15 μg) were fractionated on 8-12% acrylamide (BIO-RAD Labs., Hercules, CA) slab gels containing 0.1% SDS (Sigma-Aldrich) and transferred onto a nitrocellulose filter (Amersham Biosciences, Buckinghamshire, England) by electroblotting. Filters were incubated for 1 h in TBS, 1% Tween-20 (Sigma-Aldrich), blocked with 5% milk powder to prevent non-specific binding, and incubated overnight at 4℃ with rabbit polyclonal anti-SGLT-1 antibody (Chemicon International, Temecula, CA) diluted 1:5000 in TBS, or at room temperature with polyclonal rabbit anti-caveolin-1 antibody (Santa Cruz Biotechnology Inc.) diluted 1:200 in TBS, washed three times for 10 min each in TBS and 1% Tween-20, and incubated with the appropriate peroxidase-conjugated secondary antibody at room temperature. Bands were visualized using ECL™ Western blotting

detection deagents and autoradiography films (Amersham Biosciences). B-actin protein expression was used as a reference loading control to normalize protein expression of samples.

3.5 Statistical analysis.

Student's *t*-test (paired two-tailed) and GraphPad Prism software (GraphPad Prism Software Inc., San Diego, CA) were used for comparisons between groups. Differences were considered significant at $p<0.005$.

4. RESULTS

4.1 Synthetic glucose analogues: synthesis and screening.

Our recent findings indicate that the activation of SGLT-1 interacts with inflammatory signalling and suggest a novel role as an immunological player for this glucose transporter. High glucose levels *in vitro* and *in vivo* loads reduction of systemic pro-inflammatory signals, such as TNF-α, and the induction of endogenous IL-10 production by the host's immune cells. But high amounts of glucose that are necessary to induce these anti-inflammatory effects *in vivo* are considered a serious limitation for therapeutic application. Therefore we have collaborated with a chemical team in order to synthesize new analoge glucose, with high affinity versus SGLT-1. This chemical team is from Department of Biotecnology and Bioscience, Università degli Studi di Milano Bicocca.

In the search for non-metabolizable glucoderivatives able to "activate" the SGLT-1 transporter at pharmacological concentrations, the chemical researcher team generated a small library of naphthyl *C*-glycoside and glycitol derivatives, mostly without the use of protecting groups. We tested *in vitro* anti-inflammatory activity of different coumponds (data not shown), among them, we have selected a synthetic SGLT-1 ligand, named BLF501 (fig.1), which binds to the transporter with high potency, i.e. at concentrations 5 orders of magnitude lower than glucose.

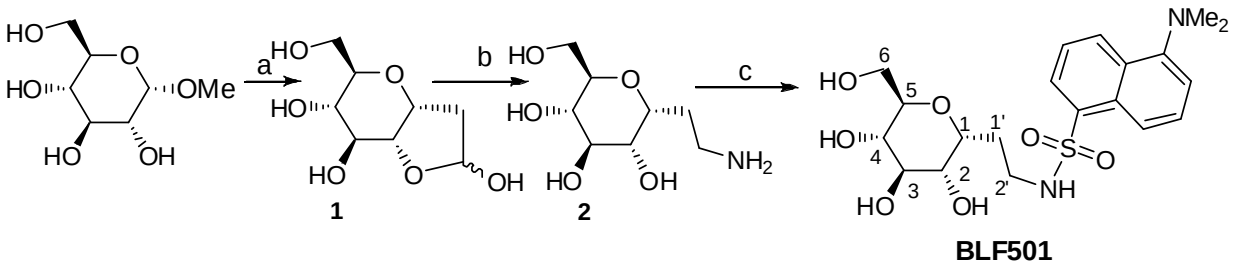

Fig. 1. Synthesis and Structure of BLF501

4.1.1 Stability studies.

BLF501, a member of the C-glycoside class, was designed to resist glucose metabolism and to retain hydrolytic stability in the acidic and basic conditions found in the gastrointestinal tract. Stability of BLF501 in different pH conditions was tested in samples prepared by dissolving 2.3 mg in 550 µl of D_2O and adjusting the pH to 1.2 through DCl addition (acidic conditions) or by dissolving 3 mg of BLF501 in 550 µl of D_2O and adjusting the pH to 12.5 through NaOD addition (basic conditions). Both samples were kept at room temperature until ^{1}H-NMR spectra were recorded at 10 min, 4.5 h and 24 h. As shown in Figure 2, neither sample evidenced degradation in 24 h.

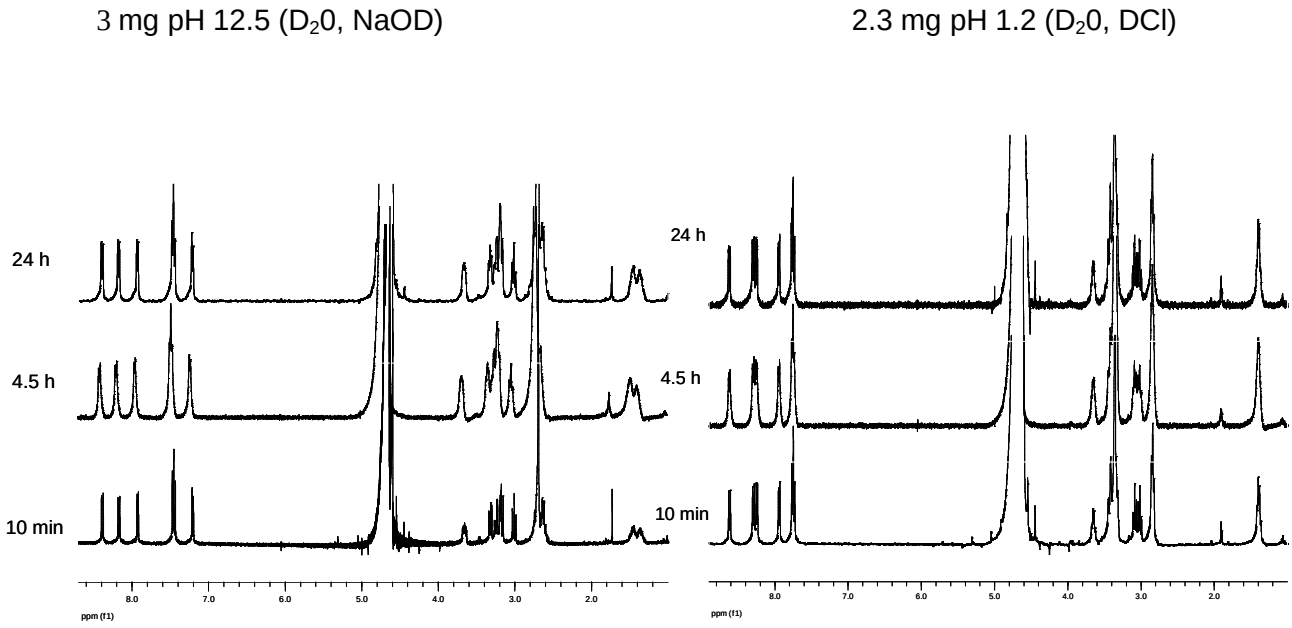

Fig. 2. ^{1}H-NMR spectra of BLF501 at pH 12.5 and at pH 1.2.

4.1.2 BLF501 affects LPS-induced IL-8 release in intestinal epithelial cells

Intestinal epithelial cells (IECs) express both the glucose transporter SGLT-1 and members of TLR family. In human and mouse IECs, TLR activation induces production of molecules such as the chemokines IL-8[15,16]. We analyzed the effect of BLF501 on IL-8 release upon LPS agonist of TLR4, in human colon carcinoma cells line HT29.

Experiments were carried out varying the BLF501 content in HT29 medium between 50 mg/l and 0,05 µg/l. Cells were cultured for 18h in different medium and stimulated for 6h with LPS (1 µg/ml). Supernatants collected after 24 h were assayed for IL-8 production. Ours resuts show that a significant reduction in IL-8 release was observed for all IECs cultured in media containing BLF501 at 50 mg/l, 5 mg/l, 50 µg/l, 5 µg/l. At 0,5 µg/l BLF501 lose more of fifty percentuage of its anti-inflammatory activity and at 0,005 µg/l BLF501 completely lose its activity (fig.3).

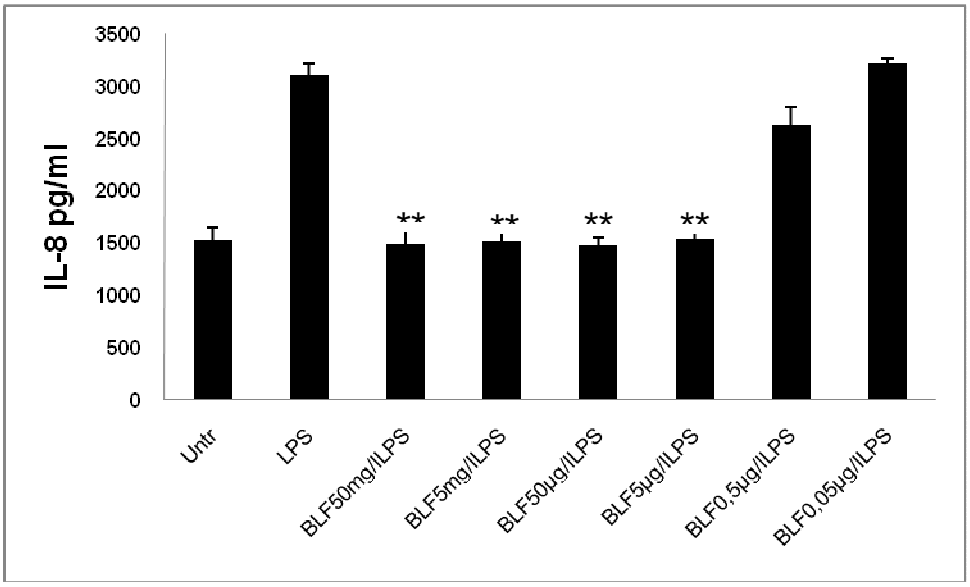

Fig.3. IL-8 production upon treatment with LPS (1 μ g/ml). BLF501 at concentrations from 50 mg/l to 0,005 µg/l.. Data are the means (±SD) of three independent experiments performed in triplicate. *, $p < 0,001$ vs LPS.

In order to determine the actual involvement of SGLT-1 in the inhibitory effect of BLF501 on IL-8 production, the assay was repeated on HT29 cells with SGLT-1 silenced through

transfection of the cells with small interfering RNA (siRNA) targeting SGLT-1 mRNA. As shown in Fig. 4 (last column) the siRNA clearly reduced the inhibitory effect of BLF501 5 µg/l on IL-8 production. This result proves the key role of the transporter and demonstrates that the biological activity of the compound is the consequence of its interaction with the transporter.

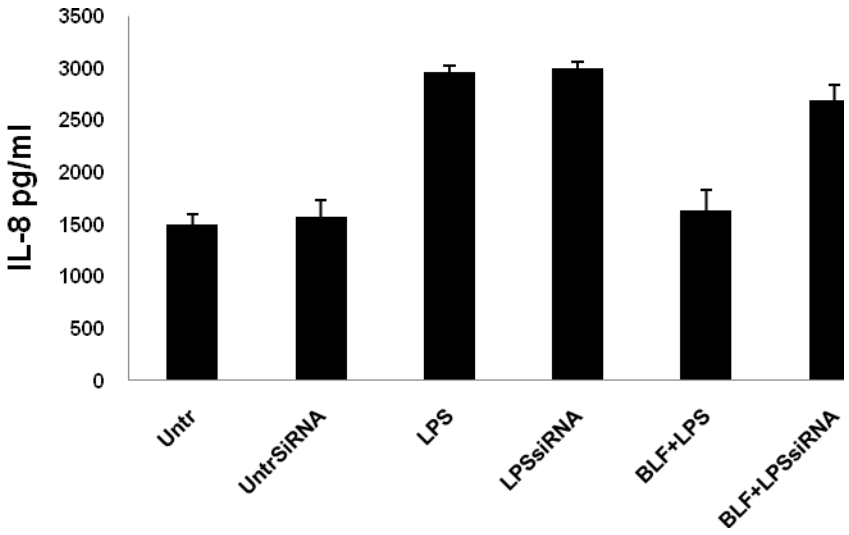

Fig. 4. IL-8 production in untreated HT29 cells, or HT29 cells treated with siRNA alone, LPS alone, LPS + siRNA, LPS + BLF501, or LPS + BLAF501 + siRNA. Data are the means (±SD) of three independent experiments performed in triplicate.

4.1.3 Protection afforded by BLF501 in LPS-induced shock in mice.

LPS plays a key role in Gram-negative sepsis by inducing production of cytokines, which mediate hyperactivation of the inflammatory system, eventually leading to death by endotoxic shock[88]; i.p. administration of LPS plus GalN provides a model of endotoxic shock in mice[89]. In our recent work[6] we show that oral administration of gluose o 3-OMG protects 100% of mice in this animal model To evaluate the effect of BLF501 in this animal model, mice (5/group) were treated i.p. with LPS (250 µg/kg) and GalN (1 g/kg) or pretreated orally with BLF-501 1h before LPS/GaIN or left untreated.

The first step was to determine the effective dose of BLF501. As can be seen from fig. 5, BLF501 afforded protection against LPS/GalN induced shock with an ED50 of 2.5 μg/kg (0.05 μg/mouse). The ED100 was 25 μg/kg (0.5 μg/mouse). Of note, 25 μg/kg is a 100,000-fold lower dose than the dose of glucose used in similar experiments, i.e. 2.5 g/kg (50 mg/mouse).

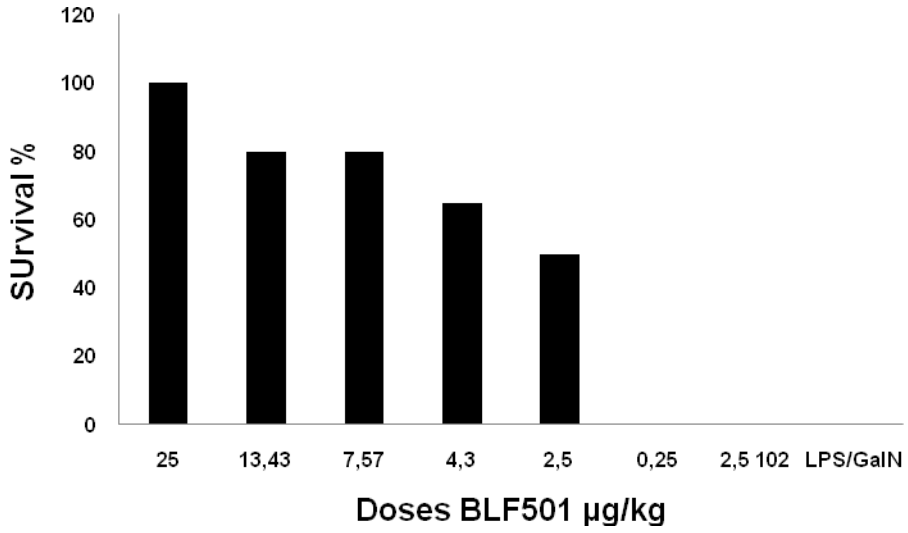

Fig. 5 Dose-response experiment of the protection afforded by p.o. administered BLF501 in LPS-induced shock in mice (n=5/group).

To increase animal number for each group we performed a second experiment, administrating oraly effective dose BLF501 25 µg/kg . A group of 10 animals was treated only with LPS (250 µg/kg) and $GalNH_2$ (1 g/kg); a second group of 10 mice was treated with LPS (250 µg/kg), $GalNH_2$ (1 g/kg) and BLF501 (25 µg/kg) administrated orally with gavage; finally a control group of mice was treated only with sterile water, and another group treated with only BLF501 (25 µg/kg). Results are reported in figure 6. As expected, in the first group of mice treatment with LPS/$GalNH_2$ induced septic shock with 100% of death within 36 h from the treatment, while in the group treated with LPS/$GalNH_2$ and BLF501 a survival of 100% of the mice along with behavior comparable to untreated

animals was observed. This result seems to confirm the great potentialities of BLF501 in the inhibition of bacteria-induced inflammatory processes and in its use as a life-saving treatment.

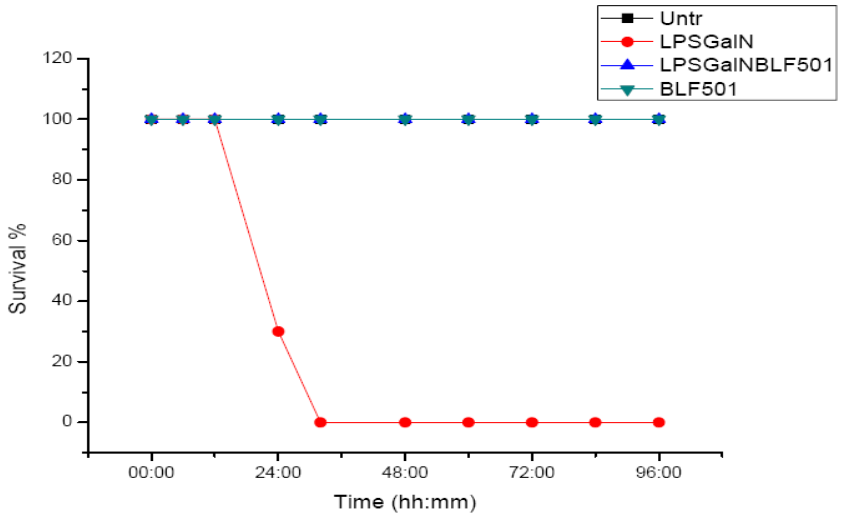

Fig. 6. Protection afforded by BLF501 25 µg/kg in LPS-induced shock in mice. Untr = untreated; LPSGalN = Mice treated with LPS/GalN alone; LPSGalNBLF501 = Mice treated with LPS/GalN + BLF501; BLF501 = Mice treated with BLF501 alone (n=10/group).

We performe a second experiment to determine inflammatory cytokine levels in plasma semple with BLF501 25 µg/kg. Figure 7 shows that BLF501, similarly to glucose, inhibits in this setting the production of the inflammatory cytokine IL-12 and induces the production of the anti-inflammatory cytokine IL-10. BLF501 alone, like glucose, is inactive in modulating serum cytokine levels.

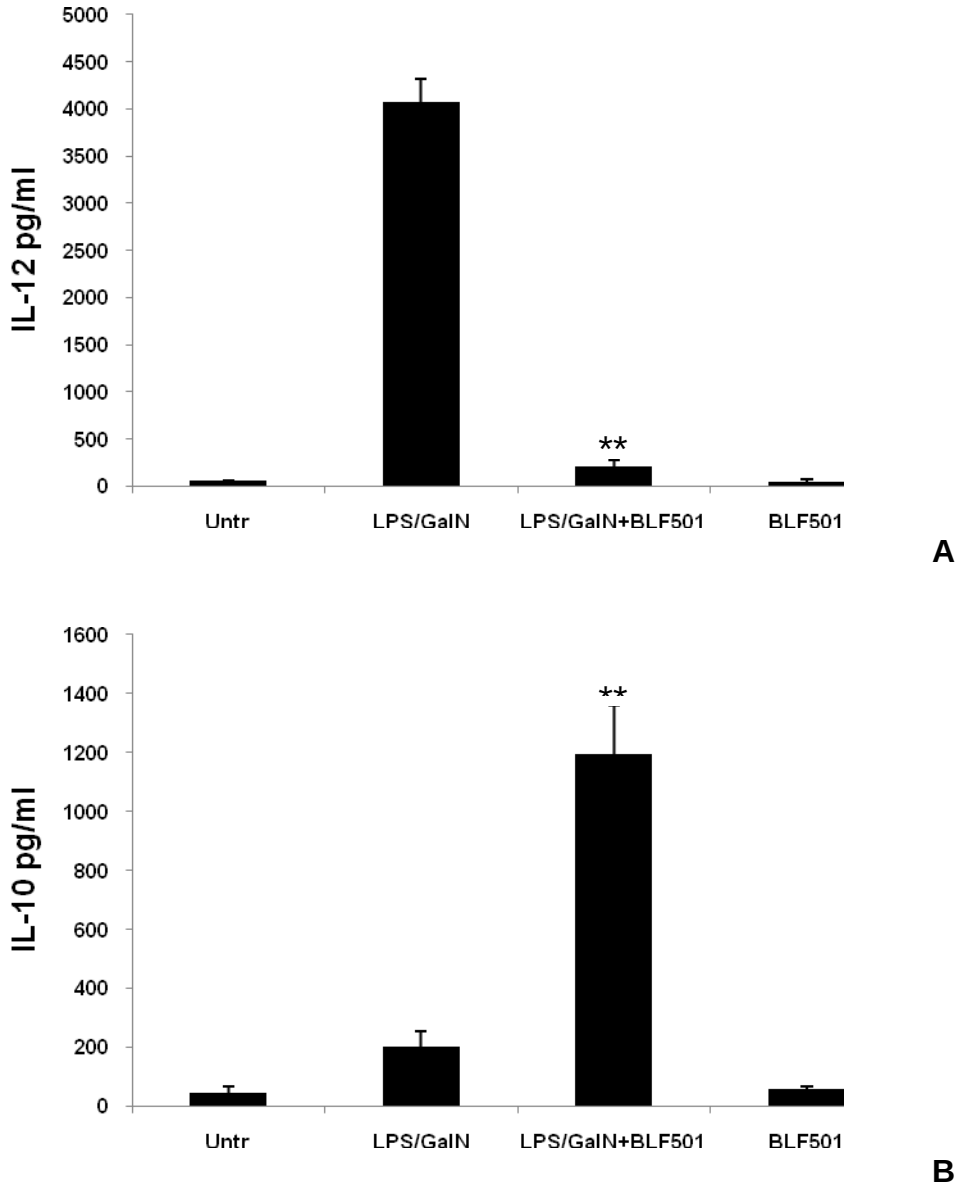

Fig. 7. Serum levels of IL-12 (A) and IL-10 (B) in untreated mice, or mice treated with LPS/GalN alone, BLF501 alone or LPS/GalN+BLF501. Untr = untreated; LPS/GalN = Mice treated with LPS/GalN alone; LPS/GalN BLF501 = Mice treated with LPS/GalN + BLF501; BLF501 = mice treated with BLF501 alone. Values represent the mean of 10 animals/group. Data are the means (±SD). *, $p < 0,001$ vs LPS/GalN.

4.2 SGLT-1 a new therapeutic target for epithelial barrier function.

4.2.1 SGLT-1 activation by BLF-501 5 µg/l effects on permeability of Caco-2 monolayer against inflammatory stimuli (INF-γ and TNF-α) and "chemical-DSS" damage.

We showed[6] that SGLT-1 activation, by high doses of oral glucose (2.5 g/kg), leads to the protection of the intestinal epithelium in a LPS-induced enterocolitis mouse model, and in particular Ussing Chamber analysis in order to valuate intestinal resistence, showed that the intestinal permeability remains similar to the one of untreated mice. This suggests that the intestinal epithelial barrier function is protected by damages associated to this inflammatory state, when SGLT-1 is activated. Complexities of the *in vivo* system make it difficult to determine effects of BLF501 administration on intestinal epithelial barrier.To determine if BLF501 can signal directly to intestinal epithelial cells we have used two inflammatory *in vitro* models, that cause dysfunction of the epithelial monolayer. Differents works have established that INF-γ and TNF-α are both required to decrease barrier function in cultured monolayer of intestinal epithelial Caco2 cells[90]. We cultured Caco2 cells on transwell filters, placed in p24, plates reaching monolayer stadium. We treated Caco-2 monolayer transwell with INF-γ and TNF-α and we have evaluated the permeability activity of Caco-2 monolayer by measuring the paracellular penetration amount of FITC-DEXTRAN (FD-3) across Caco-2 monolayer. The involvement of the paracellular pathway was confirmed by increased flux of the FD 3 paracellular marker. Addition of INF-γ and TNF-α to the lumen side of Caco-2 cells monolayers grown on permeable supports led to an immediate FD-3 permeability increased. The flux of FD-3 of INF-γ/TNF-α-treated Caco-2 cells had increased 20 ±5 fold, from 23,55 ±14 pmole/cm^2/h (control) to 174 ±22

pmole/cm^2/h (treatment) The addition of BLF501 5 µg/l, the lower efficace anti-inflammatory (as shown before) concentration, in apical medium significantly prevented an increased in permeability to FD-3 induced by INF-γ and TNF-α (fig 8). The flux of FD-3 of BLF-501 and INF-γ/TNF-α-treated Caco-2 cells is 31±16 pmole/cm^2/h comparable to untreated monolayer. BLF-501 50 µg/l prevent paracellular flux alteration induced by inflammatory stimuli.

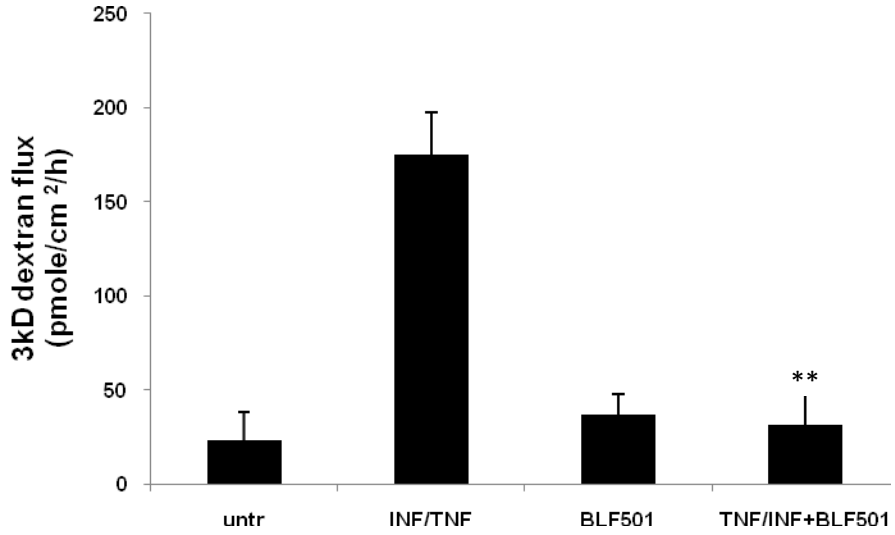

Fig 8 BLF501 protection against IFN- γ and TNF- α-damage in barrier function. Caco-2 monolayers were incubated with the indicated cytokine (IFN-γ 10 ng/ml, TNF-α 25 ng/ml) added to media in the basal chamber. Conditions were no cytokines (untr). Monolayers were assayed for permeability to 3kD fluorescein isothiocyanate-dextran. Paracellular permeability was increased only in cells exposed to IFN-γ followed by TNF-α without BLF. Data are the means (±SD) of two experiment performed in triplicate. *, $p < 0,001$ vs INF/TNF.

4.2.2 BLF501-mediated barrier functionality protection is associated to a morphological conservation of two TJ proteins.

Modulation of barrier/permeability properties is often mirrored by changes in specific TJ protein components. We have performed a series of *in vitro* experiments of immunofluorescence staining to analyze the effects of SGLT-1 activation by BLF501 on tight junctions protection. We performed immunofluorescence staining for occludin and ZO-1 in Caco2 monolayers, to analyze if BLF501 is able to protect from TNF-α- and INF-γ-induced damage.

In control, untreated monolayers, ZO-1 and occludin were predominantly localized to the apical lateral membrane, producing a characteristic “honeycomb” pattern consistent with their distribution in TJs. Addition of TNF-α- and INF-γ to medium of Caco-2 cells for 24 h clear differences in the staining patterns were noted. For occludin the staining became more punctuate and less intense consistent with a loss of protein form the cell. For ZO-1 the staining becomes more disordered and irregular. INF-γ and TNFα stimulated Caco-2 monolayers treated with BLF-501 (5 µg/l) show a ZO-1 and occludn localization similar to control monolayer (fig. 9 and 10).

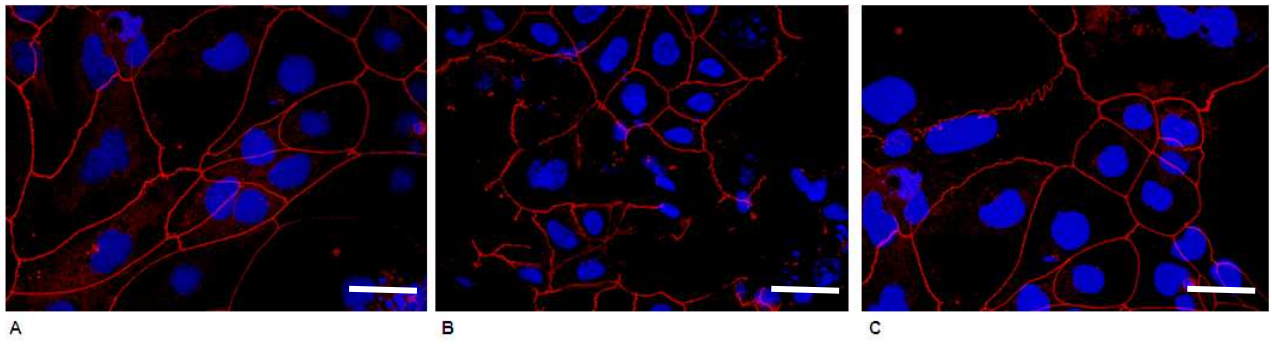

Fig.9 Staining for occludin in Caco-2 monolayer. (A) Untreated. (B) INF-γ and TNF-α treatment. (C) INF-γ snd TNF-α plus BLF501 5µl/l. In red occludin staining and in blue DAPI. These images are representative of 5 slide for each treatment. Medium added with only BLF501 µl is comparable to untreated monolayer. Bar 10 µm

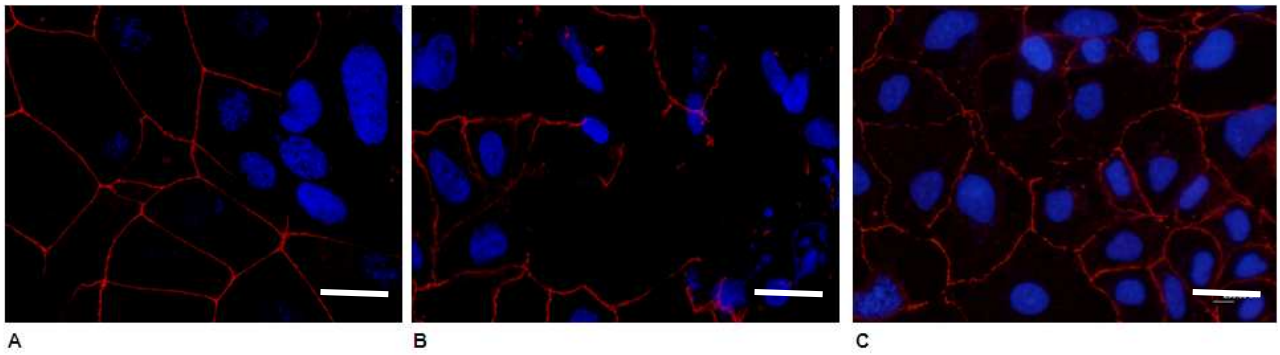

Fig.10 Staining for ZO-1 in Caco-2 monolayer. (A) Untreated. (B) INF-γ and TNF-α treatment. (C) INF-γ snd TNF-α plus BLF501 5µl/l. In red occludin staining and in blue DAPI. These images are rappresentative of 5 slide for each treatment. Medium added with only BLF501 µl is comparable to untreated monolayer. Bar 10 µm.

Moreover we performed immunofluorescence staining for occludin and ZO-1 in Caco2 monolayers, to analyze if BLF501 is able to protect from DSS-induced damage. In cells treated with DSS 5% for 24 h clear differences to untreated cells in the staining patterns were noted. For occludin and ZO-1 staining became irregular in several zone of DSS stimulated Caco-2 monolayer. Caco-2 monolayers treated with DSS and BLF-501 (5 µg/l) have a pattern of ZO-1 and occludin localization similar to control (fig. 12 and 13).

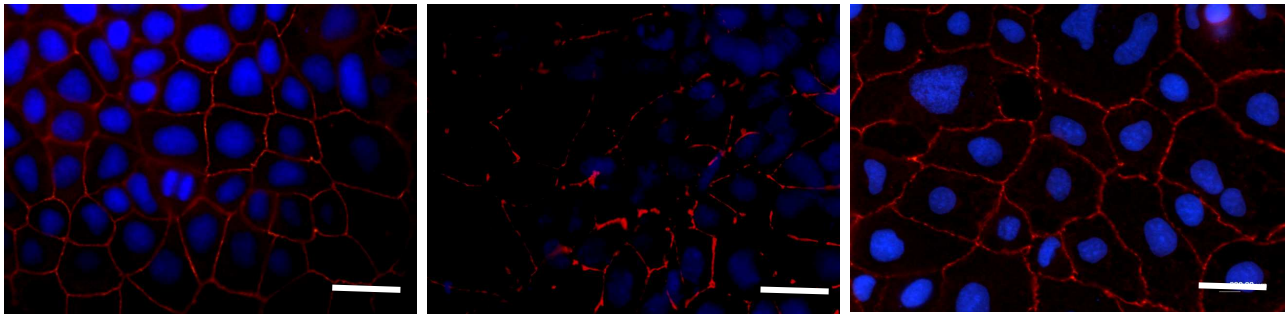

Fig.11 Staining for ZO-1 in Caco-2 monolayer. (A) Untreated. (B) DSS 5% treatment. (C) DSS 5% plus BLF501 5µl/l. In red ZO-1 staining and in blue DAPI. These images are rappresentative of 5 slide for each treatment. Medium added with only BLF501 µl is comparable to untreated monolayer.

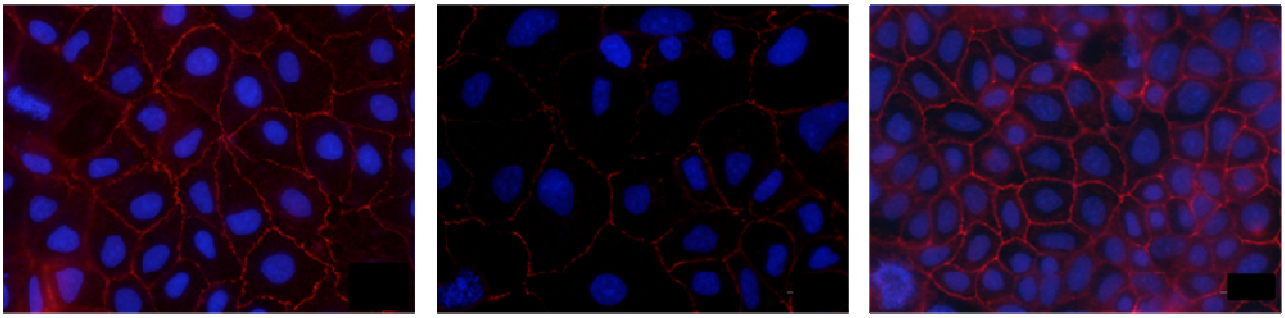

Fig.12 Staining for occludin in Caco-2 monolayer. (A) Untreated. (B) DSS 5% treatment. (C) DSS 5% plus BLF501 5µl/l. In red ZO-1 staining and in blue DAPI. These images are rappresentative of 5 slide for each treatment. Medium added with only BLF501 µl is comparable to untreated monolayer

This suggest that SGLT-1 activation by BLF501 induce protection of barrier function that in this *in vitro* model is directly distrupted by DSS. BLF-501 protects TJ indirectly inhibiting inflammatory response and directly tight junction protein.

4.2.3 BLF501 protection against inflammatory bowel disease *in vivo*

In vitro results lead us to hypothesize that SGLT-1 may be an important target in bowel inflammatory disease, where increased permeability is not simply an epiphenomenon but rather is an important aetiological event. We tested BLF501's activity in a chemically induced mouse model of acute and chronic intestinal inflammation. Different models of experimental IBD have been developed to investigate pathogenesis and to test efficacy of therapies. We have chosen dextran sodium sulphate (DSS)-induced colitis for its simplicity and reproducibility of the colonic lesions. Moreover, DSS polymers in the drinking water are directly toxic to the gut epithelial cells, affecting firstly the integrity of the mucosal barrier and then stimulating local inflammation as the secondary phenomenon [91]. For this reason we want to improve BLF.501 activity in intestinal barrier protection, which is thought to be the initial inciting event in many intestinal disorders, including IBD.

Oral ingestion of glucose and BLF501 protects mice from DSS-induce diarrhoea.

A DSS concentration of 2% (w/v) in the drinking water for 7 days induces strong colitis[92]. To evaluate the effects of glucose and BLF501 in this model, mice (10/group) were treated in the drinking water for 7 days with DSS 2% concomitantly or not with oral administration of BLF-501 (250 or 25 µg/kg) or glucose 2,5 g/kg once per day in the last four days (as described in materials and methods). DSS intake did not differ in different groups of mice.

In the following scheme animal groups (n = 10):

Aniaml group	**Treatment**
1	Untreated
2	DSS 2% only
3	DSS 2% + Glucose 2,5 g/kg
4	DSS 2% + BLF501 250 µg/kg
5	DSS 2% + BLF501 25 µg/kg
6	DSS 2% + BLF501 2,5 µg/kg
7	Glucose 2,5 g/kg only
8	BLF501 250 µg/kg
9	BLF501 25 µg/kg
10	DSS 2% + physiological solution

Colitis in the DSS model is usually strongly associated with wasting disease. Determination of weight every day to get a rough idea of colitis severity and is often indicative of differences in colitis development between experimental groups. As shown in fig 14 at 8 day the body weight significantly decreased in DSS group compared to control mice. The oral treatment with BLF 501 at doses of 250 µg/kg and 25 µg/kg recover weight loss DSS-induced; the 2,5 µg/kg dose appared to be ineffective.

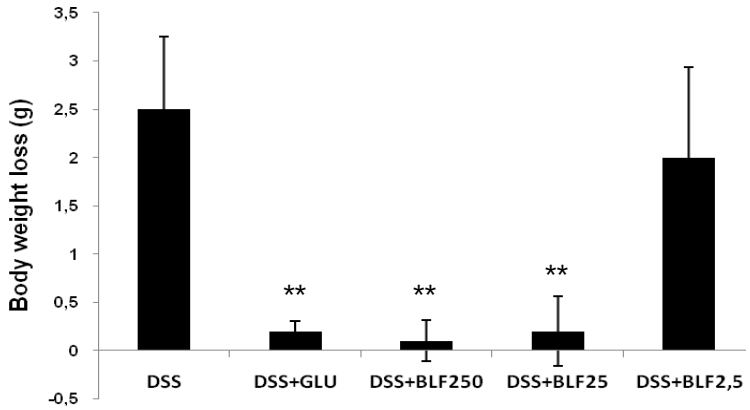

Fig.14 Body weight loss. Gramme of body weight lost after different treatments versus control group. Values represent the mean of 10 animals/group. Data are the means (±SD). **, $p < 0,001$ vs DSS.

The DSS-demages are generally located in the distal colon, whose length decreases as the disease develops. Colon mean lenght of mice group treated only with DSS decrease of 32% compared to untreated group (fig 15 B). Glucose 2,5 g/kg or BLF501 at 250 μg/kg and 25 μg/kg oral treatment of mice significantly reduced colonic shortering induced by DSS. Group of mice treated with BLF501 2,5 μg/kg and DSS shows colon lenght similar to DSS group.

About body weight and colon lenght results load us to consider 25 μg/kg like the minum effective dose of our analogue glucose in this animal model.

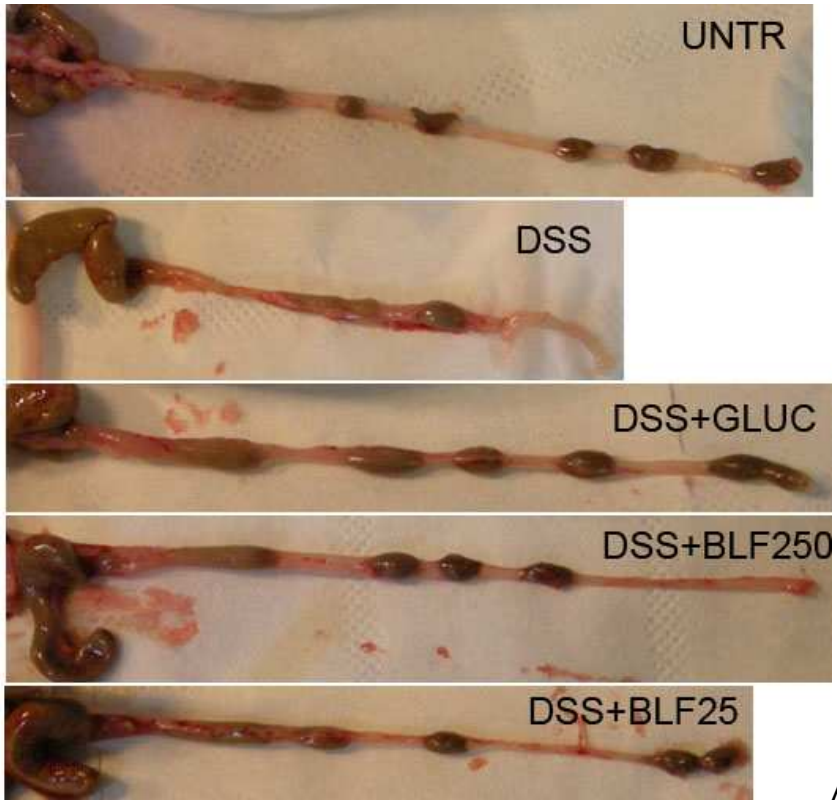

A

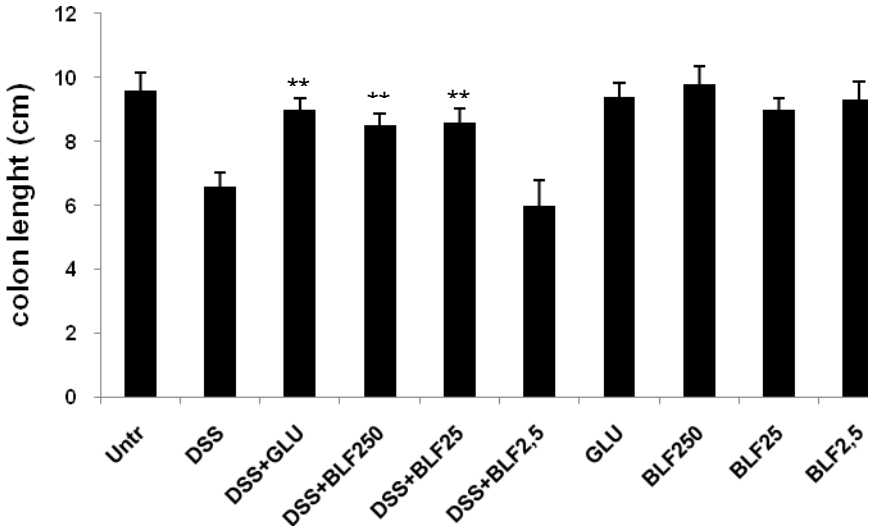

B

Fig. 15

(A) Colon rapresentative photos. Colon of mice treated with glucose or BLF501 250 μg/kg or BLF501 25 μg/kg only are similar to untreated group. BLF501 2,5 μg/kg group show colon similar to animals treated only with DSS (B) Colon length. Values represent the mean of 10 animals/group. Data are the means (±SD). **, $p < 0,01$ vs DSS.

After evaluation of colon lenght, colitis level of different group was scored using a standard parameter stool consistence. In fig. 15 A the colon photos show that DSS animals group have very soft stools with a 1,9 mean score, whereas untrated group shows normal stools with mean score 0 (fig. 16). Stool consistence of animal treated with DSS and Glucose 2,5 g/kg or BLF501 250 or 25 μg/kg is confrontable to untreated group. These results shown that oral treatment with glucose or BLF 250 or 25 μg/kg inihibit water loss, mantaining normal stool consistence.

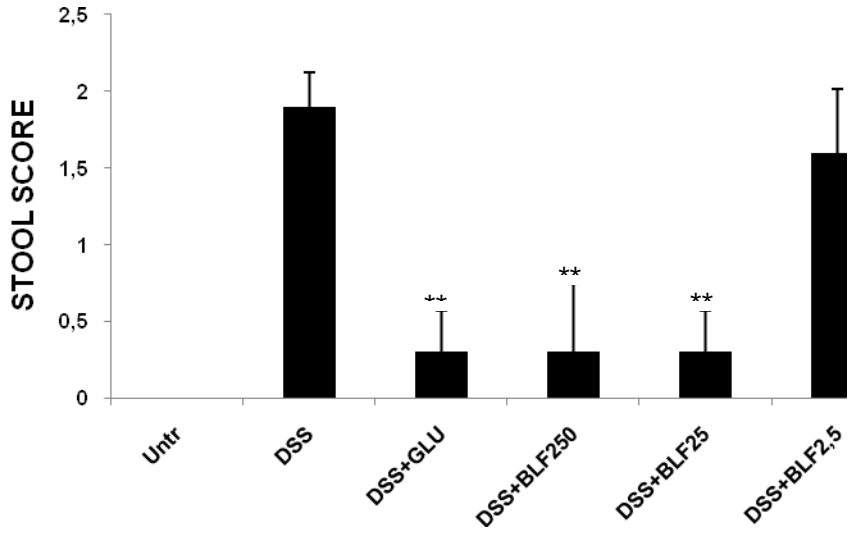

Fig 16

Scoring system for the comparative analysis of stool consistence. Values represent the mean of 10 animals/group. Data are the means (±SD). **, $p < 0,001$ vs DSS.

The most important damage DSS-induced is characterized by changes in colon mucosa, that show loss of crypts and reduction of globet cells, signs of surface epithelial regeneration, focal ulcerations, infiltration of inflammatory cells into the mucosa, and edema in the sub-mucosa. Histopathological analysis using hematoxylin-eosin staining of colon section shows that drinking water added with DSS 2% for 7 days induces crypt demage, ulceration, and infiltration of inflammatory cells in the distal colon. An histological

colitis score was calculated for 10 slide for each mouse of different groups and in fig. 18 we have reported the mean score. Score increasing has associated with inflammation develop (mean score of DSS group 3,5 vs untreated 0). Scoring system of colon section of DSS treated group plus glucose or BLF501 250 or 25 μg/kg shows protective role of SGLT1 in this animal model of acute colitis.

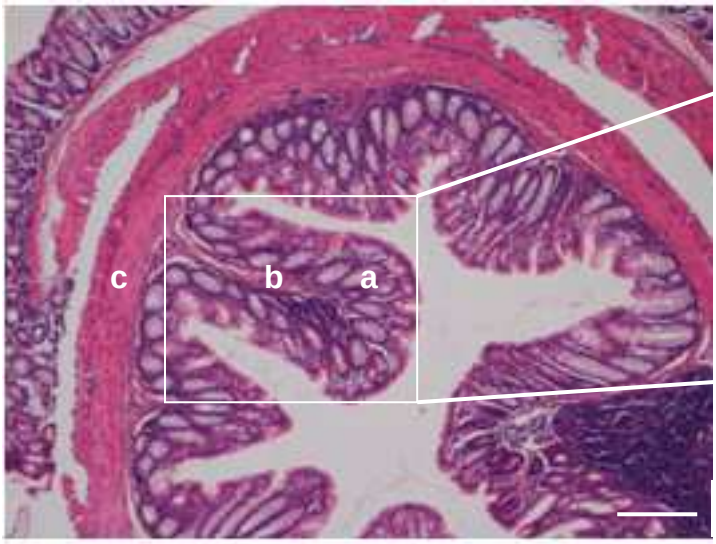

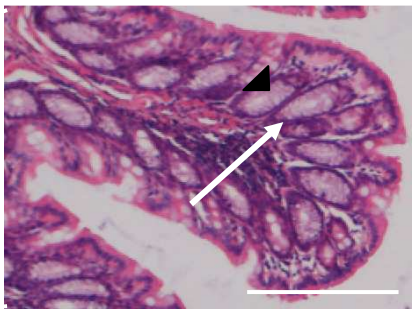

A

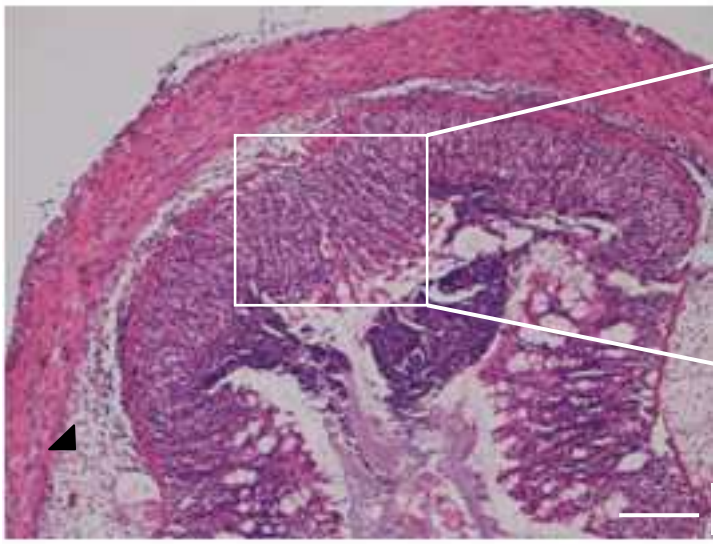

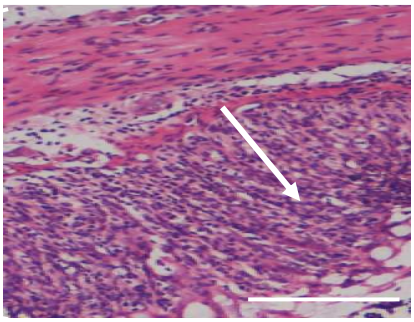

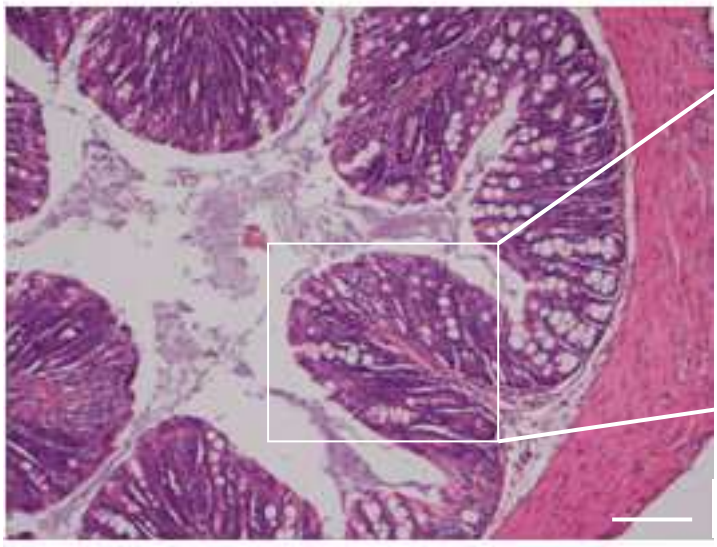

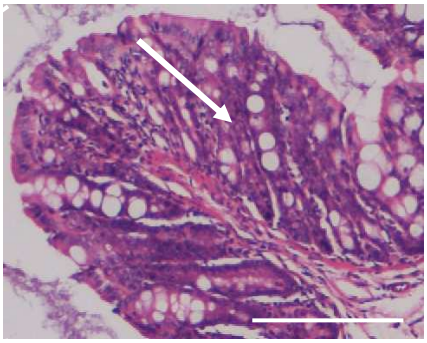

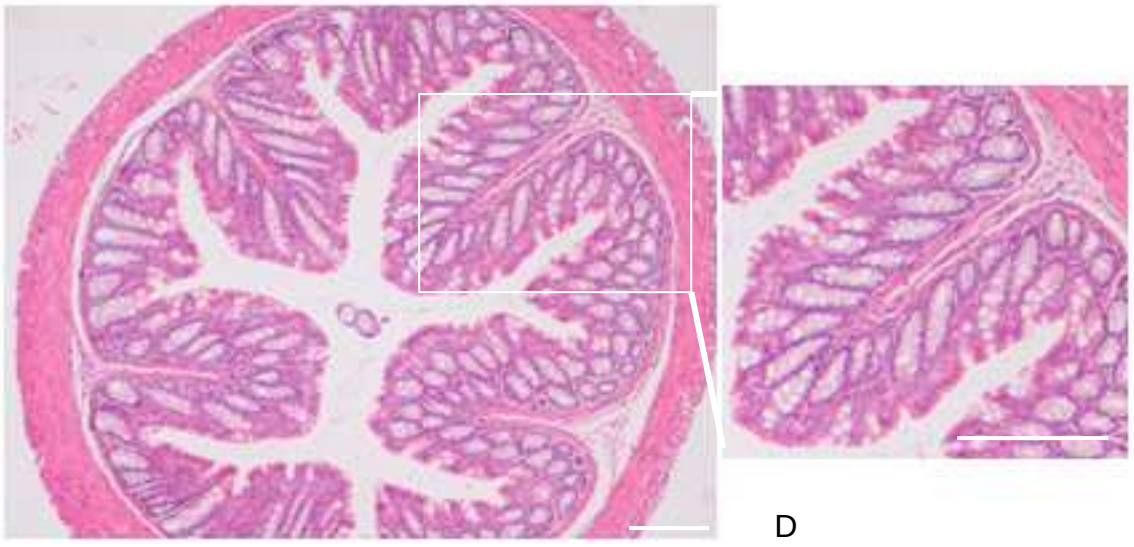

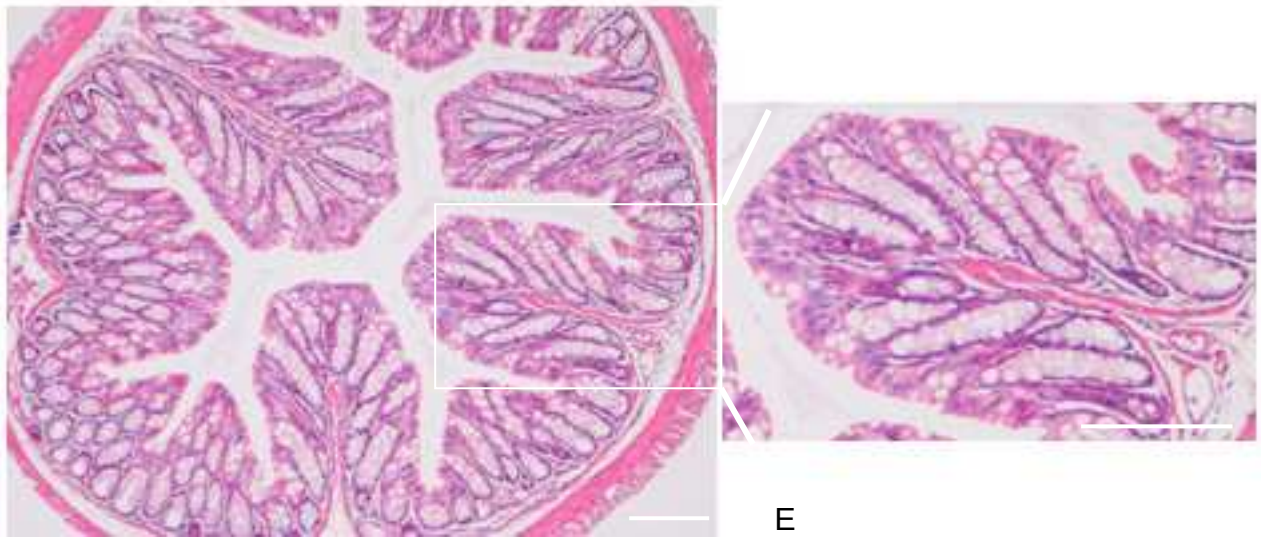

Fig 17 (A) Rapresentative colonic H&E section from mice receiving water without DSS . **a**) Lamina mucosa; **b**)Lamina submucosa; **c**)Circular and longitudinal mussle. In magnification arrow shows colon crypte with normal morphology and black arrowhead indicates globet cells. (B) Colon histology from DSS-treated group. DSS induces thickening of the colon wall, globet cells and crypt loss in large areas (in magnification arrow). Infiltration reaching the lamina submucosa (withe arrow). (C) Representative colon section of glucose 2,5 g/kg treatment in acute colitis. Normal morphology with low level of inflammation (D) H&E of BLF501 250 µg/kg and (E) BLF501 25 µg/kg, histologically comparable with control group. Bar 50 µm

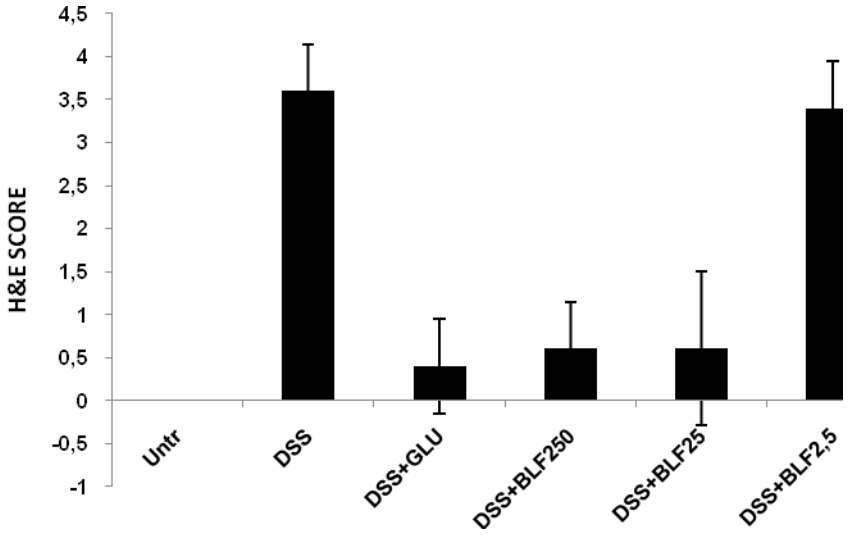

Fig. 18 Histological scores of the colon section stained with H&E. Results are representative of 10 section for five animal for eachh group. DSS mean score shows high level of inflammation with transmurall leukocite infiltration and loss of globet cells. Glucose 2,5 g/kg or BLF501 250 and 25 μg/kg oral treatment prevents and protects from mucosal demage DSS-induced.

DSS is directly toxic to gut epithelial cells of mucosal epithelium and induces a alteration of the mucosal barrier, with increase of antigens from colon lumen to lamina propria. In this animal model intestinall permeability alteration is the first step in colitis etiology/onset. Previous data have already described that an increased colon permeability is associated with colitis development after administration of DSS [93-95]. Ussing Chamber analysis of the colon of DSS-treated mice presented very low transmembrane resistance (25 ± 2,24 Ωcm^2 vs 53.4 ±2,73 Ωcm^2 for untreated mice), indicating an increased permeability, whereas in mice group treated with DSS and oral administration of glucose 2,5 g/kg and BLF501 250 and 25 μg/kg the transmembrane resistance remained similar to untreated mice (respectively 49,6 ± 1,52 Ω cm^2 or 50,4 ± 1,52 or 50,2 ± 1,2 vs 53.4 ±2,73 Ω cm^2 in untreated mice). This suggests that the increase of colon permeability DSS-induced is recovery and protects by glucose and/or BLF-501 oral administration.

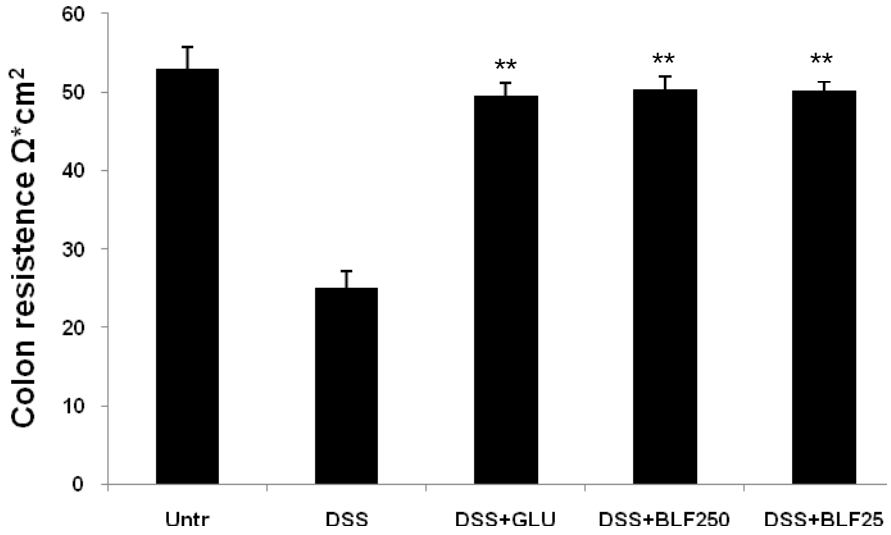

Fig 19. Colon resistence. Values represent the mean of 5 animals/group. Data are the means (±SD). **, p < 0,001 vs DSS.

This intestinal inflammation mouse model is associated with local increases in cytokines and chemokines. To test whether the DSS-induced acute colitis we observed in the BLF501-treated mice was associated with decreased inflammatory cytokines production in the intestinal mucosa. We have evaluated the level of TNF-α and IL-12. At 8 days after colitis induction, the levels of these cytokines increased significantly in the mucosa of the DSS-treated mice compared with control mice. Dextran sulphate sodium-induced increase in TNF-α and IL-12 mucosa levels were significantly suppressed by the administration of BLF-501 (fig.20 A and B). There were no significant differences in these cytokines levels between the DSS mice after given BLF-501 and the control mice.

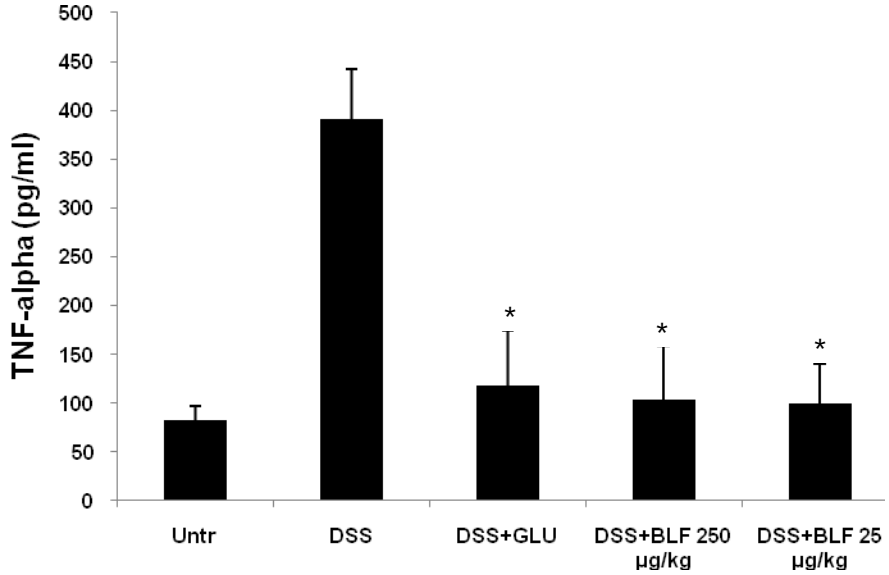

A

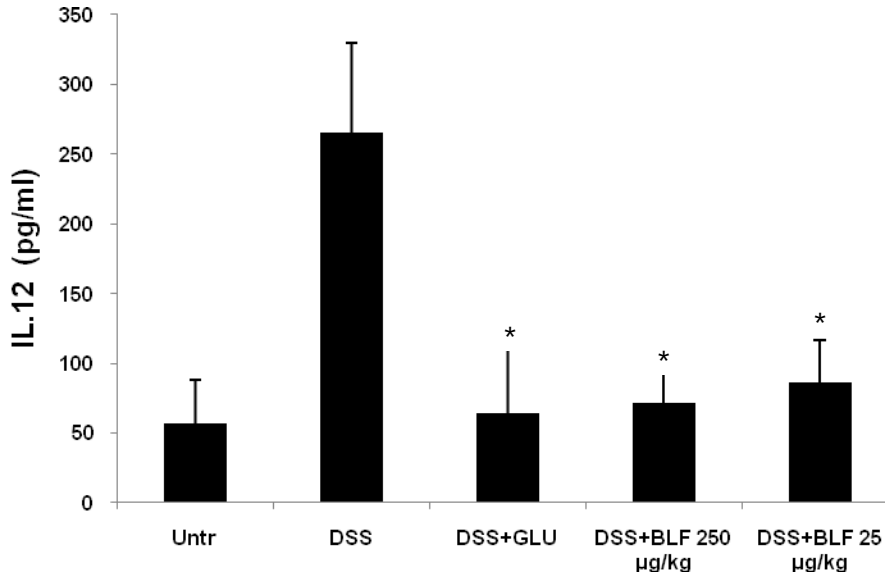

B

Fig. 20 Colonic secretion of TNF-α (A) and IL-12 (B). DSS-induced chronic colitis loads to a significant increase in colonic secretion of TNF-α and IL-12, wich was redeced by oraly administration of BLF501 25 µg/kg. Values represent the mean of 5 animals/group. Data are the means (±SD). *, $p < 0,005$ vs DSS.

Recently, IL-10 was introduced as a potential new anti-inflammatory therapy in Crohn's disease, but IL-10 treatment did not result in significantly higher remission rates or clinical improvement. The explanations for the failure of this therapeutic strategy might be that the

administered dose of IL-10 in the clinical trials, and thus the ultimate local IL-10 concentration in the intestine, might be too low to result in down-regulation of inflammation[96]. In our previous study[6], we have demonstrated that the protective effect of the activation of SGLT-1 by high doses of oral glucose (2.5 g/kg) in septic shock animal model depends from an increase of the anti-inflammatory cytokine IL-10. We evaluated by ELISA IL-10 levels in colon colture and our data (fig. 21) show that in this colitis animal model oral administration of glucose or BLF501 increase this anti-inflammatory cytokine.

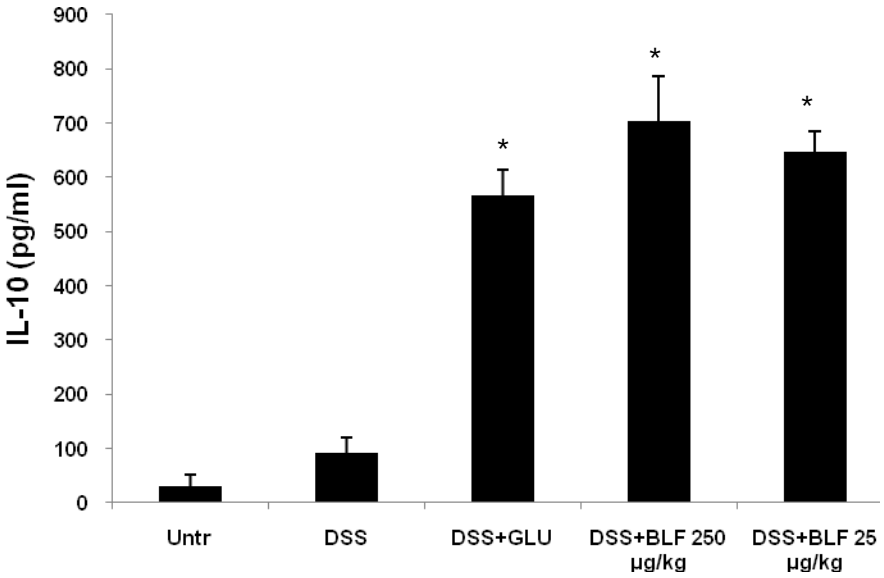

Fig 21 IL-10 levels in colonic colture DSS-induced chronic colitis loads to a insignificant increase in colonic secretion of IL-10, wich was significantly increased by oraly administration of glucose or BLF 250 and 25 µg/kg. Data are the means (±SD). *, $p < 0,005$ vs DSS.

BLF-501 oral administration protects against chemically-induced mouse model of chronic intestinal inflammation.

SGLT-1.activation by BLF501 protects against chemically-induced acute colitis mouse model, with important role in recovery of epithelial barrier intestinal barrier function. Several data in letterature show that in different animal model of Crohn disease[70,71,79] an

increased intestinal permeability has been shown before inflammation expression and the reversal of this defect can attenuate the disease.

The administration of DSS at a concentration of 2% in the drinking water for three cycles is chemically-induced mouse model of chronic intestinal inflammation. To evaluate the effect of BLF-501 in this colitis model, we have performed five animal groups of 5 mice/group. Four groups received three cycles of treatment with DSS. Each cycle consists of 2% DSS dissolved in the drinking water for 7 days, followed by a 14 days interval with normal water administration. Ten days after completion of the last DSS cycle, one group of mice received 25 µg/kg BLF501 *per os,* 4 times a week, for 3 consecutive weeks; another group of mice received 25 µg/kg BLF501 *per os* 4 times a week, for 2 consecutive weeks; the third group of mice received 25 µg/kg BLF501 *per os* 4 times a week, for 1 week only; the fourth group of mice received only three cycles of treatment with DSS, the last group of animals (control group) received normal drinking water only, during the whole time of the experiment.

Macroscopical evaluation of BLF501 25 µg action in chronic colitis.

The length of the colon decresed as the disease developed. After chronic colitis induction, in DSS administered mice the colon length was significantly shorter than control mice. A significant decrese in the shortening of the colon length was observed in mice that had received BLF-501 almost for 3 week compared with DSS-administered mice (fig. 22).

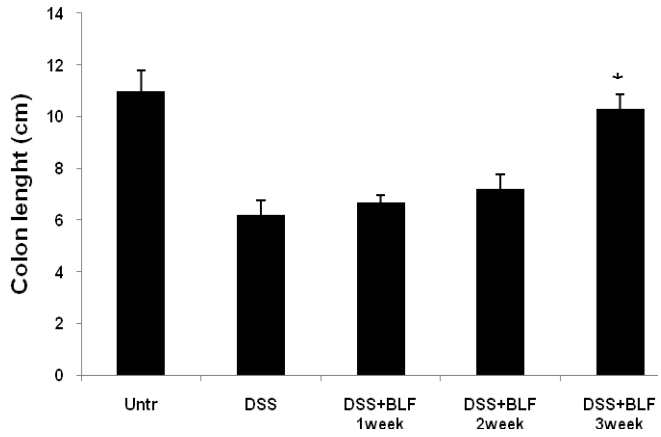

Fig 22 Distal colon length. Values represent the mean of 5 animals/group. Data are the means (±SD). *, p < 0,005 vs DSS.

,Moreover, chronic colitis level of different groups was scored using a standard parameter stool consistence. Fig. 23 show that DSS-treated group has soft stools with a 1,3 mean score, whereas untrated group shows normal stools with mean score 0. BLF501 treatment for 3 week restores completly stool consistence.

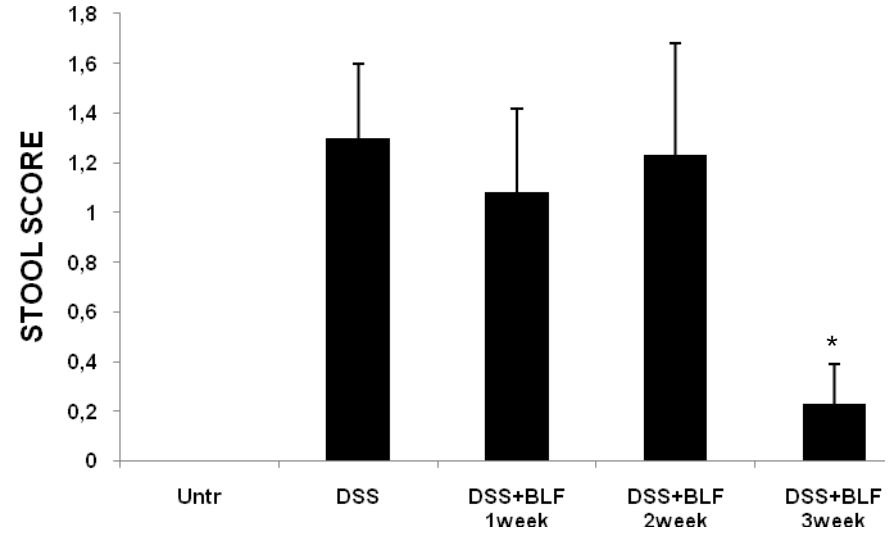

Fig 23 Scoring system for the comparative analysis of stool consistence. Values represent the mean of 5 animals/group. Data are the means (±SD). *, p < 0,005 vs DSS.

Barrier morphology and function of colon mucosal is restored in BLF-501-treated mice

Histological examination of colon tissue from DSS-treated mice showed, upon hematoxilin/eosin staining, prominent signs of inflammation with scattered, infiltrating mononuclear cells and thickening of the intestinal wall. On the other hand, very mild signs of inflammation were seen in tissue samples from animals treated with DSS and BLF501 25 µg/kg administrated for 3 week.

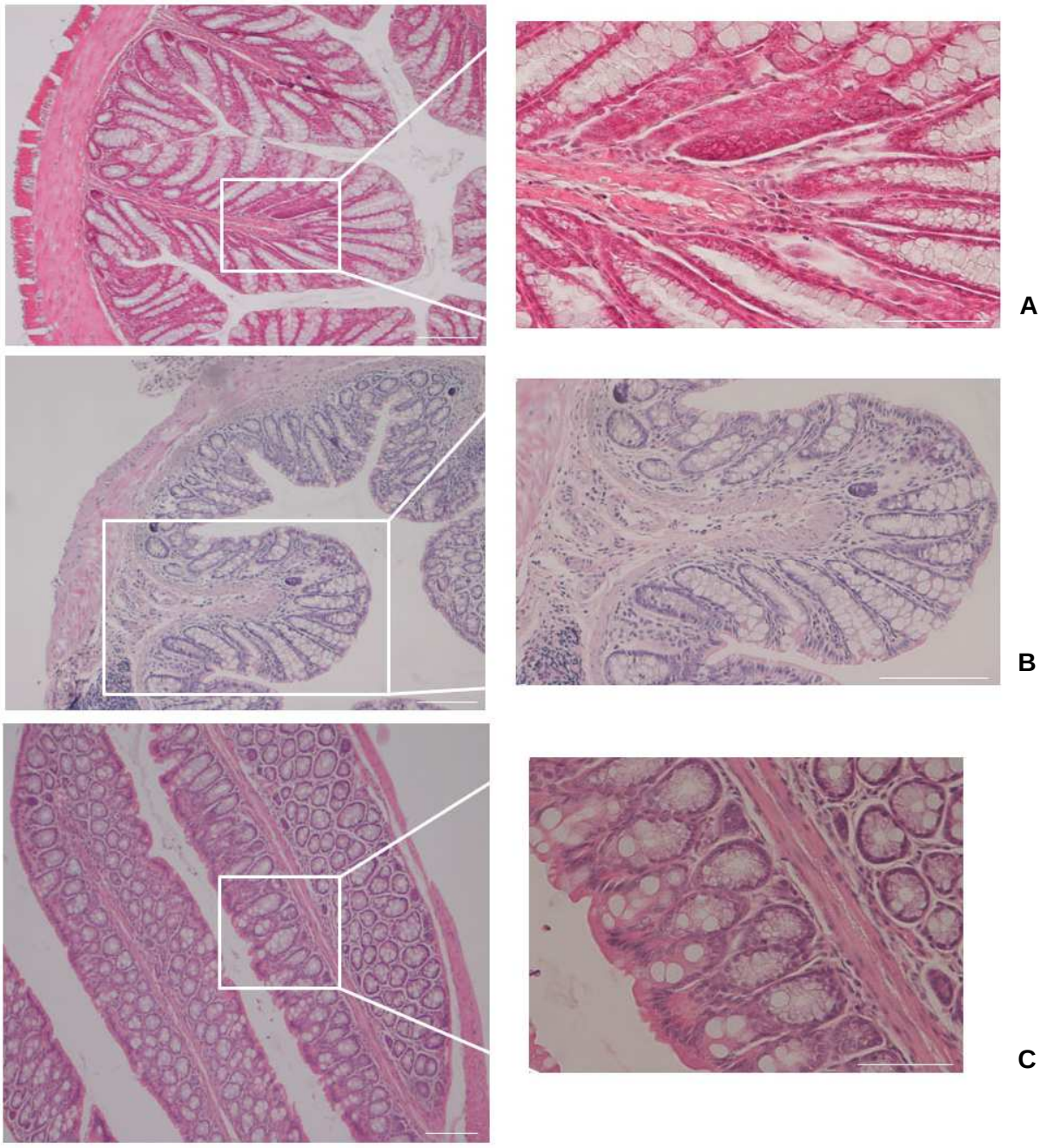

A

B

C

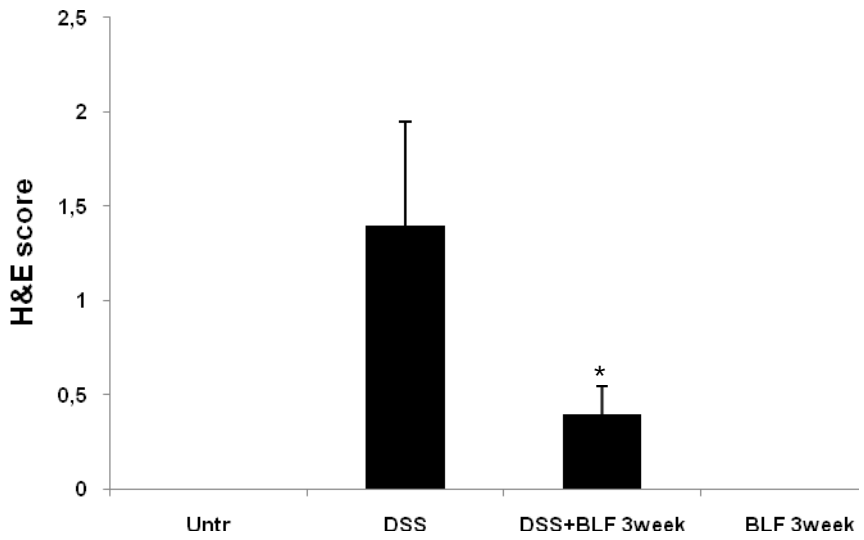

Fig 24 (A) Rapresentative colonic H&E section from mice receiving water without DSS . In magnification colon cryptes with normal morphology. (B) Colon histology from DSS-treated group. DSS induces thickening of the colon wall and infiltration reaching the lamina submucosa (in magnification). (C) Representative colon section of BLF501 25 µg/kg histologically comparable with control group. Bar 50µm (D) Histological scores of the colon section stained with H&E. Results are representative of 10 sections for each animal of different groups (n=5). DSS mean score shows high level of inflammation with transmurall leukocite infiltration. Oral administration of BLF501 25 µg/kg for 3 week restores mucosal demage DSS-induced. Data are the means (±SD). *, $p < 0,005$ vs DSS.

The intestinal epithelial barrier function is demaged in chronic inflammation, manifested by an increase in intestinal epithelial permeability. Indices of permeability typically are transepithelial resistence (TER) obtained from formalized assays using Ussing chamber. We analyzed the colon permeability in order to determine if BLF501 is able to restore the electrophysiological barrier function. Segments of colon were mounted in Ussing chambers and trans-epithelial electrical potential difference (mV) across the mucosal membrane and the short-circuit current (µAmp) were measured directly, while the transmembrane resistance was calculated as ohm x cm^2, as determined using Ohm's law. As shown in fig. 25 DSS treatment significantly reduced the barrier function of colon tissue, because loads to increase in TER, while BLF-501 oral administration restors transepithelial resistence.

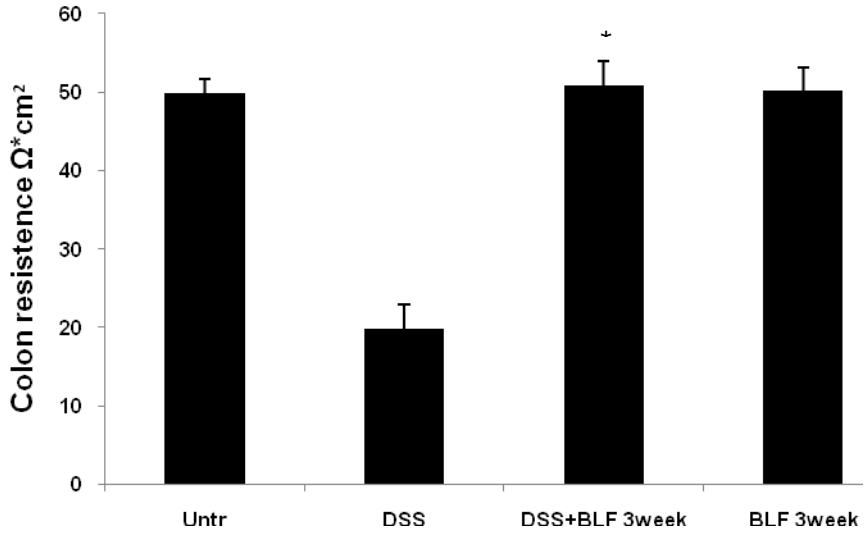

Fig.25 Colon resistence. Data are the means (±SD). *, p < 0,005 vs DSS.

Since epithelial tight junctions regulate paracellular permeability[94] and DSS induced chronic colitis is associated with increased intestinal permeability with decreased expression of occludin and ZO-1 protein. we examined the effect of BLF501 on morphological organization of these tight junction protein.

In colon of control mice, the protein occludin and ZO-1 were precisely localized to the epithelial TJ. Immunofluorescence detection of these protein (fig. 26 A, E and 27 A) show regular series of bright red lines at the apical aspect of cell junctions. In contrast the immunofluorescence signals of occludin and ZO-1 were disrupted and irregularly distributed in DSS-induced colitis (fig. 26 B and 27 B), while the signals appeared as a typical reticular pattern by the oral administration of BLF501, without any morphological alteration (fig.26 C and 24 C).

These findings suggest that the recovery of mucosal impairment in DSS-induced chronic colitis.due to oral treatment with BLF501 is associated with the restoration of the tight junction protein occludin and ZO.1.

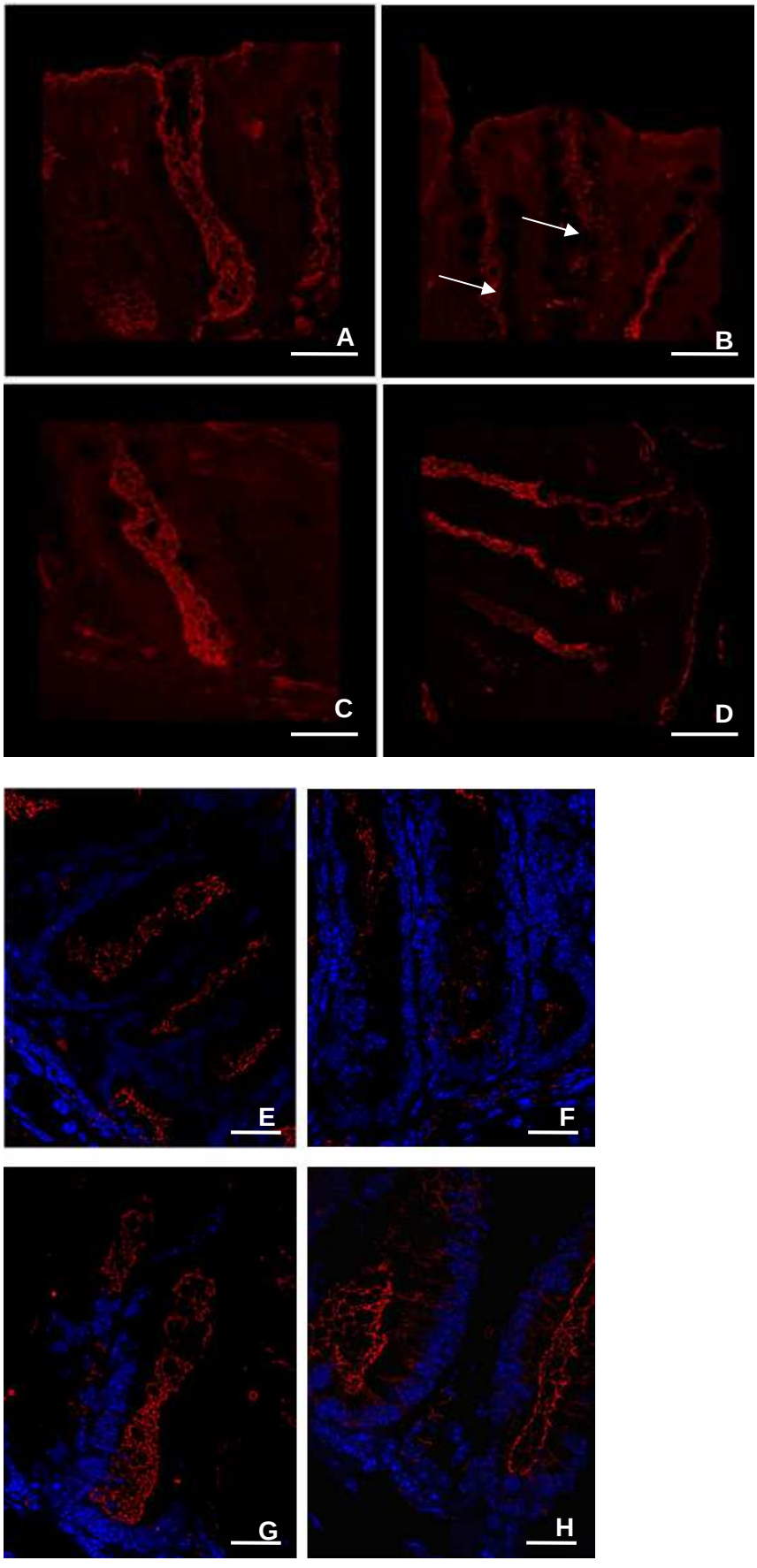
A
B
C
D
E
F
G
H

Fig 26 Immunofluorescence ZO-1 detection Confocal (A-D) and Video Confocal image (E-H). A and E) Colon section of untreated mice, ZO-1 detection (magnification 60X). ZO-1 is stained red is exclusively localized at the apical junctional complex both at the surface and in the crypts. B and F) In DSS-treated animals, a substantial redistribution of ZO-1 away from tight junctions occurred. This change was manifested by discontinuities in membrane staining, in some areas there was complete loss of staining. Withe arrows show crypt with reduced ZO-1 staining and loss of crypt morphology. C and G) Colon section of chronic DSS and BLF501 administration show a continuous and intense staining pattern similar to healthy controls. Images are representative for 5 colon section for each animals/group. Bar 25 μm

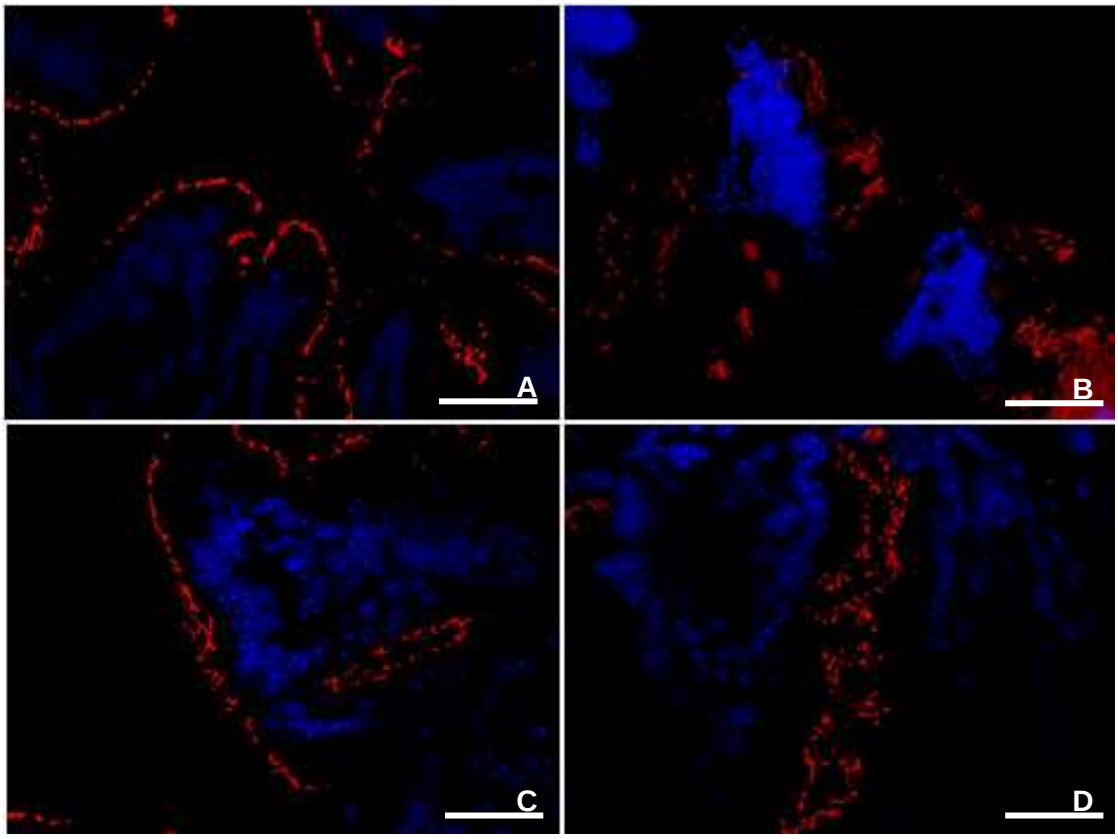

Fig. 27 Immunofluorescence for occludin. Representative images for occludin are shown for the 3 groups. The tight junction proteins are stained red, and nuclei are blue. A) Occludin exclusively localizes at the apical tight junction, and an intense apical fluorescence band is found in healthy animals. The apical staining of occludin is strongly reduced in DSS treated animals. C) In BLF501-treated animals, apical staining is preserved (arrows). Images are representative for 10 slide for each animal (n=5).

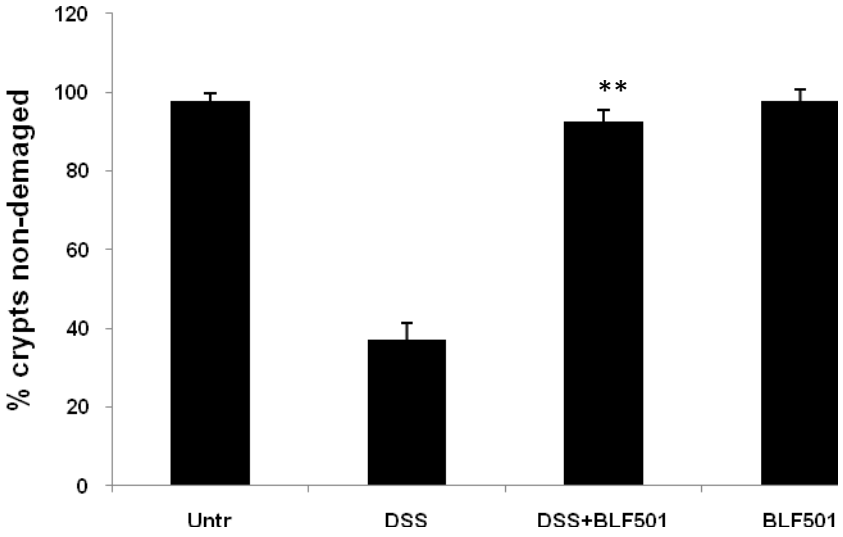

Fig.28 Graphic representation of percentage of crypts non DSS-demaged in colon section stained for occludin and ZO-1 tight junction proteins. Values represent the mean of 10 slide for each animal (5 animals/group) Data are mean (±DS) **, p < 0,001 vs DSS.

4.3 SGLT-1 a new therapeutic target in lung inflammatory disease

4.3.1 Engagement of SGLT-1 inhibits the response of human pneumocytes to LPS.

Western blot analysis (fig. 29) showed that A549 human pneumocytes express SGLT-1, consistent with findings in rat type II pneumocytes (97), while 16-HBE human bronchial epithelial did not.

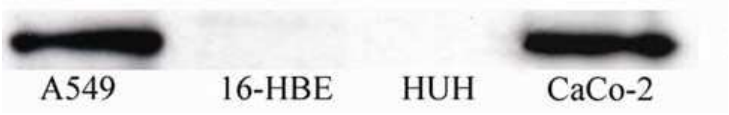

Fig.29 Western blot analysis of SGLT-1 expression in A549 human pneumocytes, 16-HBE human bronchial epithelial cells, HUH 7 human liver hepatoma cells (negative control) and CaCo-2 human colorectal carcinoma epithelial cells (positive control). B-actin expression was used as a reference loading control (data not shown).

4.3.2 BLF501 inhibits LPS-induced interleukin IL-8 production in human pneumocytes A549 cells at 100,000-fold lower concentrations than D-glucose.

To determine whether D-glucose and the synthetic D-glucose analogue BLF501 inhibit LPS-induced IL-8 production, A549 cells were cultured for 18 h in the presence of a D-glucose concentration 5-fold higher than in normal medium ("high D-glucose" medium, 27.78 mM), or in the presence of 50 µg/L of BLF501 (11.36×10^{-7} mM), and subsequently stimulated for 6 h with LPS from *Pseudomonas aeruginosa* (100 µg/ml). Both D-glucose and BLF501 suppressed IL-8 production in LPS-stimulated A549 cells to levels similar to those of unstimulated cells (fig.30 A), while the same experiments using 16-HBE human bronchial epithelial cells revealed no inhibition of LPS-induced IL-8 production by either D-glucose or BLF501 (fig. 30B). The involvement of SGLT-1 in glucose- or BLF501-induced inhibition of LPS-induced responses in A549 cells was confirmed in experiments using SGLT-1 mRNA-specific small interfering RNA (siRNA) to silence SGLT-1 expression,

resulting in the abrogation of the inhibitory effects of D-glucose and BLF501 on LPS-induced IL-8 production (fig.30 A).

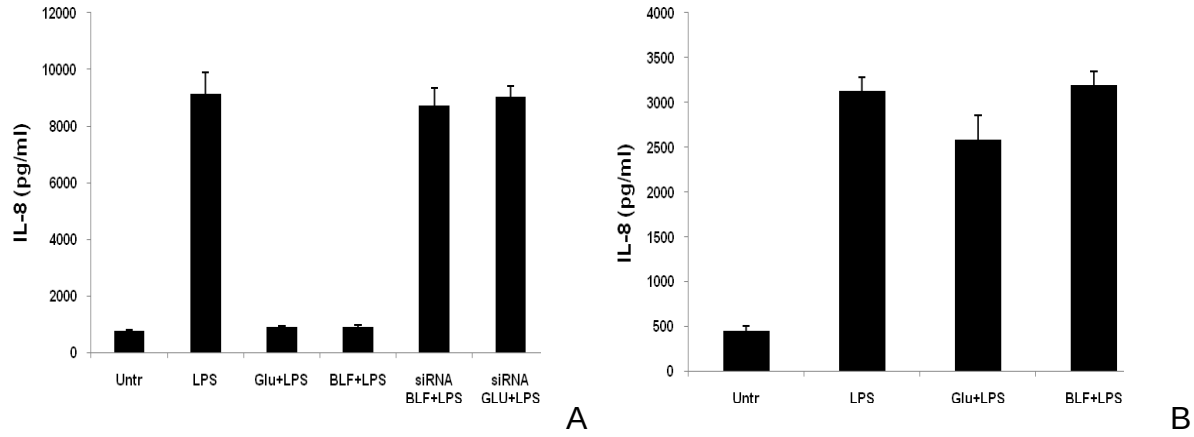

Fig.30 A) IL-8 levels in colture medium A549 after LPS pseudomonas treatment. Glucose or BLF501 B) IL-8 levels in colture medium 16-HBE

These results indicate the essential role of SGLT-1 in glucose- and BLF501-induced modulation of LPS-driven cytokine responses in human pneumocytes.

4.3.3 Protective anti-inflammatory effects induced by BLF501 engagement of SGLT-1 in lung after aerosol administration of LPS.

Immunofluorescence analysis of lung samples showed that pneumocytes expressed SGLT-1, while bronchial epithelium was not stained (fig. 31), consistent with the observations in cell lines.

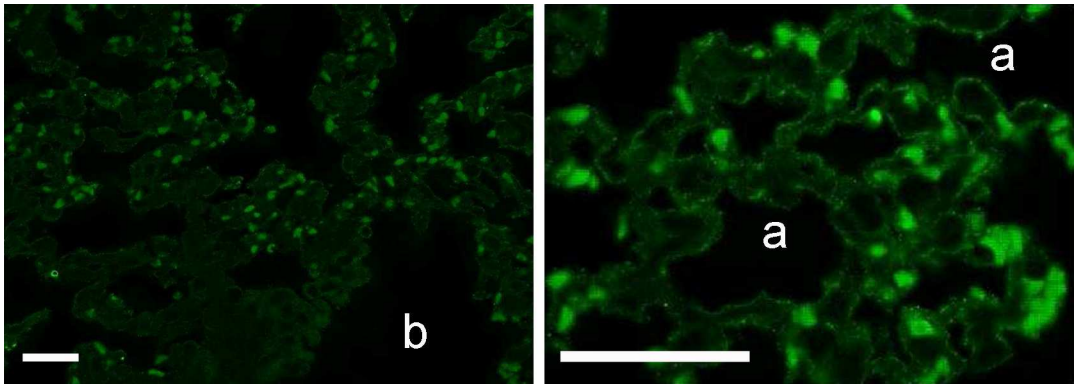

Fig 31 SGLT-1 expression in normal murine lung. Expression of SGLT-1 was detected by immunofluorescence analysis on normal alveolar pneumocytes (a), but not on normal bronchial epithelial cells (b), by incubation of lung sections with a polyclonal anti-SGLT-1 antibody (Zymed Laboratories), diluted 1:1000 in PBS, for 1 h at room temperature, followed by addition of goat anti-rabbit antibody Alexa 488, diluted 1:200 in PBS and 3% BSA, for 30 min at room temperature. Bars: 50 µm.

We then assessed whether SGLT-1 engagement exerted anti-inflammatory effects in an *in vivo* model of LPS-induced lung injury in experiments using only BLF501, since the reagent was designed and synthesized to act as a D-glucose agonist on SGLT-1 and the *in vitro* results confirmed this assumption. Thus, groups of mice (n=5/group) received BLF501 via aerosol at a dose of 266 ng/ml (total of 3 ml of administered solution), based on preliminary dose-response experiments (fig 32), or an aerosol solution containing 3 mg/ml LPS (3 ml), or both (at the above dosage but in 3 ml total) daily for 5 consecutive days. At the end of the treatment period, blood and lung samples were collected for analysis.

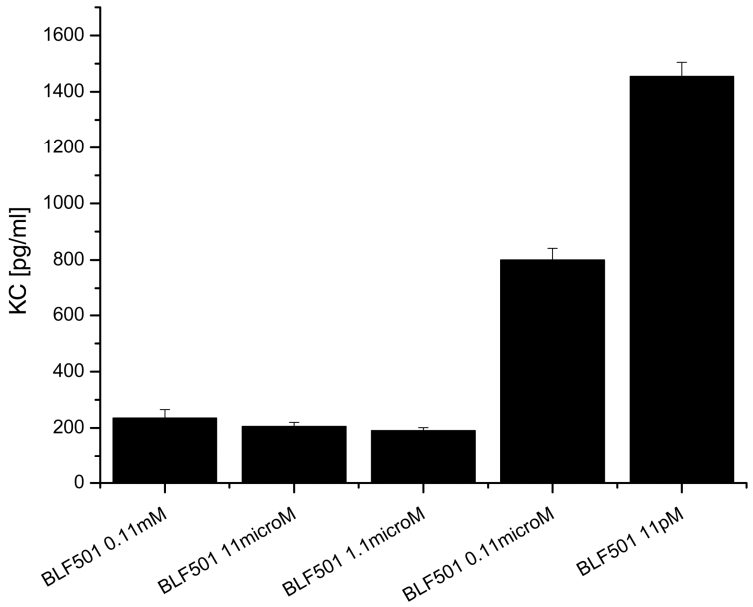

Fig 32 Dose-response of aerosol LPS-exposed mice to BLF501. Mice were exposed to LPS as described in Methods and additionally treated or not with aerosolized BLF501 in decreasing concentrations from 0.11 mM to 11 pM. The graph shows that the highest anti-inflammatory activity, evaluated based on serum KC levels, was obtained using BLF501 at a dosage of 1.1 μM. Data are mean ±S.D. (n=3/group).* $p < 0,005$.

Fig. 33 shows that lungs of mice exposed to LPS showed marked inflammatory alterations, characterized by the presence of alveolar haemorrhage and massive extravasation into the alveolar spaces of both mono- and polymorphonuclear leukocytes, aggregated in clusters, and numerous eosinophils and neutrophils. Some neutrophils were also present in bronchial spaces, associated with many macrophages. Massive alterations involved the bronchial epithelium, with areas of proliferation with rare superficial mitosis and alterations of the nuclei. By contrast, lung parenchyma of mice concomitantly treated with BLF501 and LPS revealed an almost physiological morphology, with only rare eosinophils present in alveolar septi and with pervious bronchial lumens. Immunohistochemical analysis of lung tissue for Inter-Cellular Adhesion Molecule 1 (ICAM-1) and caveolin showed that expression of both of these inflammation markers was increased in mice treated with LPS

alone, while expression in mice treated with BLF501 and LPS was comparable to that in controls.

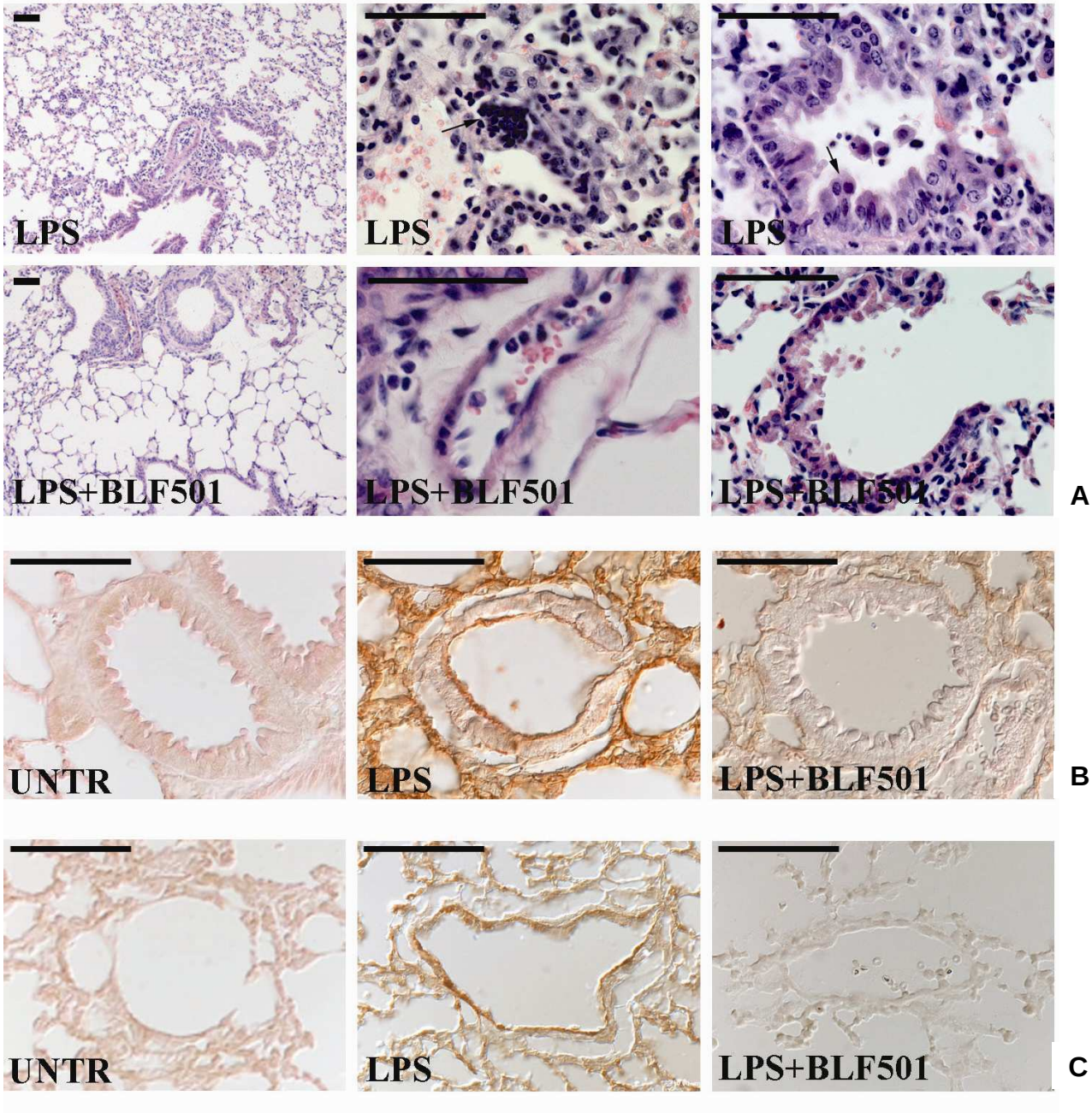

Fig. 33. Aerosolized BLF501 protects lung from injury after aerosol administration of LPS. A) Histological examination of lung samples from mice exposed to LPS, showing marked inflammatory alterations characterized by massive extravasation of leukocytes aggregated in clusters into the alveolar spaces and areas of proliferation of the bronchial epithelium (arrows). Lung samples of mice concomitantly treated with BLF501 and LPS showed no alterations of lung parenchyma. Bars: 50 µm. B) and C) Immunohistochemical analysis of lung samples using anti-

ICAM-1 (c) and anti-caveolin (d) antibodies, respectively, revealing increased expression of ICAM-1 and caveolin in mice treated with LPS alone, but expression comparable to that of controls (UNTR) in mice treated with BLF501 and LPS. Bars: 50 µm.

Analysis of the bronchoalveolar lavage fluid (BALF) revealed a massive increase in total cell numbers, with neutrophils and macrophages representing the majority of cells, in mice treated with LPS only, while alveolar spaces of LPS plus BLF501-treated mice showed cell numbers comparable to those in controls (Table 1).

	Untreated	**BLF501**	**LPS**	**BLF501+LPS**
Neutrophils	134/ml ± 15	128/ml ± 18	3450/ml ± 332	122/ml ± 20
Macrophages	32/ml ± 7	30/ml ± 8	233/ml ± 32	34/ml ± 14

Table 1. Evaluation of neutrophils and macrophages infiltrate in bronchoalveolar lavage fluid (BALF) from untreated and LPS-, BLF501-, LPS plus BLF501-treated mice (5 mice/group). Cells from BALF were fixed in formalin plus sucrose solution and deposited on glass slides by cytocentrifugation. Differential counts were performed on Giemsa-stained cytospins. Data are mean numbers of cells/ml BALF ± S.D.

Analysis of the fluid phase of BALFs for NO, a marker of cellular stress and damage[98], revealed high NO levels in LPS-treated mice, but significantly lower levels in mice treated concomitantly with BLF501 (fig. 34). Together, these data strongly suggest that BLF501 leads to marked anti-inflammatory effects *in vivo*.

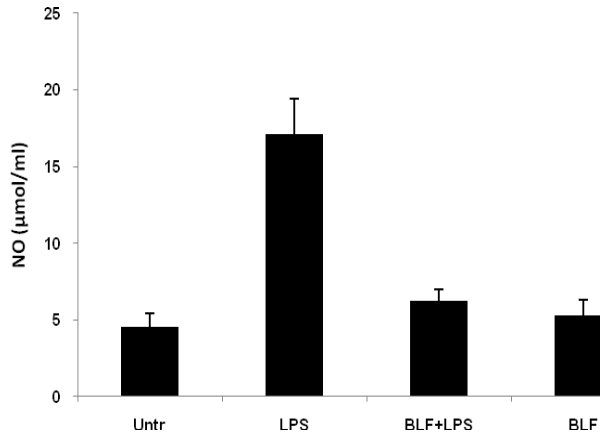

Fig. 34 NO levels in BLF fluids. BLF501 reduced NO levels, a marker of cellular stress and demage, induced by LPS administration.

4.3.4 Anti-inflammatory effects of BLF501 in an OVA-induced model of allergic asthma.

To assess whether BLF501 might inhibit other lung inflammatory conditions such as allergic asthma, we used a murine model of OVA-induced asthma, which leads to pulmonary injury characterized by intense inflammation with marked eosinophilic cellular infiltration and high levels of systemic TNF-α, IL-4 and IL-5 levels[99]. Asthma was induced in two groups of mice (n=5/group) by i.p. immunization with 100 µg OVA and 500 µg of aluminum hydroxide, followed by an aerosol of 5% (wt/vol) OVA; one of the groups received concomitant aerosol administration of BLF501 (266 ng/ml, 3 ml), while a third group remained untreated. Histological examination of lungs from OVA-treated mice showed the presence of a marked cellular infiltrate (fig. 35), with inflammatory cells aggregated all around the small blood arteries and apparently in strict contact with the external wall of the vessel, with no evidence of infiltration in the muscular tunica. An inflammatory infiltrate consisting of lymphocytes and eosinophils was also present along the external bronchial wall, while the lumen of mid-dimensional bronchi was characterized by mucus, containing several erythrocytes. A marked inflammatory infiltrate was also

observed in the alveolar septi, while bronchial cylindrical epithelial cells showed significant hyperproliferation. By contrast, mice concomitantly treated with BLF501 presented a conserved lung architecture (fig. 35), with no inflammatory infiltrate in the vascular or in the bronchial region and no mucous secretory product in the bronchial lumen. Analysis of BALFs showed a strong increase in eosinophil numbers in the lung of OVA-treated mice (4058±121 cells/ml), consistent with the induction of allergic asthma, while mice treated with BLF501 and OVA showed significantly fewer eosinophils in the alveolar spaces (142±27 cells/ml, $p = 3.3x10^{-7}$ *vs.* OVA), with numbers comparable to those of untreated mice (139±22 cells/ml).

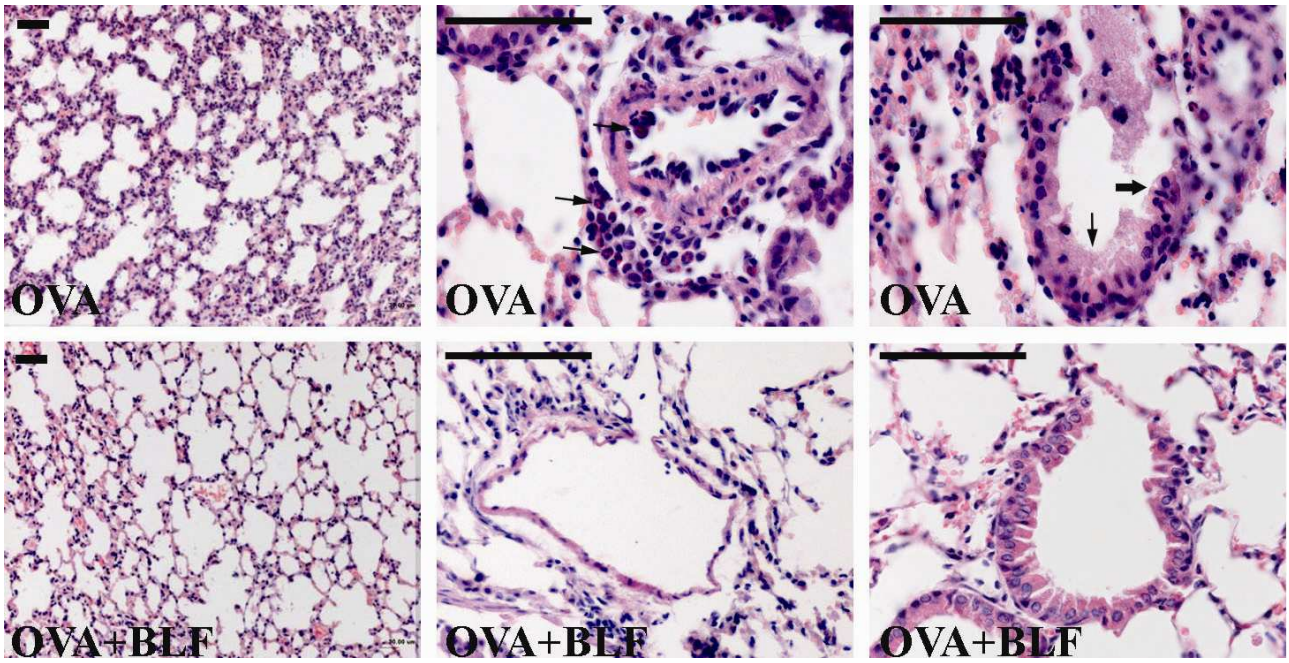

Fig. 35. Anti-inflammatory effect of aerosolized BLF501 in an OVA-induced model of allergic asthma. Histological examination of lungs of OVA-treated mice, revealing cell aggregates grouped around the small blood arteries, in strict contact with the vessel walls (thin arrows); mid-dimensional bronchi are characterized by the presence of mucus (thin arrow) and epithelial hyperproliferation (thick arrow). Mice concomitantly treated with BLF501 plus OVA showed no alterations of lung parenchyma. Bars: 50 µm.

A hallmark of inflammatory damage to the lung is the development of high-permeability edema, characterized by a high protein content in the exudate. Indeed, the protein concentration in BALFs from lungs of mice exposed to OVA was very high (0.727±0.026 mg/ml). By contrast, protein concentration in BALFs from mice treated with OVA and BLF501 was significantly lower (0.389±0.033 mg/ml, p = $1.3x10^{-4}$ *vs.* OVA) and comparable to that of untreated controls (0.375±0.036 mg/ml). NO levels in BALFs of OVA-treated mice were 19.2±1.1 µmol/ml, but 3.3±0.6 µmol/ml upon concomitant administration of BLF501 (p = $6.6x10^{-6}$*vs.* OVA), similar to those in untreated mice (2.6±0.4 µmol/ml).

Levels of IL-5 and IL-4, prototypical cytokines of allergic asthma, were elevated in sera (Fig. 36 a and b) and BALF (data not shown) from OVA- but not from BLF501 plus OVA-treated mice, whereas levels of the anti-inflammatory cytokine IL-10 were greatly increased in sera of mice receiving BLF501 plus OVA but similar in controls and in mice treated with OVA alone; no IL-10 production was observed in mice treated with BLF501 alone (Fig. 36 d).

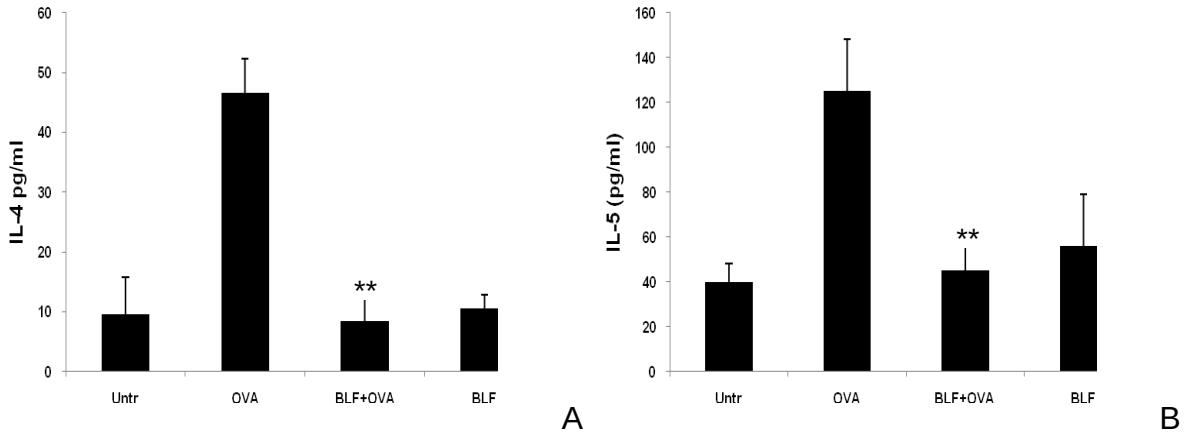

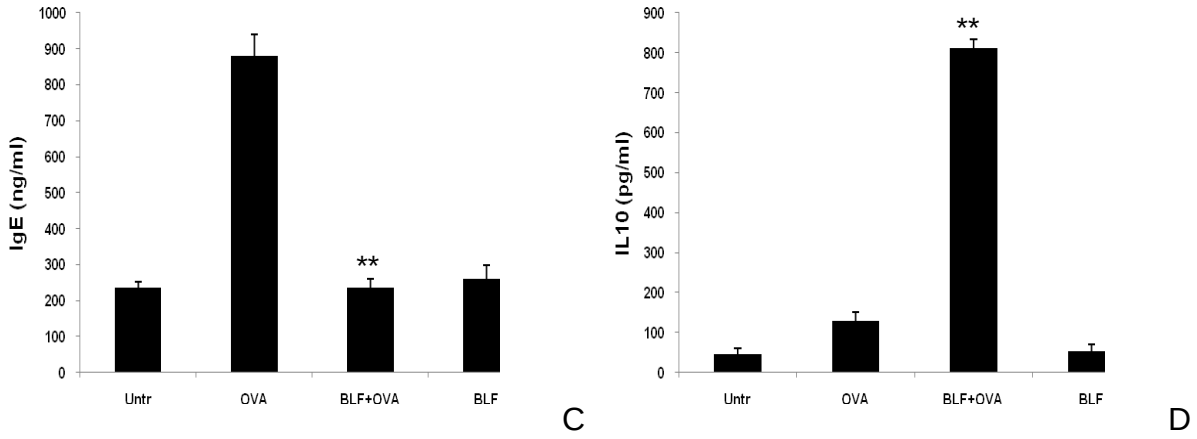

Fig. 36**.** Anti-inflammatory effect of aerosolized BLF501 in an OVA-induced model of allergic asthma. A-D) Levels of IL-4, IL-5, IL-10, and anti-OVA IgE, respectively, in sera of untreated mice (UNTR) or OVA-, BLF501- or OVA plus BLF501-treated mice. Data are mean ± S.D. (n=5/group). **p <0,001.vs OVA.

Analysis of serum Immunoglobulin E (IgE) levels, which are increased in airway inflammation in asthma, in mice treated with aerosolized OVA, with or without BLF501 administration, revealed significantly increased levels of anti-OVA IgE in asthmatic mice compared with those of control mice, while administration of BLF501 led to a significant decrease in these specific IgE levels (Fig. 36c).

Together, these results demonstrate that BLF501 exerts potent anti-inflammatory effects in an animal model of allergic asthma.

4.3.5 Orally administered BLF501 inhibits OVA-induced lung inflammation.

We previously showed that engagement of intestinal epithelial cells SGLT-1 by orally administered glucose induces systemic production of protective anti-inflammatory cytokines[6]. To determine whether the anti-inflammatory effects of BLF501 might also be observed upon oral administration, mice receiving OVA were orally treated or not with

BLF501 (25 µg/kg), and serum, BALF and lung samples collected at the end of treatments were analyzed as those for mice treated with aerosolized BLF501. The results with respect to eosinophilic infiltrate, serum and BALF protein content, and cytokine and anti-OVA IgE levels (Fig. 37 a and b) were comparable to those obtained with aerosolized BLF501. By contrast, no protection was observed after intravenous BLF501 administration (data not shown).

Based on our previous finding in liver inflammation conditions that SGLT-1 activation is efficacious in triggering an anti-inflammatory activity only in the presence of a danger signal[7], we focused on identifying the danger signal that might be involved in the protection in the asthma model. In many lung diseases, including chronic bronchitis, chronic obstructive pulmonary disease, acute lung injury, acute respiratory distress syndrome and asthma, Tumor Necrosis Factor (TNF)-α plays a major role [100]. To test whether TNF-α might constitute the major danger signal in the asthma model, we monitored serum levels of this cytokine at various time-points during 1 month in OVA-treated and OVA plus orally BLF501-treated mice (Fig. 37c). Sera of mice treated only with OVA presented two peaks of TNF-α on the 1st and 7th day of treatment, corresponding to the two sensitizations with OVA and aluminum hydroxide; levels remained constant at about 100 pg/ml and increased again from the 12th day during the 5 days of OVA aerosol administration, reaching levels of about 230 pg/ml until day 22, when TNF-α levels decreased again but only to 80-200 pg/ml. While sera of mice concomitantly treated with OVA and oral BLF501 both during the sensitization phase and the challenge phase presented peak levels of TNF-α at the same time points as the OVA-only group, levels were consistently much lower than in the OVA-only group (Fig. 37c). Thus, TNF-α is produced even in the presence BLF501 treatment.

To investigate the role of TNF-α in the effects of BLF501 on OVA-induced asthma, we examined the lung morphology and serum/BALF cytokine levels in mice treated for 5 days with aerosolized OVA only, or with OVA plus BLF501, or with OVA, BLF501 and 5 µg of an anti-TNF-α neutralizing antibody, administered i.p. on the 4th and 5th day of OVA administration (n=5 mice/group). Interestingly, the concomitant administration of anti-TNF-α antibody blocked the protective effect of BLF501, with mice showing signs of inflammatory injury similar to those in OVA-treated mice (data not shown). These results point to a crucial role for circulating, threshold levels of TNF-α as a danger signal that contributes to BLF501-mediated protection in this OVA-induced model of allergic asthma.

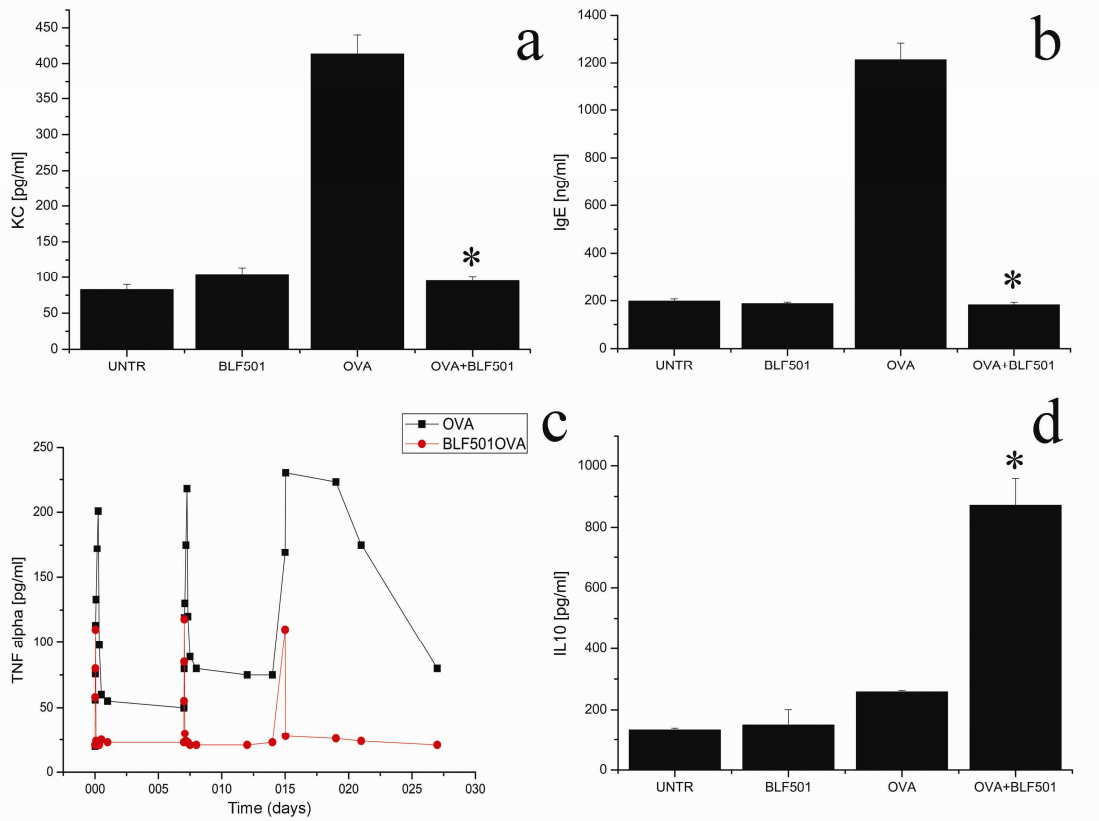

Fig. 37. Anti-inflammatory effects of orally administered BLF501 in an OVA-induced model of allergic asthma and involvement of dendritic cells. a, b) Levels of KC and anti-OVA IgE in sera of untreated mice (UNTR) or of OVA-, BLF501- and OVA plus BLF501-treated mice. Data are mean ± S.D. (n=5/group). * $p = 5.18 \times 10^{-6}$ (a) and $p = 7.33 \times 10^{-6}$ (b) vs. OVA. **c)** Serum levels of TNF-α in a time-course experiment: peak production occurred at the same time points in both the OVA plus BLF501 (-●-) and the OVA-only group (-■-), but levels were consistently lower in the former. Data

are mean values (n=5/group). **d)** IL-10 levels in supernatants of lung-derived CD11c+ cells from untreated mice (UNTR) or OVA-, BLF501- and OVA plus BLF501-treated mice. Cells were plated at the same cell density for all treatment groups. Data are mean ±S.D. (n=5/group) ** p <0,001 vs. OVA.

4.3.6.Hsp27 mediates the anti-inflammatory effects of BLF501 through induction of IL-10 production by dendritic cells.

The anti-inflammatory effects of BLF501 might be due to the production of an anti-inflammatory cytokine, such as IL-10, in response to engagement of SGLT-1, and a second signal, such as TNF-α. Indeed, IL-10 levels were only slightly increased in OVA-treated animals, but markedly increased in mice treated with BLF501 and OVA**.** On the other hand, no IL-10 production was observed in mice treated only with BLF501. Moreover, we previously showed that anti-IL-10 antibodies abrogate the protective activity following SGLT-1 activation[6,7]. To investigate in more detail the induction of systemic IL-10 production in response to BLF501, we tested whether dendritic cells (DCs), the main IL-10-producing cells[101], were involved in the increase of systemic IL-10 in response to OVA and BLF501. Thus, groups of mice (n=5/group) were treated as above with OVA alone or with BLF501 plus OVA; untreated mice and mice treated only with BLF501 served as controls. At the end of treatment, lungs were collected, enzymatically digested, and pulmonary CD11c+ DCs were isolated by magnetic cell sorting. After 18-h culture of these cells at equivalent cell densities, supernatants were collected and tested for IL-10 levels. The cells isolated from the BLF501 plus OVA group produced high levels of IL-10, greatly exceeding those from cells derived from the other groups (fig. 37 d). Moreover, the number of DCs obtained from mice treated with BLF501 plus OVA was significantly higher than that from the other groups [mean number of cells/lung ± S.D.: 4087±301 for BLF501 plus OVA; 216±35 for untreated ($p = 6.6x10^{-6}$ *vs.* BLF501+OVA); 357±39 for OVA-only (p =

$9.2x10^{-6}$ *vs.* BLF501+OVA); and 282±42 for BLF501-only ($p = 4.8x10^{-6}$ *vs.* BLF501+OVA) (5 mice/group)].

Unlike epithelial cells, DCs do not express SGLT-1 and are unable to respond to BLF501 on their own, suggesting a role for a signaling molecule in linking epithelial cell production of SGLT-1 with DC production of IL-10. Based on data indicating that extracellular stress proteins, such as heat-shock protein (hsp) 27, act as “signaling" molecules for the innate immune system[102] and induce anti-inflammatory mediators, including IL-10 [103], we first assessed hsp27 production in the culture supernatant of HT-29 human colon carcinoma cells stimulated with TNF-α, in the absence or presence of BLF501; high levels of hsp27 were produced in response to TNF-α and BLF501, but not to TNF-α or BLF501 alone (Fig. 38a).

To test whether hsp27 production in response to BLF501 plus TNF-α was able to induce IL-10 production, a monolayer of HT-29 cells grown to confluence in the upper part of a Transwell system was co-incubated with human monocyte-derived dendritic cells (MoDCs) in the bottom wells, so that only molecules secreted at the basolateral side of HT-29 cells might reach the co-cultured MoDCs. In response to TNF-α plus BLF501, enterocytes induced the production of high IL-10 levels by the MoDCs (Fig. 38b).

Consistent with the *in vitro* results, analysis of sera from mice treated with OVA alone or OVA plus BLF501 or left untreated revealed high-level production of hsp25, the murine analogue of human hsp27, only in the OVA plus BLF501-treated animals (Fig. 38c).

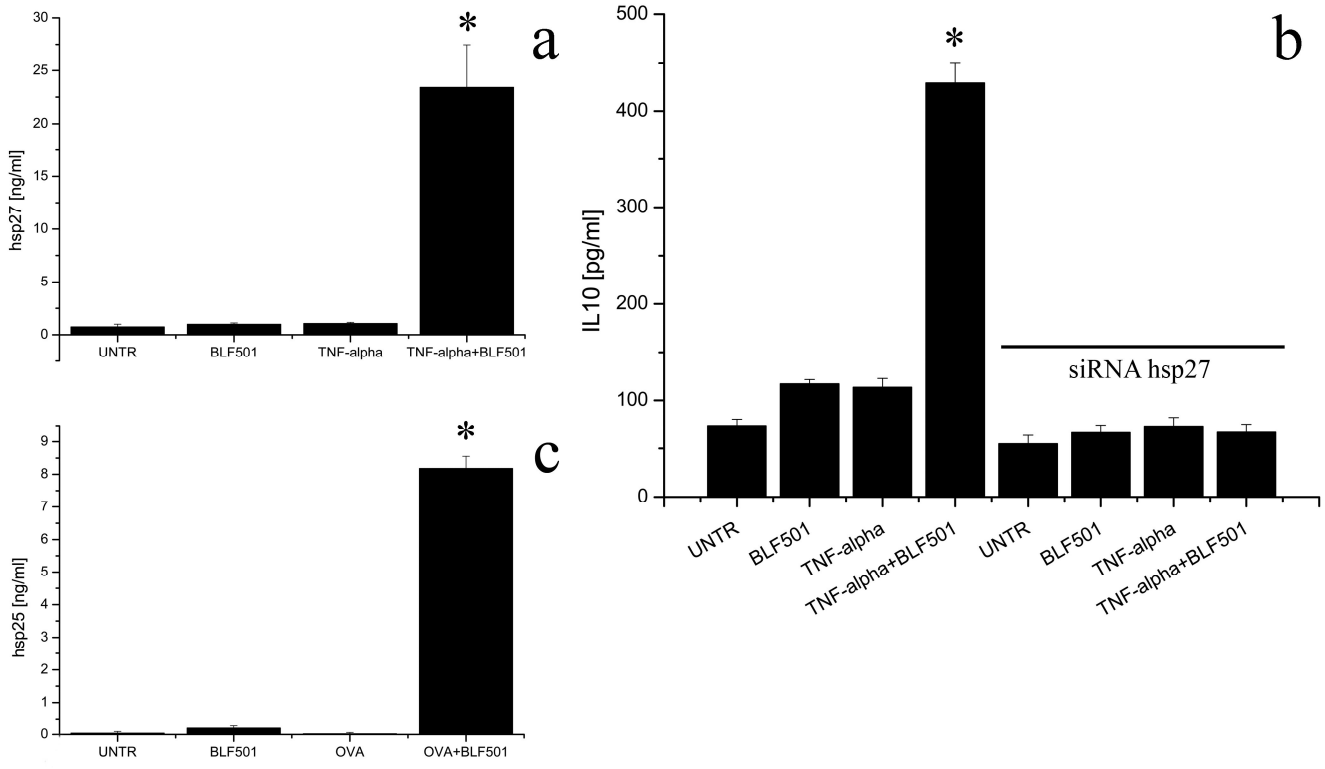

Fig 38. Role of hsp27/hsp25 in BLF501 activity. a) Hsp27 levels in supernatants of HT-29 human colon carcinoma cells in response to TNF-α, BLF501 or TNF-α plus BLF501. Data are mean ±S.D. (n=5/treatment) * p = 2.53×10^{-4} vs. TNF-α. b) IL-10 levels in supernatants of dendritic cells (MoDCs) in the presence of enterocytes stimulated with TNF-α, BLF501, or both, or unstimulated. Data are mean □ S.D. (n=5/treatment) * p = 3.37×10^{-6} vs. TNF-α. **c)** Hsp25 levels in sera from mice treated with OVA, BLF501, or both or untreated (UNTR). Data are mean ±S.D. (n=5/group) * p = 1.35×10^{-6} vs. OVA.

5. DISCUSSION

SGLT-1 is a co-transporter able to absorb D-glucose, against a concentration gradient, together with Na^+. The expression of SGLT-1 on the apical membrane of enterocytes, the cells that line the gut and overlook to the intestinal lumen, is fundamental in order to obtain the maximum D-glucose absorption from the digested alimentary bolo that transits through the gut. Presented results show a novel role of SGLT-1: this protein when is appropriately activated modulates the immune response and protect barrier function.

Accumulating data support the notion that SGLT1 orchestrates a number of fundamental cellular processes besides its canonical absorptive function. Previous reports showed that activation of SGLT1 induced the recruitment of GLUT2 to the brush border membrane for diffusive glucose transport via a PKCb-dependent pathway.[103,104] Others documented that cotransport of Na^+ with glucose triggered the activation of Akt and phosphorylation of cytoskeleton-associated ezrin, leading to recruitment of Na^+/H^+ antiport (NHE3) to apical membrane that facilitated absorption of sodium and hydrogen in intestines[105,106] Our recent study demonstrated that activation of SGLT1 suppressed bacterial LPS-induced NFkB signaling in intestinal epithelial cells, and suggested that SGLT1 has a novel immunomodulatory role. Moreover, oral ingestion, but not intraperitoneal administration of glucose, attenuated proinflammatory cytokine production and protected endotoxemic mice from lethal septic shock[6,7]. Clinically, oral rehydration therapy that targets SGLT1 to drive passive diffusion of water is a widely used supportive therapy for diarrheal patients. Early enteral nutrition (EN) is advocated for patients with multiple pathologies for its known benefit in lowering the risk of septic complications compared with parenteral supplementation. One area that has gained much attention in nutrition therapy nowadays

is preoperative oral carbohydrate loading[107,108]. All these studies show SGLT1-mediated nutritive and non-nutritive functions.

5.1 Dansyl C-Glycoside as a novel agent against endotoxic shock.

The activation of the transcription factor NFkB and the production of IL-8 induced by LPS or CpG-ODN via TLRs is inhibited by D-glucose. This inhibition has been found to be mediated by the activation of sodium-dependent glucose transporter-1 (SGLT-1). Moreover, in a murine model of endotoxic shock, oral ingestion of glucose was found to protect 100% of mice[6,7]. These studies suggest that activated SGLT-1 may be a promising target for inhibition of bacteria-induced inflammatory processes and lifesaving treatments, assuming a novel role as an immunological player. The main drawback of this activation is the high level of glucose that must be administrated (2.5 g/kg) in vivo so to achieve protection, and the evident impacts on the metabolism. In this contest we have collaborated with a chemical team from in the search of non-metabolisable glucoderivatives able to “activate” the SGLT-1 transporter at much lower concentration, in order to achieve the protection against damages induced by LPSs while avoiding the disadvantages caused by high glucose concentration.

A preliminary screening of the members of the library was carried out by detecting the level of IL-8, which is often used as quantitative marker of inflammation severity, in human HT29 cell line released upon treatment with LPS. Most interesting was the activity of compound called BLF501 that maintained the same effect on the reduction of IL-8 production also at lowest concentration. Our results show that a significant reduction in IL-8 release was observed for all IECs cultured in media containing BLF501 at 50 mg/l, 5

mg/l, 50 µg/l, 5 µg/l. At 0,5 µg/l BLF501 lose more of fifty percentuage of its anti-inflammatory activity and at 0,005 µg/l BLF501 completely lose its activity.

We then decided to better investigate the activity of BLF501**.** In order to determine the effective involvement of the glucose transporter-1 (SGLT-1) in the observed biological result just reported we carried out the detection of the level of IL-8 released upon treatment with LPS in human HT29 cell line SGLT-1 knockdown. SGLT-1 was silenced by small interfering RNA (siRNA) transfection. The silencing experiment clearly influence the efficacy of BLF501 in the modulation of the inflammatory processes.

We finally investigated the effective biological activity of BLF501 in vivo. These studies were carried out on the mouse model of lethal septic shock. Results as expected in the group of mice treated only with LPS/$GalNH_2$ induced septic shock with 100% of death within 36 h from the treatment, while for the group treated with LPS/$GalNH_2$ and BLF501 a survival of 100% of the mice along with a behaviour comparable to untreated animals was observed. This result seems to confirm the great potentialities of BLF501 as inhibition of bacteria-induced inflammatory processes and life-saving treatments and the mice mortality was down to the 0%, thus achieving a life saving treatment.

These data presented show a novel compound able to “activate” the SGLT-1 transporter, and seem to confirm its role as a novel immunological player. BLF501 has been demonstrated to be able to exert a protective effect, both in vitro and in vivo, towards damages induced by LPS, through it’s interaction with SGLT-1 when administrated orally at very low concentration. The intriguing of this work is the development of an highly active agonists for SGLT-1: in fact, existing molecules targeting this transporter aim to block its activity, in order to avoid glucose absorption into the cell. Differently, our molecule have

been planned as extremely effective activators of SGLT-1, given the recent knowledge regarding the positive effects of its activation in inflammatory processes.

5.2 BLF501 as a novel agent against colitis animal model.

Our data obtained from the present study suggest that the activation of SGLT-1 from the novel C-Glycoside derivative BLF501, may constitute a new pharmacological agent for treatment of IBD. Oral administration of BLF-501 in a chemically-induced mouse model of acute and chronic intestinal inflammation leads to inhibition of inflammatory response and restore intestinal epithelial barrier function. In IBD, the observed hyper-permeable properties of the intestinal epithelium appear to have interwined early roles in the initiation of this disease. The conventional treatments for IBD as corticosteroids, mesalamine, and immunosuppressants, provide mostly to block downstream inflammatory events, without protect directly epithelial barrier. Now, novel therapies are created to address not only the clinical consequences of the disease but in root cause(s). Based upon this analysis BLF501 may be considered a novel therapeutical agent for IBD.

Complexities of in vivo system make it difficult to determine BLF-501 effects on intestinal epithelial cells. Therefore we have performed a series of *in vitro* experiments to test BLF501 activity in a cultured intestinal epithelial monolayer damaged by inflammatory and chemically stimuli. Recently, much of the work exploring mechanisms by which intestinal epithelial barrier function is regulated has been performed using cultured intestinal epithelial cell lines. Sanders et al.[109] have shown a convenient and sensitive method to examine intestinal monolayer permeability. Transmonolayer movement of Fluorescein Dextran likely represents paracellular and not transcellular flux. *In vitro* studies [90] have shown that INF-γ and TNF-α treatment in cultured Caco-2 induces paracellular alteration

and increase FD-3 flux. Addition of FD of size 3 kD to apical surface of Caco-2 monolayer untreated leads to 23 pmole/cm^2/h, but a incubation of Caco-2 monolayer with TNF-α and INF-γ added medium leads to increased flux at 174 pmole/cm^2/h. We evaluated that BLF501 5 μg/l protects paracellular pathway against INF-γ and TNF-α damage. Recent work[90] have shown that none of the seven NFk-B inhibitor tested were able to prevent INF-γ/TNF-α-induced barrier dysfunction, this us leads to hypothesizes that SGLT-1 activation protects barrier dysfunction by a mechanism that does not depend on his demonstrated NFk-B inhibition activity [6]. Moreover data [90,91] have shown that in INF-γ/TNF-α permeability alteration does not involve TNF-α induced apoptosis, but is mediated by down-regulation of tight junction protein ZO-1 and occludin. Indeed, modulation of permeability properties is mirrored by changes in specific TJ protein components. Images obtained by Confocal and Video Confocal microscopy of immunofluorescence staining of occludin and ZO-1 show that SGLT-1 activation by BLF501 stabilizes TJ-protein localization preventing INF--γ/TNF-α-mediated degradation. BLF501 is very effective at preventing functional (FD-3 flux) and morphological (TJ protein) permeability defects induced by inflammatory stimuli.

The potential of BLF501 to ameliorate already established permeability increased was also examined in a second *in vitro* model of degradation of TJ mediated by DSS that is directly toxic to epithelial cells. We treated Caco-2 monolayer transwell with DSS 5% and we have evaluated the permeability activity of Caco-2 monolayer by measuring the paracellular penetration amount of FD-3 across Caco-2 monolayer. The flux of FD-3 of DSS-treated Caco-2 cells had increased 30-fold by 1 hour, from 50 pmole/cm^2/h (control) to 270 pmole/cm^2/h after 24 h DSS treatment. The FD-3 permeability increased following incubation with DSS 5%, the addition of BLF501 (5 μg/l) in apical medium significantly

prevented an increased in permeability to FD-3 induced by DSS. The flux of FD-3 in BLF-501 and DSS-treated Caco-2 cells is 20 pmole/cm^2/h. BLF-501 treatment of Caco-2 monolayer prevent DSS-induced barrier loss. Our results shows that SGLT-1 activation by BLF501 induce protection of barrier function that in this *in vitro* model is directly distrupted by DSS. BLF-501 protects directly TJ maintaining barrier functionality.

In our previous work our data obtained by Ussing Chamber analysis of colon samples have shown that the increase in colon permeability, which may be observed in a enterocolitis mouse model, is avoided when animal are concomitantly treated with oral glucose. This results and data *in vitro* leads to hypothesizes that BLF-501 may be protect intestinal mucosal barrier in mouse model of intestinal inflammatory disease. We firstly have perform *in vivo* experiments utilizing a chemically-induced mouse model of intestinal inflammation, which is the most commonly used IBD animal model: feeding mice for several days with DSS polymers in the drinking water induces an acute colitis characterized by bloody diarrhea, intestinal ulcerations and infiltrations with granulocytes. It is generally believed that DSS is directly toxic to gut epithelial cells of the basal crypts and affects the integrity of the mucosal barrier. The administration of DSS at a concentration of 2% in the drinking water for three cycles will result in development of chronic colitis. The DSS-colitis model shares many clinical and pathological features of human ulcerative colitis with regard to ulceration and loss of barrier function. Although the exact action of DSS is not fully understood, it is believed that DSS causes mucosal injury and destroys the barrier function, leading to inflammation. DSS has been shown to increase mucosal permeability in mice and reduce TER in intestinal cell monolayer[93-95]. Therefore, the DSS model is an appropriate model to investigate the effect of oral administration of BLF-501. Using this model, we found that mice with chronic colitis BLF-

501-treated not presents typical mucosal injury, shows a weight recovery and not develops severe clinical symptoms, including bleeding and dehydratation. Having shown this BLF-501 protective effects *in vitro* of barrier function, we investigated the capacity of BLF-501 oral administration to control barrier intestinal permeability *in vivo.* Data obtained by Ussing chamber analysis shown that chronic treatment with DSS leads to increased colon permeability compared with control mice, oral administration of BLF-501 induce in a intestinal permeability recovery.

The TJ seal the paracellular space and regulate the permeability of the mucosal barrier. The tight junction are the ordered structure formed by multiprotein complexes consisting of transmembrane proteins, as occludin and nonmembrane proteins, as ZO-1. The TJ protein has been reported to be deregulated in IBD. We have analyzed occludin and ZO-1 localization in colon tissue of different treatments and we have evaluated that intestinal permeability recovery observed with Ussing Chamber analysis is mediated by TJ protein protection. These results suggest that the BLF-501-mediated action involves stabilization of epithelial junction complex also *in vivo*. SGLT-1 activation plays an important role in restoring mucosal integrity in DSS-induced chronic intestinal inflammation. These reparative mechanisms could restablish intact barrier function and structure to protect the mucosa against entry of bacteria and forgein antigens into colonic tissue and bloodstream

More recently, IL-10 was suggested as a potential new anti-inflammatory therapy for Crohn's disease, but this treatment did not result in significantly higher remission rates or clinical improvement; the explanation for the failure of this therapeutic strategy is that the administered dose of IL-10 in clinical trials, and therefore the ultimate local IL-10 concentration in the intestine, might be too low to down-regulate the inflammatory status[96]. We demonstrate that oral administration of BLF-501 modulates pro-inflammatory and anti-

inflammatory cytokines in the colon, resulted in recovery of acute and chronic colitis. In the present study, we observed that activation of pro-inflammatory cytokines, such as TNF-α, and IL-12 in DSS acute and chronic colitis was suppressed by oral administration of BLF-501. We have observed a marked increase of IL-10 levels in mice treated with BLF-501 and acute and chronic cycles of DSS in comparison with DSS alone or with untreated mice. The continuous IL-10 production from immune system components, guaranteeing an endogenous source of this anti-inflammatory cytokine, is able, to down-modulate the inflammatory response, avoiding the problems linked to the classical IL-10 therapy.

5,3 BLF501 as a novel agent against inflammatory lung disease.

Our results in two experimental models of inflammatory lung disease, i.e., mice exposed to aerosolized LPS and the model of OVA-induced asthma, show that engagement of the glucose transporter SGLT-1 induces potent anti-inflammatory effects in lungs. As an SGLT-1 ligand, we used the synthetic glucose analogue BLF501, a synthetic C-glucoside derivative, identified by *in vitro* screening for SGLT-1 ligands that might elicit anti-inflammatory effects similar to those induced by glucose but at much lower concentrations compatible with possible therapeutic applications.

In the first model analyzed, exposure of mice to aerosolized LPS led to acute respiratory distress, accompanied by widespread destruction of the alveolar and endothelial epithelia, as well as flooding of the alveolar spaces with proteinaceous exudates containing large amounts of neutrophils[110-112]. This is the consequence of LPS binding to TLRs, followed by the expression of proinflammatory cytokines (TNF-α and IL-1β), chemokines (keratinocyte-derived chemokine KC or IL-8, and adhesion molecules (ICAM-1 and vascular cell

adhesion molecule-1 VCAM-1), which induce the extravasation of neutrophils across endothelial and epithelial barriers that separate the bloodstream from the pulmonary air spaces[110,111]. By contrast, mice treated with LPS and aerosolized BLF501 presented a normal lung parenchyma, without cellular depots within the alveoli. Immunohistochemical analysis of lung sections showed a marked increase in ICAM-1 and caveolin expression in mice treated with LPS alone, but not upon treatment with LPS and BLF501. Moreover, analysis of the BALFs revealed high levels of NO in LPS-treated animals, but not in mice also treated with BLF501. It is noteworthy that the engagement of SGLT-1 by BLF501 *per se* did not influence inflammatory parameters since mice receiving BLF501 alone were comparable in all respects to untreated control mice.

A similar protective activity of BLF501 was observed in OVA-induced allergic asthma, a model that differs considerably from LPS-induced lung injury with respect to pathogenesis but not in the inflammatory outcomes, including the abundant cellular infiltrates in lung parenchyma and increased serum levels of pro-inflammatory chemokines and cytokines. Lung tissue from BLF501-treated mice did not exhibit depots of alveolar lymphocytes or blood infiltrates, and BALFs revealed no accumulation of neutrophils or eosinophils. The reduction of leukocyte in filtration observed in OVA plus BLF501 treated mice may play a pivotal role in the induction of anti-inflammatory effects observed in this setting, since neutrophils are considered primary effector cells in the alveolo-capillary damage that accompanies lung inflammation[112]. Moreover, serum levels of IL-4 and IL-5, prototypical cytokines involved in the pathogenesis of asthma, and of IgE were elevated in mice treated with OVA alone but normal in OVA plus BLF501-treated mice, which also showed dramatically increased serum levels of the anti-inflammatory cytokine IL-10.

A high protein content was observed in the BALFs from mice treated with OVA alone, consistent with the presence of high-permeability pulmonary edema, whereas BALF protein concentrations in BLF501-treated mice was comparable to that of untreated mice or mice treated with BLF501 alone. Thus, BLF501 effectively decreased abnormal lung vascular permeability and promoted resolution of lung edema, suggesting that this reagent protects the integrity of the alveolo-capillary membrane.

BLF501 had protective activity in OVA-induced asthma even when orally administered, while intravenous administration did not lead to a protective effect. These findings suggested an engagement of SGLT-1 expressed in intestinal epithelial cell by orally administered BLF501 that induces a direct or indirect release of anti-inflammatory molecules. In fact, mice orally treated with BLF501 and OVA had very high systemic levels of IL-10, an anti-inflammatory cytokine produced mainly by DCs and monocytes[113]. Accordingly, administration of recombinant IL-10 has been shown to increase survival in mice undergoing sepsis, while IL-10 gene therapy significantly attenuates sepsis-induced multi-organ failure[114]. Thus, IL-10 produced by DCs and monocytes would be the final mediator of the systemic anti-inflammatory effects induced by BLF501, which, though orally administered, exerts anti-inflammatory activity in the lung compartment through these soluble mediators. DCs do not express SGLT-1, but they produce IL-10 when activated by hsp27[115,116]. Our *in vitro* data showed that hsp27 is strongly secreted by SGLT-1-positive epithelial cells HT-29, upon stimulation with TNF-α in the presence of BLF501, and the co-culture of TNF-α/ BLF501-treated HT-29 cells with MoDCs cells led to the production of high levels of IL-10 by DCs. This production of IL-10 was completely eliminated upon silencing of hsp27 expression in HT29 cells . *In vivo,* hsp 25 serum levels, murine homologue of hsp27, were dramatically increased in mice treated with OVA and

BLF501. Together, these findings strongly suggest that hsp25/hsp27 mediates activation of SGLT-1 and production of IL-10 by DCs.

The present data showing that BLF501 exerts potent anti-inflammatory effects in two different experimental models of inflammatory lung diseases provide direction to a new pharmacological approach for treatment of inflammatory lung diseases. Thus, the SGLT-1 ligand synthetic glucose analogue BLF501 might serve in the therapeutic intervention of lung inflammation, especially in allergic asthma, a disease of increasing world-wide prevalence with still unmet clinical needs.

REFERENCES

1. Diez-Sampedro A, Eskandari S, Wright EM and Hirayama BA. Na+-to sugar stoichiometry of SGLT1. *Am J Physiol Renal Physiol* 2001; 280:F278±F282.
2. Elfeber K, Kohler A, Lutzenburg M, Osswald C, Galla HJ, Witte OW, Koepsell H. Localization of the Na+-D-glucose cotransporter SGLT1 in the blood-brain barrier. *Histochem Cell Biol* 2004; 121:201-207.
3. Miyamoto K, Hase K, Takagi T, Fujii T, Taketani Y, Minami H, Oka T, Nakabou Y. Differential responses of intestinal glucose transporter mRNA transcripts to levels of dietary sugars. *Biochem J* 1993; 295 (Pt 1):211-215.
4. Veyhl M, Spangenberg J, Puschel B, Poppe R, Dekel C, Fritzsch G, Haase W, Koepsell H. Cloning of a membraneassociated protein which modifies activity and properties of the Na(+)-D-glucose cotransporter. *J Biol Chem* 1993; 268: 25041 25053.
5. Ikari A, Nakano M, Kawano K, Suketa Y. Up-regulation of sodium-dependent glucose transporter by interaction with heat shock protein 70. *J Biol Chem* 2002; 277:33338-33343.
6. Palazzo M, Gariboldi S, Zanobbio L, Selleri S, Dusio GF, Mauro V, Rossini A, Balsari A, Rumio C. Sodium-dependent glucose transporter-1 as a novel immunological player in the intestinal mucosa. J Immunol. 181: 3126–3136 (2008).
7. Zanobbio L, Palazzo M, Gariboldi S, Dusio GF, Cardani D, Mauro V, Marcucci F, Balsari A, Rumio C. Intestinal glucose uptake protects liver from LPS/D-GalN, acetaminophen and alpha-amanitin in mice. Am J Pathol. 175:1066-1076 (2009).
8. Pilewski J.M. et al Role of CFTR in arway disease. Physiol. Rev. 79, S215-S255 (199).
9. Heazlewood C.K. et al.. Aberrant mucin assembly in mice causes endoplasmic reticulum stress and spontaneous inflammation reseimbling ulcerative colitis. PLos. Med. (2008)
10. Ayabe T, Satchell DP, Wilson CL, Parks WC, Selsted ME, and Ouellette AJ. Secretion of microbicidal α-defensins by intestinal Paneth cells in response to bacteria. *Nat Immun* 2000; 1:113–118.
11. Gewirtz AT, Navas TA, Lyons S, Godowski PJ and Madara JL. Cutting edge: bacterial flagellin activates basolaterally expressed TLR5 to induce epithelial proinflammatory gene expression. *J Immunol* 2001; 167:1882–1885.
12. Hooper LV, Stappenbeck TS, Hong CV, and Gordon JI. Angiogenins: a new class of microbicidal proteins involved in innate immunity. *Nat Immun* 2003; 4: 269–273
13. Barton GM, Medzhitov R. Control of adaptive immune responses by Toll-like receptors. *Curr Opin Immunol* 2002; 14:380–383.

14. Matzinger P. An innate sense of danger. *Ann NY Acad Sci* 2002; 961:341–342.
15. Palazzo M, Balsari A, Rossini A, Selleri S, Calcaterra C, Gariboldi S, Zanobbio L, Arnaboldi F, Shirai YF, Serrao G, Rumio C. Activation of enteroendocrine cells via Toll-like receptors induces hormone, chemokine and defensin secretion. J. Immunol, 2007;178: 4296-4303
16. Cario E, Rosenberg IM, Brandwein SL, Beck PL, Reinecker HC and Podolsky DK. Lipopolysaccharide activates distinct signaling pathways in intestinal epithelial cell lines expressing Toll-like receptors. *J Immunol* 2000; 164: 966–972.
17. Ortega-Cava CF, Ishihara S, Rumi MA, Kawashima K, Ishimura N, Kazumori H, Udagawa J, Kadowaki Y, and Kinoshita Y. Strategic compartmentalization of Tolllike receptor 4 in the mouse gut. *J Immunol* 2003; 170: 3977–3985.
18. Hermiston, M. L. & Gordon, J. I. *In vivo* analysis of cadherin function in the mouse intestinal epithelium: essential roles in adhesion, maintenance of differentiation, and regulation of programmed cell death. *J. Cell Biol.* 129, 489–506 (1995).
19. .Furuse M, Fujita K, Hiiragi T, Fujimoto K, Tsukita S. 1998. Claudin-1 and -2: novel integral membrane proteins localizing at tight junctions with no sequence similarity to occludin. *J. Cell Biol.* 141:1539–50
20. Furuse M, Tsukita S. 2006. Claudins in occluding junctions of humans and flies. *Trends Cell Biol.* 16:181–88
21. Van Itallie CM, Anderson JM. 2006. Claudins and epithelial paracellular transport. *Annu. Rev. Physiol.* 68:403–29
22. Van ItallieCM,Fanning AS, Anderson JM. 2003. Reversal of charge selectivity in cation or anion-selective epithelial lines by expression of different claudins. *Am. J. Physiol. Renal Physiol.* 285:F1078–84
23. Yu ASL, ChengMH,Angelow S, Gunzel D, Kanzawa SA, et al. 2009. Molecular basis for cation selectivity in claudin-2-based paracellular pores: identification of an electrostatic interaction site. *J. Gen. Physiol.* 133:111–27
24. Itoh M, Furuse M, Morita K, Kubota K, Saitou M, Tsukita S. 1999. Direct binding of three tight junction–associated MAGUKs, ZO-1, ZO-2, and ZO-3, with the COOH termini of claudins. *J. Cell Biol.* 147:1351–63
25. Jesaitis LA, Goodenough DA. 1994. Molecular characterization and tissue distribution of ZO-2, a tight junction protein homologous to ZO-1 and the *Drosophila* discs–large tumor suppressor protein. *J. Cell Biol.* 124:949–61

26. Haskins J, Gu L,Wittchen ES, Hibbard J, Stevenson BR. 1998. ZO-3, a novel member of the MAGUK protein family found at the tight junction, interacts with ZO-1 and occludin. *J. Cell Biol.* 141:199–208

27. Umeda K, Ikenouchi J, Katahira-Tayama S, Furuse K, Sasaki H, et al. 2006. ZO-1 and ZO-2 independently determine where claudins are polymerized in tight-junction strand formation. *Cell* 126:741–54

28. Furuse M, Hirase T, Itoh M, Nagafuchi A, Yonemura S, Tsukita S. 1993. Occludin: a novel integral membrane protein localizing at tight junctions. *J. Cell Biol.* 123:1777−88

29. McCarthy KM, Skare IB, Stankewich MC, Furuse M, Tsukita S, et al. 1996. Occludin is a functional component of the tight junction. *J. Cell Sci.* 109:2287−98

30. Chen Y, Merzdorf C, Paul DL, Goodenough DA. 1997. COOH terminus of occludin is required for tight junction barrier function in early *Xenopus* embryos. *J. Cell Biol.* 138:891−99

31. Cordenonsi M, Mazzon E, De Rigo L, Baraldo S, Meggio F, Citi S. 1997. Occludin dephosphorylation in early development of *Xenopus laevis*. *J. Cell Sci.* 110:3131−39

32. Sakakibara A, Furuse M, Saitou M, Ando-Akatsuka Y, Tsukita S. 1997. Possible involvement of phosphorylation of occludin in tight junction formation. *J. Cell Biol.* 137:1393−401

33. Wong V, Gumbiner BM. 1997. A synthetic peptide corresponding to the extracellular domain of occluding perturbs the tight junction permeability barrier. *J. Cell Biol.* 136:399−409

34. Shen L, Turner JR. 2005. Actin depolymerization disrupts tight junctions via caveolae-mediated endocytosis *Mol. Biol. Cell* 16:3919−36.

35. Mitic LL, Unger VM, Anderson JM. 2003. Expression, solubilization, and biochemical characterization of the tight junction transmembrane protein claudin 4. *Protein Sci.* 12:218−27

36. Saitou M, Furuse M, Sasaki H, Schulzke JD, Fromm M, et al. 2000. Complex phenotype of mice lacking occludin, a component of tight junction strands. *Mol. Biol. Cell* 11:4131−42

37. Schulzke JD, Gitter AH, Mankertz J, Spiegel S, Seidler U, et al. 2005. Epithelial transport and barrier function in occludin-deficient mice. *Biochim. Biophys. Acta* 1669:34−42

38. Ikenouchi J, Furuse M, Furuse K, Sasaki H, Tsukita S. 2005. Tricellulin constitutes a novel barrier at tricellular contacts of epithelial cells. *J. Cell Biol.* 171:939−45

39. Riazuddin S, Ahmed ZM, Fanning AS, Lagziel A, Kitajiri S, et al. 2006. Tricellulin is a tight-junction protein necessary for hearing. *Am. J. Hum. Genet.* 79:1040−51

40. Turner JR, Rill BK, Carlson SL, Carnes D, Kerner R, et al. 1997. Physiological regulation of epithelial tight junctions is associated with myosin light-chain phosphorylation. *Am. J. Physiol.* 273:C1378−85

41. Turner JR, Cohen DE, Mrsny RJ, Madara JL. 2000. Noninvasive in vivo analysis of human small intestinal paracellular absorption: regulation by Na+-glucose cotransport. *Dig. Dis. Sci.* 45:2122−26.

42. Madara JL, Pappenheimer JR. 1987. Structural basis for physiological regulation of paracellular pathways in intestinal epithelia. *J. Membr. Biol.* 100:149−64

43. Yuhan R, Koutsouris A, Savkovic SD, Hecht G. 1997. Enteropathogenic *Escherichia coli*−induced myosin light chain phosphorylation alters intestinal epithelial permeability. *Gastroenterology* 113:1873−82

44. Spitz J, Yuhan R, Koutsouris A, Blatt C, Alverdy J, Hecht G. 1995. Enteropathogenic *Escherichia coli* adherence to intestinal epithelial monolayers diminishes barrier function. *Am. J. Physiol.* 268:G374−79.

45. Madara, J. L. & Stafford, J. Interferon-gamma directly affects barrier function of cultured intestinal epithelial monolayers. *J. Clin. Invest.* 83, 724–727 (1989).

46. Taylor, C. T., Dzus, A. L. & Colgan, S. P. Autocrine regulation of epithelial permeability by hypoxia: role for polarized release of tumour necrosis factor-α. *Gastroenterology* 114, 657–668 (1998).

47. Mullin, J. M., Laughlin, K. V., Marano, C. W., Russo, L. M. & Soler, A. P. Modulation of tumour necrosis factor-induced increase in renal (LLC-PK1) transepithelial permeability. *Am. J. Physiol.* 263, F915–F924 (1992).

48. Mazzon, E. & Cuzzocrea, S. Role of TNF-α in lung tight junction alteration in mouse model of acute lung inflammation. *Respir. Res.* 8, 75 (2007).

49. Baker, O. J. *et al.* Proinflammatory cytokines tumour necrosis factor-α and interferon-γ alter tight junction structure and function in the rat parotid gland Par-C10 cell line. *Am. J. Physiol. Cell Physiol.* 295, C1191–C1201 (2008).
50. Tiruppathi, C., Naqvi, T., Sandoval, R., Mehta, D. & Malik, A. B. Synergistic effects of tumour necrosis factor-α and thrombin in increasing endothelial permeability. *Am. J. Physiol. Lung Cell. Mol. Physiol.* 281, L958–L968 (2001).
51. Baert, F. J. *et al.* Tumour necrosis factor α antibody (infliximab) therapy profoundly downregulates the inflammation in Crohn's ileocolitis. *Gastroenterology* 116, 22–28 (1999).
52. Tamion, F. *et al.* Gut ischemia and mesenteric synthesis of inflammatory cytokines after hemorrhagic or endotoxic shock. *Am. J. Physiol.* 273, G314–G321 (1997).
53. Brown, G. R. *et al.* Tumour necrosis factor inhibitor ameliorates murine intestinal graft-versus-host disease. *Gastroenterology* 116, 593–601 (1999).
54. Clayburgh, D. R. *et al.* Epithelial myosin light chain kinase-dependent barrier dysfunction mediates T cell activation-induced diarrhea *in vivo*. *J. Clin. Invest.* 115, 2702–2715 (2005).
55. Zolotarevsky, Y. *et al.* A membrane-permeant peptide that inhibits MLC kinase restores barrier function in *in vitro* models of intestinal disease. *Gastroenterology* 123, 163–172 (2002).
56. Ma, T. Y., Boivin, M. A., Ye, D., Pedram, A. & Said, H. M. Mechanism of TNF-α modulation of Caco-2 intestinal epithelial tight junction barrier: role of myosin lightchain
57. kinase protein expression. *Am. J. Physiol. Gastrointest. Liver Physiol.* 288, G422–G430 (2005).
58. McKenzie, J. A. & Ridley, A. J. Roles of Rho/ROCK and MLCK in TNF-α-induced changes in endothelial morphology and permeability. *J. Cell. Physiol.* 213, 221–228 (2007).
59. Blair, S. A., Kane, S. V., Clayburgh, D. R. & Turner, J. R. Epithelial myosin light chain kinase expression and activity are upregulated in inflammatory bowel disease. *Lab. Invest.* 86, 191–201 (2006).
60. Schwarz, B. T. *et al.* LIGHT signals directly to intestinal epithelia to cause barrier dysfunction via cytoskeletal and endocytic mechanisms. *Gastroenterology* 132, 2383–2394 (2007).
61. Al-Sadi, R., Ye, D., Dokladny, K. & Ma, T. Y. Mechanism of IL-1β-induced increase in intestinal epithelial tight junction permeability. *J. Immunol.* 180, 5653–5661 (2008).
62. Wroblewski, L. E. *et al.* Helicobacter pylori dysregulation of gastric epithelial tight junctions by urease-mediated myosin II activation. *Gastroenterology* 136, 236–246 (2009).

63. Scott, K. G., Meddings, J. B., Kirk, D. R., Lees-Miller, S. P. & Buret, A. G. Intestinal infection with Giardia spp. reduces epithelial barrier function in a myosin light chain kinase-dependent fashion. *Gastroenterology* 123, 1179–1190 (2002).

64. Moriez, R. *et al.* Myosin light chain kinase is involved in lipopolysaccharide-induced disruption of colonic epithelial barrier and bacterial translocation in rats. *Am. J. Pathol.* 167, 1071–1079 (2005).

65. Eutamene, H. *et al.* LPS-induced lung inflammation is linked to increased epithelial permeability: role of MLCK. *Eur. Respir. J.* 25, 789–796 (2005).

66. Ferrier, L. *et al.* Impairment of the intestinal barrier by ethanol involves enteric microflora and mast cell activation in rodents. *Am. J. Pathol.* 168, 1148–1154 (2006).

67. Podolsky D. Inflammatory bowel disease. N. England J. Med. 347:417-429

68. Strober W, et al. The fundamental basis of inflammatory bowel disease. J Clin Invest, (2007) Mar;117(3):514-521

69. Fuss, I., et al.. Non classical CD1d-restricted NK T cells that produce IL-13 characterize an atipica Th2 response in ulcerative colitis. *J. Clin. Invest.* 113:1490–1497 (2004).

70. Arietta MC et al. Reducing small intestinal permeability attenuates colitis in the IL-10 gene-deficient mouse. *Gut* 2009; 58;41-48.

71. Arietta MC et al. Alteration in intestinal permeability. *Gut*. 55:1512-1520 (2006).

72. Feagan, B. Et al. Maintenance therapy for inflammatory bowel disease. *Am. J. Gastroenterol.* 98 (Suppl. 12):S6–S17. 5 (2003).

73. Siegel C.and Sands, B.. Practical management of inflammatory bowel disease patients taking immunomodulators. *Aliment. Pharmacol. Ther.*22:1–16 (2005)

74. Madsen, K. L. *et al.* Interleukin-10 gene-deficient mice develop a primary intestinal permeability defect in response to enteric microflora. *Inflamm. Bowel Dis.* 5, 262–270 (1999).

75. Olson, T. S. *et al.* The primary defect in experimental ileitis originates from a nonhematopoietic source. *J. Exp. Med.* 203, 541–552 (2006).

76. Wyatt, J., Vogelsang, H., Hubl, W., Waldhoer, T. & Lochs, H. Intestinal permeability and the prediction of relapse in Crohn's disease. *Lancet* 341, 1437–1439 (1993).

77. Hollander, D. Crohn's disease — a permeability disorder of the tight junction? *Gut* 29, 1621–1624 (1988).

78. Irvine, E. J. & Marshall, J. K. Increased intestinal permeability precedes the onset of Crohn's disease in a subject with familial risk. *Gastroenterology* 119, 1740–1744 (2000).

79. Y. Zolotarevsky, G. Hecht, A. Koutsouris, D.E. Gonzalez, C. Quan, J. Tom, R.J. Mrsny, J.R. Turner, A membranepermeant peptide that inhibits MLC kinase restores barrier function in in vitro models of intestinal disease, Gastroenterology 123 (2002) 163– 172.

80. Sibille Y, Reynolds HY. Macrophages and polymorphonuclear neutrophils in lung defence and injury. *Am Rev Respir Dis* 1990; 141:471–501.

81. Polito AJ, Proud D. Epithelial cells as regulators of airway inflammation. *J Allergy Clin Immunol* 1998; 102: 714–718

82. Massion PP, Inoue H, Richman-Eisenstat J, et al. Novel Pseudomonas product stimulates interleukin-8 production in airway epithelial cells in vitro. *J Clin nvest* 1994; 93:26–32

83. Crapo JD, Harmsen AG, Sherman MP, Musson RA. Pulmonary immunobiology and inflammation in pulmonary diseases. *Am J Respir Crit Care Med* 2000; 162:1983–1986

84. Kowalski MP et al. Host resistance to lung infection mediated by major vault protein in epithelial cells. *Science* 2007; 317(5834):130–132.

85. Schutte BC and McCray PB. [beta]-defensins in lung host defense. *Annu Rev Physiol 2002; 64*:709–748

86. Bals R, Wang X, Zasloff M, Wilson JM. The peptide antibiotic LL-37/hCAP-18 is expressed in epithelia of the human lung where it has broad antimicrobial activity at the airway surface. *Proc Natl Acad Sci USA* 1998;95:9541-6

87. Moser C, Weiner DJ, Lysenko E, Bals R, Weiser JN, Wilson JM. Betadefensin 1 contributes to pulmonary innate immunity in mice. *Infect Immun* 2002; 70:3068-72.

88. Cohen, J. 2002. The immunopathogenesis of sepsis. *Nature* 420: 885–891.

89. Galanos, C., M. A. Freudenberg, and W. Reutter. 1979. Galactosamine-induced sensitization to the lethal effects of endotoxin. *Proc. Natl. Acad. Sci. USA* 76: 5939–5943.

90. Wang, W.V. Graham, Y. Wang, E.D. Witkoski, B. T. Schwarz and J.R. Turner. Interferon-γ and tumor necrosis factor-α synergize to induce intestinal epithelial barrier dysfunction by

up-regulation Myosin chain kinase axpression. American Journal of Phatology 2005, 166 409-419.

91. Okayasu I. Et al .A novel method in the induction of reliable experimental acute and chronic colitis in mice. *Gastroenterology*. 98,694-702 (1990).

92. Wirtz S, et al. Chemically induced mouse models of intestinal inflammation. Nat Protoc, 2007; 2(3): 541-546.

93. Vetrano S. et al Unique role of junctional adhesion molecule-a in maintaining mucosal homeostasis in inflammatory bowel disease. Gastroenterology 2008 Jul;135(1):173-84. Epub 2008 Apr 11.

94. Poritz LS. Et al. Loss of the tight junction protein ZO.1 in dextran sulfate sodium induced colitis. J. Surg. Res. 2007 1;140(1):12-9.

95. Liu XC et al. Balsalazine decreases intestinal mucosal permeability of dextran sulfate sodium-induced colitis in mice. Acta Pharmacol. Sin. 2009 30(7):987-93

96. Herfarth H., et al. IL-10 therapy in Crohn's disease: at the crossroads. Gut, 2002; 50: 146-147..

97. Mamchaoui, K., Makhloufi, Y., and Saumon, G. Glucose transporter gene expression in freshly isolated and cultured rat pneumocytes. *Acta Physiol. Scandinavica* 2002 175:19-24

98. Wu, T.L., et al.. A panel of multiple markers associated with chronic systemic inflammation and the risk of atherogenesis is detectable in asthma and chronic obstructive pulmonary disease. *J. Clin. Lab. Anal.* 2007 21:367-371.

99. Hessel, E.M., et al.. Development of airway hyperresponsiveness is dependent on interferon-gamma and independent of eosinophil infiltration. *Am. J. Respir. Cell. Mol. Biol.* 1997 16:325-334.

100 Mukhopadhyay, S., Hoidal, J.R., and Mukherjee, T.K.. Role of TNF alpha in pulmonary pathophysiology. *Respir. Res.* 2006 7:125.

101 Ogawa, Y., Duru, E.A., and Ameredes, B.T. Role of IL-10 in the resolution of airway inflammation. *Curr. Mol. Med.* 2008.8:437-445.

102 Wheeler, D.S., and Wong, H.R.. Heat shock response and acute lung injury. *Free Radic. Biol. Med.* 2007 42:1-14

103 Kellett GL, Helliwell PA. The diffusive component of intestinal glucose absorption is mediated by the glucose-induced recruitment of GLUT2 to the brush-border membrane. Biochem J 2000;350(Part 1):155–162.

104 Kellett GL. The facilitated component of intestinal glucose absorption. J Physiol 2001;531(Part 3):585–595.

105 Hu Z, Wang Y, Graham WV, Su L, Musch MW and Turner JR. MAPKAPK-2 is a critical signaling intermediate in NHE3 activation following Na-Glucose

106 Zhao H, Shiue H, Palkon S, et al. Ezrin regulates NHE3 translocation and activation after Na+-glucose cotransport. Proc Natl Acad Sci USA. 2004;101:9485–9490.

107 Fearon KC, Ljungqvist O, Von Meyenfeldt M, et al. Enhanced recovery after surgery: a consensus review of clinical care for patients undergoing colonic resection. Clin Nutr 2005;24:466–477.

108. Martindale RG, Maerz LL. Management of perioperative nutrition. Curr Opin Crit Care 2006;12:290–294.

109 Sanders SE, Madara JL, McGuirk DK, Gelman DS, Colgan SP. Assessment of inflammatory events in epithelial permeability: a rapid screening method using fluorescein dextrans. Epithelil Cell Biol 4(1):25-34. 1995.

110 Bachofen, M., and Weibel, E.R.. Structural alterations of lung parenchyma in the adult respiratory distress syndrome. *Clin. Chest Med.* 1982 3:35-56.

111 Kline, J.N., et al.. Variable airway responsiveness to inhaled lipopolysaccharide. *Am. J. Respir. Crit. Care Med.* 1999 160:297-303.

112 Arbour, N.C., et al.. TLR4 mutations are associated with endotoxin hyporesponsiveness in humans. *Nat. Genet.* 2000 25:187-191.

113 Ogawa, Y., Duru, E.A., and Ameredes, B.T.. Role of IL-10 in the resolution of airway inflammation. *Curr. Mol. Med.* 2008 8:437-445

114 Howard, M., Muchamuel, T., Andrade, S., and Menon, S.. Interleukin 10 protects mice from lethal endotoxemia. *J. Exp. Med.* 1993 177:1205-1208.

115 Xu, W., et al.. Human peritoneal macrophages show functional characteristics of M-CSF-driven anti-inflammatory type 2 macrophages. *Eur. J. Immunol.* 2007 37:1594-1599.

116 Laudanski, K., De, A., and Miller-Graziano, C. 2007. Exogenous heat shock protein 27 uniquely blocks differentiation of monocytes to dendritic cells. *Eur. J. Immunol.* 37:2812-2824